EXPERIMENTAL INVESTIGATION OF A NON-THERMAL

ATMOSPHERIC PRESSURE PLASMA JET
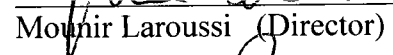
by

Asma Begum
B.Sc. August 1999, Dhaka University
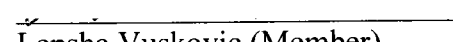M.Sc. December 2001, Dhaka University

A Dissertation Submitted to the Faculty of
Old Dominion University in Partial Fulfillment of the
Requirement for the Degree of

DOCTOR OF PHILOSOPHY

ELECTRICAL AND COMPUTER ENGINEERING

OLD DOMINION UNIVERSITY
August 2010

Approved by:

_____
Mounir Laroussi (Director)

_____
Sacharia Albin   (Member)

_____
Lepsha Vuskovic (Member)

_____
Frederic D. McKenzie (Member)

ABSTRACT

EXPERIMENTAL INVESTIGATION OF NON-THERMAL ATMOSPHERIC PRESSURE PLASMA JET

Asma Begum
Old Dominion University, 2010
Director: Dr. Mounir Laroussi

An atmospheric pressure non-thermal plasma jet/bullet is the flowing plasma outside the discharge chamber. It is widely used in plasma medicine and surface decontamination. It is also used in surface treatment and material deposition. A dielectric barrier configured plasma pencil is used to generate the plasma jet in the helium gas channel, which comes out from the discharge chamber in the ambient atmosphere. A unipolar square pulse voltage is used to create discharge in the helium channel. The main objective of this dissertation is to understand the formation of the plasma jet from the plasma pencil, and the propagation of the plasma jet in the ambient atmosphere where the effect of the external electric field is almost zero. Before investigating the formation and propagation phenomenon of the plasma jet, common physical properties of plasma jets are determined by using the imaging technique and optical emission spectroscopy. The first goal of this dissertation is to establish the laminar helium gas flow channel through a plasma pencil. For this reason, the critical Reynolds number of helium gas flow through the outlet of the plasma is calculated. This result is justified by observing the image of the plasma jet for different feed gas flow rates. The change of the shape and size of the plasma jet with applied voltage, pulse width, and feed gas flow rate is also investigated. The temperature of the plasma jet is measured by using an Hg- thermometer.

The formation position, formation time, and the criterion of the plasma jet formation from the discharge chamber of a plasma pencil are investigated by imaging technique, optical emission spectroscopy, and electrical measurement technique. It shows that the plasma jet forms at the surface of the grounded dielectric as a positive plasma front. The formation time of the plasma jet decreases with applied voltage. The maximum power, total power, and average energy to the system and to the discharge are calculated

from the total current, discharge current, input potential, and gap potential of the plasma pencil. The calculated average input power with applied voltage to the discharge shows that 56% of the input power is used in the discharge. The total charge in the discharge chamber is calculated by integrating the discharge current waveform. The critical charge in the discharge chamber required to generate a plasma jet is also determined.

The propagation phenomenon of the plasma bullet in the ambient atmosphere has been investigated from the velocity curves of the plasma bullet along the jet axis for different applied voltages, pulse widths, and feed gas flow rates. The plasma bullet's velocity is measured by using two different techniques: i) imaging technique and ii) electrical technique. In imaging technique, ultra-fast ICCD images of the plasma jet have been taken at different times and positions, and from the change of position of the plasma bullet's front with time plasma bullet velocity is calculated. In the electrical technique, from the spatial and temporal evolution of the jet current along the jet axis, the plasma bullet velocity is calculated. It shows that the plasma bullet velocity curve has three distinct phases: transition phase, propagation phase, and collapse of the plasma bullet. The transition phase and the propagation phase of the plasma bullet have been explained to understand the plasma properties in the plasma bullet. A correlation between the average plasma bullet velocity, length of the plasma jet, and the operating pulse width is established, which can be used in the modeling of the plasma bullet's propagation. The change of the shape and the inner structure of the plasma bullet are observed along the propagation pathway of the plasma bullet. The contraction of the plasma bullet is investigated from the head-on view image and the electric field due to the cross-section of the plasma bullet. It shows that the contraction of the plasma bullet occurs because of a cone-shape electric field line in front of the plasma bullet. The average reduced electric field and the power density have been estimated by using a simple model. The electron density of the plasma jet along the jet axis is estimated from the jet current density and the spatial and temporal differences between the consecutive jet current peaks along the jet axis. The estimated electron density in the plasma bullet is in the order of 10^{11} cm^{-3}. The effect of applied voltage and gas flow rate on the electron density is also investigated.

The spatial evolution of the different species along the jet axis is investigated by optical emission spectroscopy. The evolution of the different species follows the same shape as the plasma bullet velocity curve. Along the transition phase, the plasma chemistry is dominated by excited state of ionized molecular nitrogen, helium metastable, and high energy electrons. Along the propagation phase, the plasma chemistry is dominated by the first negative system of nitrogen and some of the long lived metastable helium. The local reduced electric field and electron density along the jet axis are measured from the intensity of the nitrogen bands and it is compared with the results obtained from the measurement by using a dielectric probe. The maximum local reduced electric field is 350 Td for the applied voltage of 6 kV. The estimated electron density is in the same order (10^{11} cm^{-3}) for both measurements.

ACKNOWLEDGMENTS

I would like to express my gratitude and thanks to my research advisor Dr. Mounir Laroussi, who was always been beside me to support me with his knowledge, scientific intuition, to correct me whenever research was not going right, and to help to develop my scientific writing. His knowledge and dedication about science and engineering has helped me to grow as a researcher. I am grateful and would like to thank specially Dr. Sacharia Albin, Department of Electrical and Computer Engineering, ODU and Dr. Lepsha Vuskovic, Department of Physics, ODU. Without their help it would have been quite impossible to complete my Ph.D. in this short time.

I would like to thank all of my coworkers whose support and contribution made my research life very easy. I will gratefully remember Julien Jarrige, Erdinc Karakas, N. Mericam-Bourdet, and T. Akan who helped me throughout my experiments in last couple of years.

My friends Senthilraja Singaravelu and Janardan Upadhay in the Department of Physics, ODU, were always beside me to share my sad and happy moments. I will cherish their friendship. Thank you.

Finally and most importantly, from bottom of my heart, I want to specially thank, my parents. Without you all I would not be who I am today. Above all, my warm and special thanks for the understanding, patience, and huge support of my husband, Rasel Pervez and my son, Reek Pervez. Without them, it would be quite impossible to continue my research during my stay in the USA.

TABLE OF CONTENTS

LIST OF TABLES

LIST OF FIGURES

CHAPTER I

INTRODUCTION

I.1. MOTIVATION

Plasma is the fourth state of matter, which is quasi-neutral gas composed of charges (ions and electrons), excited, and neutral particles. Plasma is a chemically active ionized medium. As low pressure plasma generation requires vacuum system, in the last decade, there has been growing interest in the use of atmospheric pressure plasma because of practical applications. The applications for plasma are range from material processing and particle deposition to plasma medicine. Most of the atmospheric pressure plasma sources are obtained with corona discharges [1] and Dielectric Barrier Discharges (DBD) [2, 3]. The researcher created an atmospheric pressure (760 Torr) gas environment in a chamber to generate atmospheric pressure plasma. In the surface treatment, the sample is normally placed inside the discharge chamber and these plasmas are exposed directly to the surface of the sample.

Among many of the atmospheric pressure plasma sources, atmospheric pressure plasma jets are gaining growing attention because of its remote exposure of facilities on the sample. The phenomenon of the Atmospheric Pressure Plasma Jet (APPJ) dates back to 1960s when it was generated as a local thermodynamic equilibrium plasma jet [4]. Later on, APPJs were produced in various distinct designs and under different conditions [5-7]. Atmospheric pressure arc jet and plasma torches generate thermal equilibrium plasma, known as thermal plasma. These plasmas are at high temperature and may damage the sample surface. Koinuma and his group [6] obtained an APPJ in micro beam plasma generator in 1992. It was later named a cold plasma torch. Generally, the gas temperature of cold/low temperature plasma torch is around room temperature and the electron temperature is much higher than the gas temperature. Figure I.1 shows the general technique of the plasma jet generation process. The basic tools to generate a plasma jet are: i) gas flow channel, and ii) the ignition of a discharge in that channel. The discharge starts from the high voltage electrode and develops along the feed gas flow channel. This partially/weakly ionized gas channel outside the discharge zone is called

---

This dissertation follows the style of *Physical Review E.*

the plasma jet. These plasma jets are not confined within an externally applied electric field. It is convenient to use this type of plasma for indirect surface treatment. It is believed that the only way to create the plasma jet is by blowing out the plasma plume from the discharge chamber into the ambient air by gas flow. However, experiments have shown [8, 9] that the jet phenomenon is strictly an electrical discharge in a gas stream.
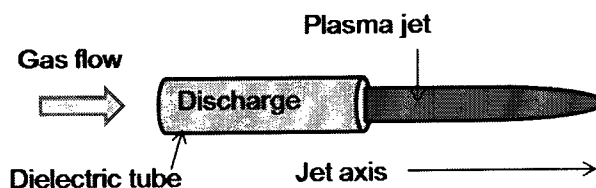
FIG. I.1. Schematic of the plasma jet generator.

Several types of plasma jets have been developed by different researchers around the world; most of them use Radio Frequency (RF) power supplies [10]. However, discharges ignited by pulse power have been found to be more efficient with enhanced gas phase chemistry at the same input power [11, 12]. Short high voltage pulses can give almost instantaneous high energy to the electrons. Atmospheric pressure plasma jets are generated in Dielectric Barrier Discharge (DBD) by using pulsed power provides plasma as bullets in the ambient atmosphere where the gas temperature remains around room temperature. These plasma jets are mostly used in biomedicine [13-17] and surface treatment. Some jets can propagate in ambient air for more than 11cm.

Depending on the applications of the plasma jet different research teams around the world have worked on different types of plasma jet reactors. Most of the developments are focused on the device geometry and their applications. Table I.1 shows some of the plasma jets, their operating conditions and applications.

Table I.1. Different kinds of plasma jet, their operating conditions, and applications.

Type of plasma jet	Operation conditions	Applications
AC driven plasma jet	AV = Few kVs f = 5-50 kHz Gas temperature: 300-750 K Jet length: ~5 cm Feed gas: He, Ar, N_2	Bio-application [8], change the wettability of a thin polymer film [18, 19], Surface treatment [20]
RF driven plasma jet	f = 5-40 MHz Gas temperature: 300-1000 K Jet length: ~ 2 cm Feed gas: He, Ar, N_2 mixed with H_2/ tetramethoxysilane/ silane (SiH4), with precursors.	Surface treatment [21], etching of silicon [22], deposition of SiO_2 and TiO_2 [23, 24], bacteria killing [25].
Pulsed DC driven plasma jet	AV = kV range PW = nanosecond to microsecond f = 2-10 kHz Gas temperature: 300-500 K Feed gas: He, Ar, N_2 Jet length: ~ 11 cm.	Killing various types of bacteria and blood coagulation. [13, 26-30]

I.2. STATEMENT OF THE PROBLEM

Although a large number of different plasma jets have been developed over the years, the physical phenomena of their formation and propagation are not well understood. Most of the developments in the plasma jet are focused on the device geometry and their applications. Teschke and his group [8] showed that the plasma jet generated by an RF power supply is a train of plasma bullets/plumes. Laroussi and Lu [30] designed "Plasma Pencil" to generate plasma jet for bio application. This plasma pencil, designed with a dielectric barrier double electrode configuration, generates a plasma jet 5-8 cm long in the ambient atmosphere by using pulsed DC power supply. Lu and Laroussi [31] showed that the plasma jet is, in fact, a train of plasma bullets travelling at supersonic velocities (Fig. I.2a). They used an ICCD camera to take images of the plasma jet in the nanosecond range and traced the spatial and temporal evolution of the plasma jet. They measured the plasma bullet velocity as shown in Fig. I.2b. The plasma bullet propagates with extremely high velocity (order of 10^5 m/sec). Lu and Laroussi found that the discharge current waveform of the plasma pencil is different from the regular DBD's discharge current waveform. The discharge current waveform shown in Fig. I.3 illustrates that there are two positive current peaks (identified as 1 and 2). In a regular DBD, only one positive current peak is observed. The correlation between the discharge current waveform and the ICCD image of the discharge chamber shows that the second positive current peak in the discharge current waveform corresponds to the formation of the plasma jet [31]. It has been shown that the plasma jet comes out through the outlet of the plasma pencil when the second positive discharge current starts to increase. These unusual properties of the plasma jet led to investigations aimed at elucidating the formation and propagation process of the plasma jet.

This hypersonic velocity of the plasma jet is compared with the progression process of the cathode directed streamer propagation [31]. This streamer model, developed by Dawson and Win [32], explains the propagation of the cathode-directed streamers in a low external electric field. The streamer is a strong primary avalanche which amplifies the external electric field and leads to the formation of a weakly ionized plasma channel behind it. The streamer theory was developed by Raether, Loeb and Meek & Craggs. In the positive streamer, high energy photons emitted from the excited

molecules and atoms at the avalanches provides photoionization in front of the discharge to initiate second avalanches. The electrons in the secondary avalanches travel backwards, and create a plasma channel. Shi et al [33] invoked an ionization wave model to explain the plasma bullet propagation. In the ionization wave model a plasma bullet is assumed to be produced by an ionization wave front. It is predicted that the high velocity of the plasma front is due to the ponderomotive force [34], electron diffusion, and breakdown wave [35] in the gas channel. In the ionization wave propagation model, the gas breakdown mechanism is the same as the streamer breakdown mechanism.

The plasma jet propagates in the ambient atmosphere and the feed gas mixes with air along the jet axis. The gas temperature in the plasma jet measured from nitrogen emission band is around room temperature. The investigation of the plasma jet properties for different operating conditions is important to have a better control on plasma jet applications. To understand the plasma jet propagation, this dissertation deals with the experimental investigation of jet's plasma properties and ionization mechanisms along the feed gas flow axis. Four fundamental issues will be discussed in this work: i) physical properties of the plasma jet, ii) formation of the plasma jet from the discharge chamber, iii) plasma jet velocity and its contraction, and iv) jet current density and the electron density along the jet axis, which gives the information about the ionization mechanism.
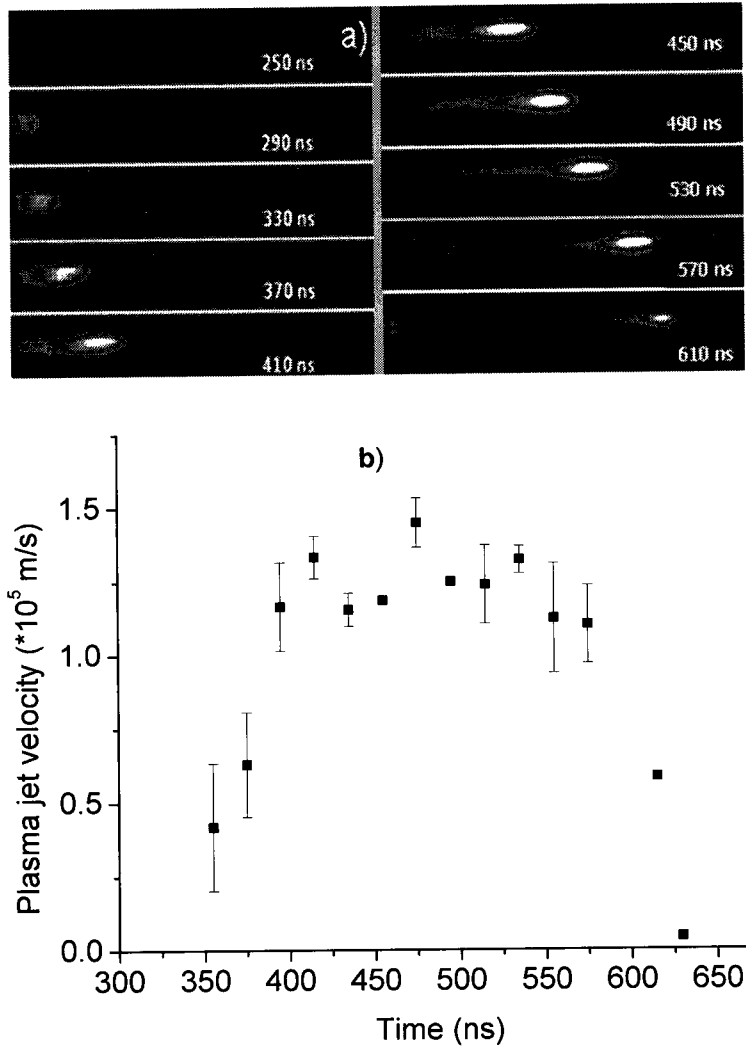
FIG. I.2. Plasma jet velocity: a) ICCD image of the plasma jet for 40 ns delay, which indicates the position of the plasma jet and the required time for the plasma jet to reach that position, and b) plasma jet velocity measured from ICCD images of the plasma jet.
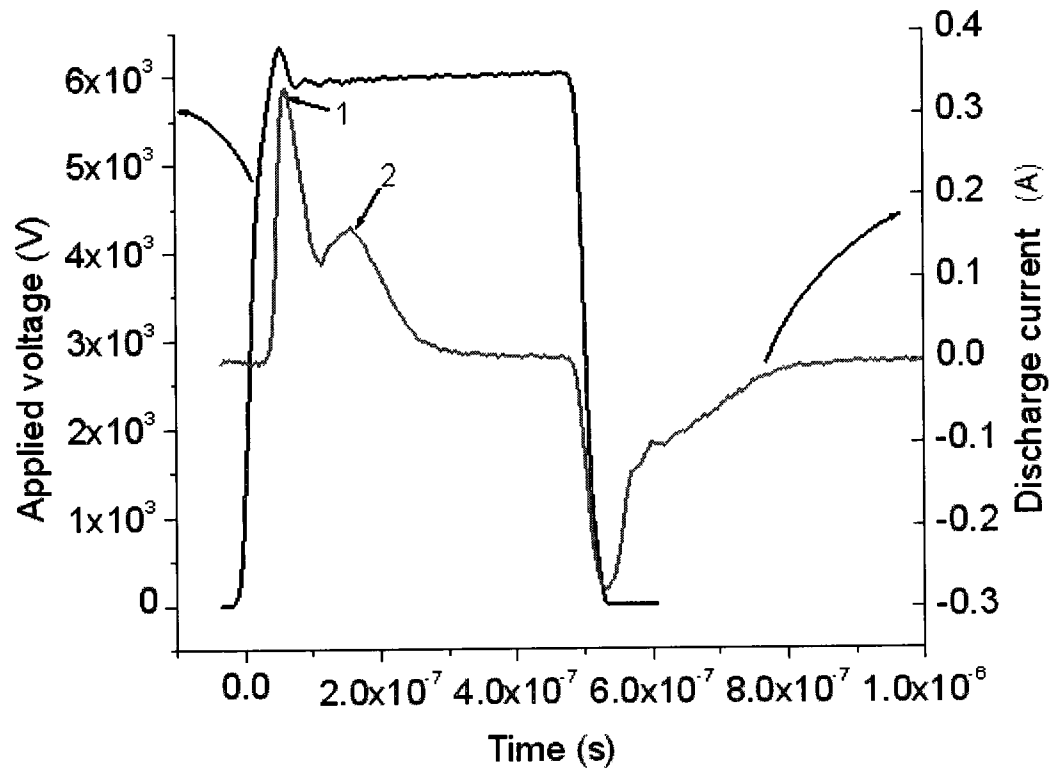
FIG. I.3. Discharge current and applied voltage waveform of the plasma pencil: discharge current has two positive current peaks and a negative current peak and the applied voltage waveform for the pulse duration of 550 ns.

I.3. OVERVIEW AND SCOPE OF THE DISSERTATION

This dissertation addresses the foregoing issues step by step. Chapter II discuss about the experimental detail, which is important to conduct the experiment for plasma jet investigation. A double dielectric barrier configured plasma pencil was used to generate a plasma jet. In this chapter, the geometry of the plasma pencil and the operating conditions of the plasma pencil are described in detail. It presents all the details about the measurement tools and their operation in the experiment to get the expected results.

Before investigating the formation and propagation of the plasma jet/bullet, the fundamental properties of the plasma jet need to be identified. Chapter III presents the physical properties of the plasma jet. Importance of the feed gas flow, operating input voltage, and pulse width on the plasma jet have been investigated to understand the physical properties such as shape, size, and temperature of the plasma jet. The effect of input power on the temperature of the plasma jet for different feed gas flow rates are investigated in Section III.3.3. The chemical property of the jet plasma is also observed in this chapter from the emission spectrum of the plasma jet.

Chapter IV is dedicated to the investigation of the plasma jet formation. Electrical and imaging techniques are used to investigate the plasma jet formation phenomenon. The plasma pencil is configured as a dielectric barrier discharge and the plasma jet form from the discharge chamber of the plasma pencil; for this reason the discharge inside the device (between the electrodes) was studied to understand the formation of the plasma jet. The average input power to the discharge, electron density, and the dissipated energy to the discharge were investigated. The energy loss and the critical charge required to generate a plasma jet are studied in Chapter IV.

In Chapter V, the propagation of the plasma jet was studied from the velocity curve of the plasma bullet. From the images of the plasma jet and the spatially resolved jet current, the plasma bullet velocity is measured for different applied voltages, pulse widths, and feed gas flow rates. The average plasma bullet velocity is correlated with the pulse width and the length of the plasma jet. The contraction of the plasma bullet along its propagation axis is observed and is explained by calculating the electric field due to the charge in the plasma bullet. The average power density, reduced electric field, and the

electron density in the plasma bullet along the jet axis are estimated from the jet current along the jet axis.

The spatial evolution of the different excited species in the plasma jet gives the idea of the evolution of the plasma bullet's chemistry along the jet axis. In Chapter VI, the spatial evolution of the different excited species is observed from the change of the emission intensity from the different excited species in the plasma bullet for different applied voltages, pulse widths, and feed gas flow rates.

The effect of the dielectric barrier on the plasma jet formation and propagation are included in Appendix A. In this appendix, the formation and the propagation of three different plasma jets, with a dielectric barrier and no dielectric barrier is observed. The observations are compared with each other to understand the effect of dielectric barrier on the formation of the plasma bullet.

The calculation of the linear capacitance of the plasma jet and the electric field in the space due to a charged ring are presented in Appendix B. The electric field measurement by using a dielectric probe is a direct contact method. For this reason, the reduced electric field and the electron density along the jet axis are calculated from the emission intensity ratio of the first negative system and the second positive system of nitrogen. The reduced EF and electron density calculated from the intensity ratio of the emission lines is presented here. As the electron mobility changes with reduced EF and the gas composite, the electron mobility for different amount of He/Air mixture and different reduced EF is presented in Appendix B.

Finally in Chapter VII, the conclusion about this research is presented. In this chapter, the findings from this work and the future work plans are discussed.

CHAPTER II

EXPERIMENT

II.1. EXPERIMENTAL SET-UP

An experimental set-up was built to study the hypersonic flow of the plasma jet/bullet in the ambient atmosphere. The plasma jet in the ambient atmosphere itself provided some advantages to the researcher for experimental investigations. The most important advantage in this experimental investigation is that the experimental set-up does not require any chamber. It is a small scale table top experimental set-up. It is so sensitive to the environmental conditions like temperature and humidity of the atmosphere that the reproduction of an exactly similar result at different times and places for the same operating conditions is hard. The results of the similar experiments conducted at different times and places may give slightly different values, but the shape of the curve is always the same. The plasma pencil, which was used to generate the plasma jet, is small in dimension. This device consists of two parallel ring electrodes attached to two dielectric (alumina) disks, placed 0.5 cm apart in a dielectric cylinder. The diameter of the alumina disk is 3 cm. To allow a feed gas flow through the chamber, 0.3 cm diameter hole is perforated on the dielectric disk. The schematic of the plasma pencil is shown in Fig. II.1. One of the ring electrodes is connected to the high voltage, and the second electrode is kept grounded. The whole system is placed in an ambient atmosphere. The feed gas flows from the high voltage end to the grounded dielectric and comes out in the ambient air through the outlet on the grounded dielectric.
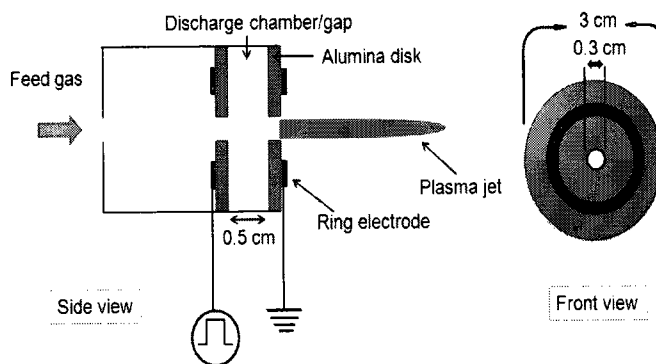
FIG. II.1. Schematic of the plasma pencil.

Pure helium gas is feed into the plasma pencil through the inlet, which mixes with air in the discharge chamber and comes out through the outlet of the plasma pencil. This creates a helium gas channel in the atmosphere air. The pressure inside and outside of the plasma pencil is in atmospheric pressure. A Bronkhorst digital mass flow meter is used to control the feed gas flow rate. This regulator allows the gas flow within 1-20 l/min. For this experimental condition the feed gas flow rate is maintained within 1.15-10 l/min. The schematic of the experimental set-up is shown in Fig. II.2.
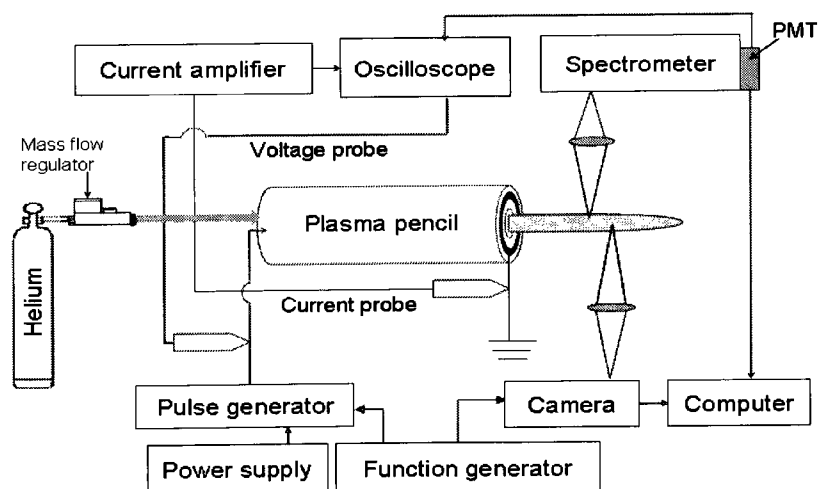
FIG. II.2. Schematic of the experimental setup.

II.1.1. Power Supply

A Spellman SL 1200 high voltage power supply from which, one can get the available maximum output voltage of 10 kV, is used to give the power supply to the DFI PVX-4110 pulse generator. This pulse generator support maximum 10 kV input voltage. The maximum output voltage pulse is 10 kV. Tektronix AFG 3000 function generator has 12 standard waveforms and arbitrary waveform capability. The square wave voltage pulse of 200-2000 ns pulse width is generated to operate the plasma pencil. The rise and fall time of the pulse is 20 ns. The output of the function generator is connected to the gate of the pulse generator. The separation between the electrodes in the plasma pencil is only 0.5 cm, so for very high operating applied voltage there is arcing inside the discharge chamber, which is unexpected for the jet applications. The maximum amplitude of the applied voltage used in these experiments is 8 kV.

II.1.2. ICCD Camera

A Di-cam Pro ICCD camera was used to take the image of the plasma jet. This camera can capture the image of an object, which is moving with hypersonic velocity. It was used to take the image of the plasma jet to observe the temporal and spatial evolution of the plasma bullet. The minimum exposure time and the delay time, which one user can set to the camera, are 10 ns and 3 ns, respectively; moreover the camera has a system delay of 85 ns. By connecting the trigger input of the camera with the function generator, the camera can be triggered with the input pulse. In this way, the camera is synchronized with the applied voltage pulse. As this camera takes the image of the moving plasma jet at the time, which is set in the camera, the temporal evolution of the plasma is observed from the images of the plasma jet. The ICCD image of a measuring scale, which is set along the jet axis from the outlet of the plasma pencil, is taken to find the position of the plasma bullet along the jet axis. By comparing the image of the scale with the image of the plasma jet, the position of the plasma jet front and the required time for the plasma jet to reach that position can be found. The total time to take an image by the camera is equal to the sum of the given time delay, exposure time, and the system delay. Maintaining a fixed delay, by increasing the exposure time one can take the image of the whole plasma

jet. As the plasma bullet is not bright enough, the minimum exposure time does not give a bright image of the plasma jet. If one wants to get a bright image of the plasma jet, he/she need to increases the exposure time, but this will change the total time. So, one would not get the image of the plasma bullet at an expected time/position. By increasing the number of loops for a fixed delay and exposure time, one can increase the number of the same image, which will be overlapped. In this way one can increase the intensity of the image without increasing the exposure time.

II.1.3. Flow Measurement

As diameter of the feed gas channel is very small, an Alnor micro manometer (pitote) is used to measure the gas flow velocity. It measures the pressure and calculates the velocity and the volumetric flow rate of the feed gas for a user input duct size and shape. This pitote is placed in the feed gas channel to measure the gas velocity. The measurements of the feed gas velocity by using this pitote have an error of 15%. The measurement error is high at the end of the gas channel, because the feed gas is highly diffused at the end of the gas channel, and its diameter is also too small for accurate feed gas velocity measurement by using this pitote.

II.1.3. Electrical Investigation

To investigate the electrical characteristics of the plasma jet generated by the plasma pencil, a Tektronix TDS784D oscilloscope, a Tektronix TM502A current amplifier and current probe, and a Tektronix P6015A high voltage probe were used. All the electric measurements are taken with an average of 500 acquisitions. As the applied voltage to the plasma pencil is in the kilovolt range, a high voltage probe is required to measure the voltage. The current is measured both across the high voltage electrode and the grounded electrode of the plasma pencil. The outlet of the plasma pencil is at the grounded dielectric so the characteristic of the current waveform at the grounded electrode of the plasma pencil is important to understand the plasma jet formation. For this reason, the current of the plasma pencil is measured at the grounded electrode.

There are many diagnostic techniques to characterize the plasma. One of the most used plasma diagnostic tools is Langmuir probe. With a Langmuir probe, a small conducting material is inserted into the discharge and biased negatively and positively to collect the current. This probe is not applicable in the atmospheric pressure plasma. It entirely changes the shape and the chemistry in the small sized plasma jet. It is also hard to place close to the outlet ($z < 1.5$ cm) of the plasma pencil, because of the possibility of arcing. If there is not well-defined ground electrode, double probes are usually used in a plasma diagnostic. A bias voltage is usually applied between two probes. When a probe is placed close to the plasma jet in the radial position, a fine line of plasma is created between the plasma jet and the probe, and when the probe is placed into the plasma jet all plasma is concentrated at a point on the probe. It requires a very high positive bias voltage to get the saturation current, which will give the electron density. The high bias voltage totally changes the properties of the train of plasma bullets, and affects the plasma inside the chamber.

Figure II.3a shows the position of the plasma jet front with time when there is a conducting plate/no conducting plate in front of the plasma jet. The metal plate is placed on three different positions on the plasma jet's propagation pathway. It shows that the plasma jet front accelerates when it is close to the metal plate. The distorted images of the plasma jet front in the presence of the metal plate at 4.5 cm and 5 cm on the jet axis are shown in Fig. II.3b. It shows that the jet front is elongated along the axis when it is close to the metal plate. This elongated plasma front is identified as the perturbed jet front. The metal plate on the jet axis plays as a ground electrode and when the plasma jet comes close to the plate, the potential difference between the plate and the plasma jet accelerates the ions in the plasma and the jet becomes distorted. This acceleration of the different species especially electron enhance the plasma chemistry. At a high applied voltage, another discharge is created on the plate when the plasma bullet is close to the metal plate.
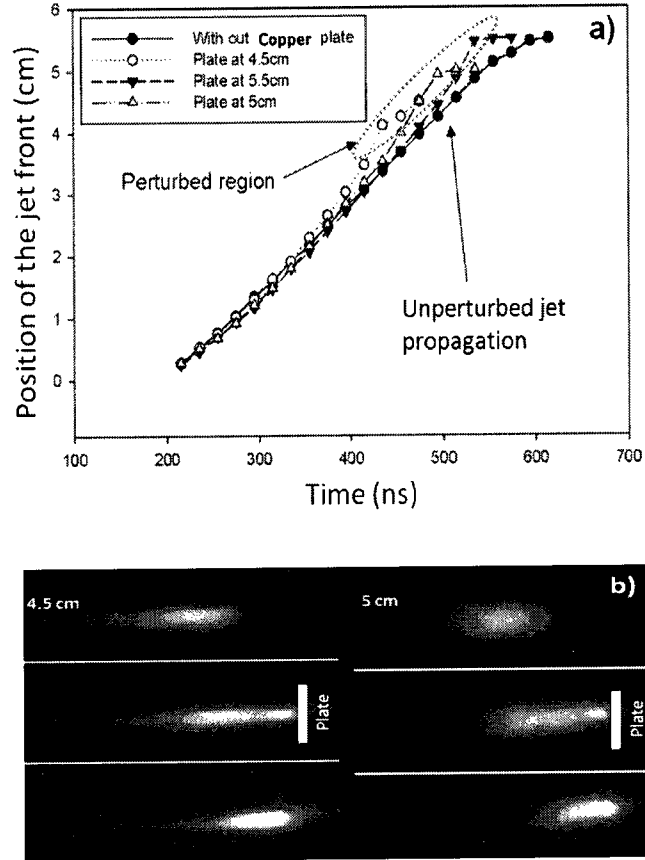
FIG. II.3. Perturbation of the plasma jet close to the conducting plate: a) position of the plasma jet front (with/without metal plate) with time, b) image of the perturbed plasma jet front.

For the characterization of the plasma jet, a lab-made probe was used to measure the jet current. This probe is made of a small copper plate covered by a dielectric sheet. The schematic of this dielectric probe is shown in Fig. II.4. The advantage of this probe is that it can be placed close to the outlet of the plasma pencil. There is no possibility of arcing. The image of the plasma bullet is taken at the probe-plasma interaction point. The plasma chemistry and the shape of the plasma bullet at the surface of the probe do not show a significant change. The plasma has the tendency of spreading over the dielectric surface. Considering this property of the plasma, the probe area is kept as small as possible so the plasma jet front after reaching the probe surface does not have enough space to spread over. In this way the enhancement of the plasma chemistry on the probe surface is controlled. The dielectric probe is connected to the ground through a 1 kilo ohm resistor, and it is placed at different positions along the jet axis. As the plasma jet touches the probe, the whole system (plasma, probe, and resistor) builds a RC circuit. The time constant (RC) of the circuit is very small compared to the time duration of the voltage pulse, so the circuit works as a differentiator, and the peak current measured across the resistor is the total current of the plasma jet. A known current is applied to the probe surface and the current passed through the wire is measured to observe the response of the probe. All the measurements taken by using this probe are with a zero biased potential. In this measurement large electron flux and a small ion flux, both are collected in the same time. As there is no external EF and the plasma bullet is an isolated plasma volume per pulse, the plasma bullet and the dielectric probe maintain a potential difference, which accelerates the electron first and then the ions. So the first peak current in the jet current waveform is due to the electron current.
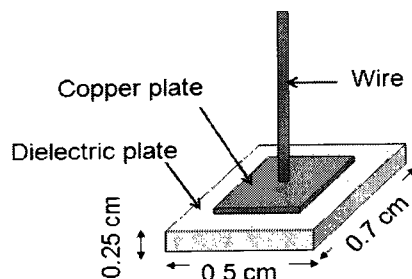
FIG. II.4. Schematic of the dielectric probe.

II.1.4. Optical Investigation

As the emission spectroscopy is a non-intrusive method for plasma diagnostics, the emission spectrum of the plasma jet is taken by using Spectra pro-500i spectrometer. It includes two 1,200 groves per millimeter grating. Its scan range is 0-1400 nm with the minimum step of 0.0025 nm. The spectrometer had a focal length of 500 mm. The exit slit of the spectrometer is connected to a photomultiplier. The output of the photomultiplier is connected to the computer to collect the emission spectrum. To get the temporal evolution of any specific line, the wavelength of the line is set as the operation wavelength, and the out put of the photomultiplier is connected to an oscilloscope. The wavelength of the spectrometer is calibrated by Hg-lamp but the intensity is not calibrated. To understand the spatial and temporal evolution of the different plasma species and to calculate the local reduced electric field of the plasma jet, the intensities of different emission bands need to be obtained. All the acquisitions are taken at every 0.3 cm of the jet axis with 0.004 nm step and 100 ms integration time. A lens is focused at the mid point of the plasma jet cross section to collect the light from the plasma jet. In this way, it is possible to acquire data from a small volume of plasma. Figure II.5 shows the schematic of the experimental set-up to acquire the emission line from the plasma jet.
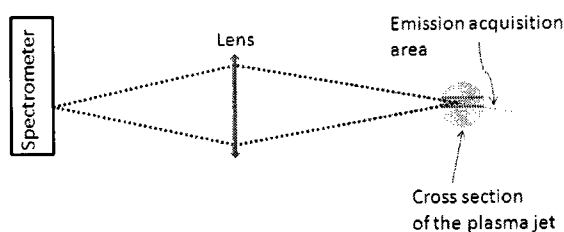
FIG. II.5. Schematic of the acquisition of the emission from the cross-section area of the plasma jet.

CHAPTER III

BASIC CHARACTERISTICS OF PLASMA JET

III.1. INTRODUCTION

The plasma jet investigation shows that the feed gas flow rate plays an important role on the plasma jet's size, shape and chemistry [36- 38]. In describing fluid flow, the velocity of the fluid is of first importance. The feed gas velocity in ambient atmosphere gradually decreases along the stream line and finally it fully defuses into the atmospheric air. The length of the feed gas channel depends on the gas flow rate. Depending on the application, one likes to operate the gas jet in a laminar flow or in a turbulent flow. Osborne Reynolds studied these states of flow and he found that when the flow velocity is low, the flow has a straight single line – called a laminar flow. When the increasing flow velocity reaches a certain critical value it is called the turbulent flow. A turbulent flow leads to a rapid mixing of the gas jet with surrounding atmosphere. A stable gas flow is important to improve the controllability of the plasma jet in material processing or in bio-medicine [39, 16]. In the present work stable helium laminar jets were generated under different operating conditions. The importance of the Gas Flow Rate (GFR) on the size, shape, and the temperature of the plasma jet were investigated. The effect of the magnitude of the applied voltage and pulse width on the length and shape of the jet have been studied by using imaging technique. The emission spectrum of the plasma jet provides an insight into the chemistry of the plasma jet.

III.2. EXPERIMENTAL SET-UP

The image of the plasma jet was taken by placing an ICCD camera at the tangential position to the jet axis. To take the image of the whole plasma jet the camera was set with the exposure time of 900 ns and delay of 100 ns. The feed gas velocity without discharge was measured by using a pitote. To take this measurement this pitote was placed at different positions on the gas flow channel. The jet temperature measurement by using thermocouple was impossible. The average jet temperature was

measured by using regular Hg-thermometer. The schematic of the experimental set-up is shown in Fig. III.1a and b. The plasma jet normally spreads over dielectric surfaces. This spreading of the plasma increases the temperature of the plume. To prevent the heat energy loss by the surface spreading, an insulator was used around the mercury bulb. The plasma jet was exposed to the mercury bulb for 5-6 minutes (until the temperature reached a stable point) for each measurement.
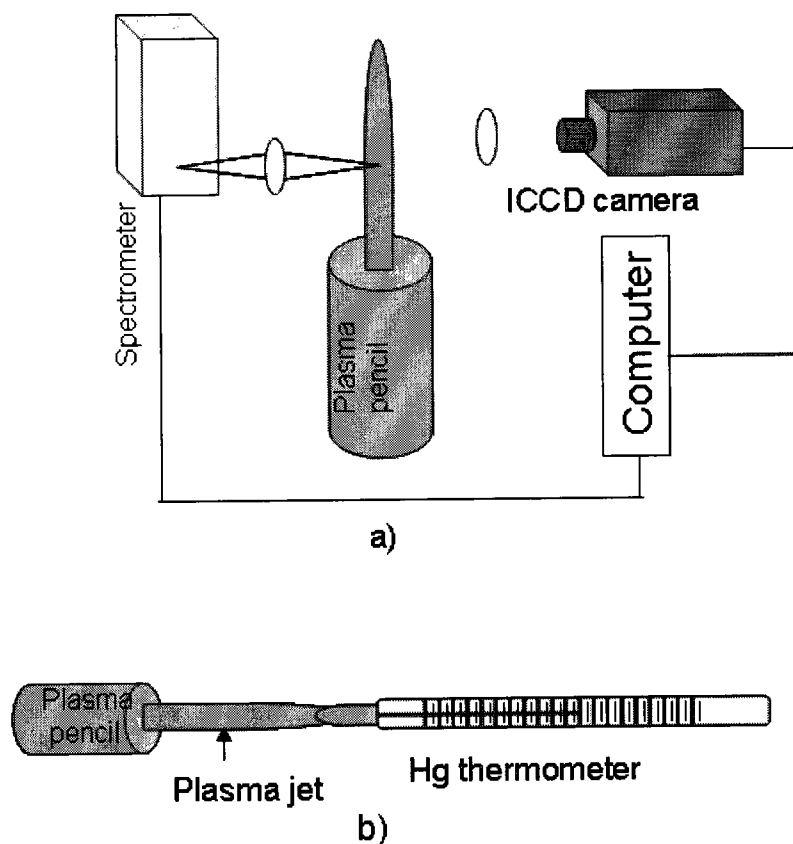
FIG. III.1. Experimental setup: a) emission spectroscopy and imaging of the plasma jet, b) temperature measurement of the plasma jet.

III.3. RESULTS

III.3.1. Effect of Gas Flow Rate on Plasma Jet

The plasma jet always expands along the neutral gas channel. It follows the gas stream line even if the gas flow is unstable. Figure III.2 shows that the plasma is following the feed gas channel even when the flow was diverted by placing a paper barrier on its axis. The gas flow in the atmosphere has three distinct stages: i) laminar flow, ii) turbulent flow, and iii) diffuse gas channel. In the atmosphere, where the volume of the feed gas is very low the gas channel is diffused in the ambient air. As the volume of the flowing gas depends on the cross-sectional area of the jet and the gas velocity, the length of the gas channel can be predicted from the gas flow velocity along the flow axis. The gas velocities along the jet's axis for three different GFRs are shown in Fig. III.3. The flow velocity decreases along the jet axis. For the GFR of 1.42 l/min, the gas velocity is measurable until 3.5 cm of the jet axis, whereas for the GRF of 2.8 l/min the measurable gas velocity is until 6 cm along the jet axis. The gas channel is diffused after 7.5 cm of the axis for the GFR of 5.6 l/min.

FIG. III.2. Importance of feed gas flow channel.
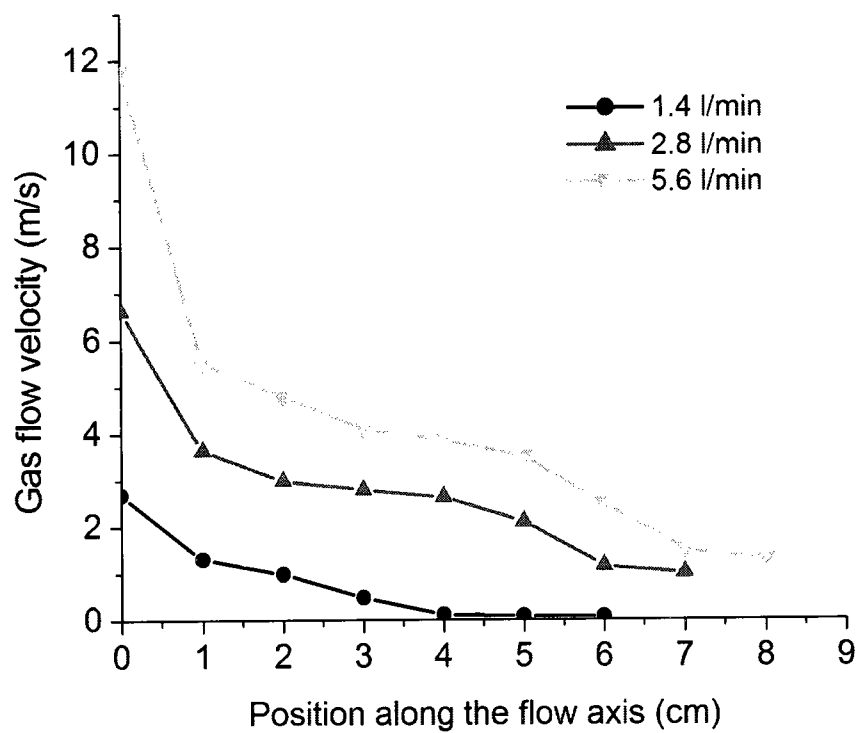
FIG. III.3. Feed gas flow velocity along the flow channel.

The Reynolds number is an important parameter to determine the laminar and the turbulent gas flow regimes [40-42]. Reynolds number of a flowing gas in the ambient atmosphere depends on the gas velocity, the diameter of the gas channel and the viscosity. In this case, the outlet diameter of the plasma pencil is D = 3 mm, gas flow rate is 2.81 l/min. For these conditions, the Reynolds number is calculated from the following equation,

$$R_e = \frac{4Q_{sc}}{\mu(T)\pi D}\frac{MP_0}{RT_0}$$

(Equ. III.1)

where, Q_{sc} = Flow rate (m^3/s)

M = Molar Weight (kg/mol) = 4×10^{-3} kg/mol (for Helium)

P_0 = Pressure = 101325 Pa

D = Diameter of the nozzle = 3×10^{-3} m

R = Ideal gas constant = $8.314*10^3$ Nm/kmol. K

T_0 = 273 K

$\mu(T)$ = Dynamic viscosity.

The dynamic viscosity depends on the gas temperature. The dynamic viscosity is given by,

$$\mu(T) = \mu_0 \frac{T_0 + C}{T + C}\left(\frac{T}{T_0}\right)^{\frac{3}{2}}$$

(Equ. III.2)

where, C = 79.4 is Sutherland's constant, and μ_0 = 19×10^{-6} Pa.s is the dynamic viscosity of helium at the temperature of 273 K. For the gas flow rate of 2.8 l/min, the calculated Reynolds number is 214. The calculated Reynolds numbers for different helium GFRs are shown in Fig. III.4. According to the literature, the critical Reynolds number for helium gas flow in air is 830 [40]. The critical Reynolds number of helium inside a tube is 1760 [43].
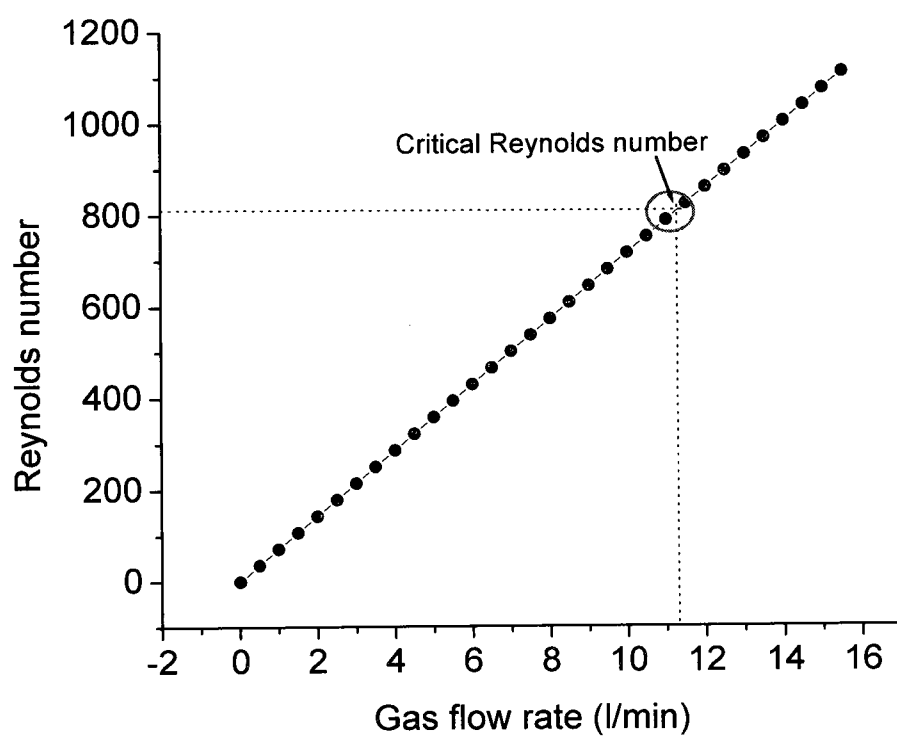
FIG. III.4. Calculated Reynolds number for different gas flow rates.

The helium flow reaches the critical Reynolds number at the GFR of 11.25 l/min. The gas channel diameter increases with flow velocity. The air diffusion in the feed gas channel changes with the velocity and the diameter of the gas channel. The required time scale to diffuse air along the gas channel's radius is $\frac{r^2}{D_{dif}}$. Here, r is the radius of the jet and D_{dif} is the diffusion coefficient. The jet's diameter decreases along the jet's axis; so the required diffusion time scale decreases along the axis. For this reason the amount of diffused air in the gas channel increases along the jet axis.

Fig. III.5 shows the relationship between the gas flow rate and the length of the plasma jet for specific operating conditions: AV = 5 kV, PW = 500 ns and f = 4 kHz. The jet's length increases with the GFR and reaches optimum at the GFR of 3.5 l/min. With further increases of GFR from 3.5 l/min, the length of the plasma jet decreases and the diameter of the plasma jet increases. For the gas flow rate of 1.4 l/min the jet's length is around 2.45 cm, whereas the length of the gas channel is 3 cm, and for the GFR of 2.81 l/min the length of the plasma jet is 3.6 cm, which is short compared to the length of the gas channel. If the energy absorbed by the plasma is not high enough, even in the presence of a gas channel, the plasma jet stops propagating. Therefore, the length of the jet depends on the presence of the feed gas channel and the discharge energy deposited into that channel. The shape of the plasma jet also changes with GFR. Fig. III.6a shows that for a low gas flow rate, the plasma jet is very thin and curved upward. An increased gas flow rate changes its shape, it becomes straight and its diameter increases. The gas jet propagates in straight line as long the neutral channel is not too diffuse. After that more dense air works as an obstacle and the jet propagates upwards. The low mass of helium with less momentum causes it to go upward. A dimensionless parameter, Richardson number [42, 44], can characterize this buoyancy effect of the gas jet. The Richardson number is given by, $R_i = gD(\rho_a - \rho_{jet})/\rho_{jet}V^2$, where D is the diameter of the gas channel, g is the gravitational acceleration, ρ_a is the density of air, and ρ_{jet} is the density of the feed gas. For a very low flow velocity, $R_i > 1$ and the jet is bent. For the GFR of 1.14 l/min and at the position of 2.7 cm along the jet's axis, the feed gas velocity is V = 0.5 m/sec gas and the calculated feed gas density is ρ_{jet} = 0.13 kg/m^3. The calculated Richardson number is R_i = 1.116 and the jet shows a buoyancy effect. Fig. III.6b shows that at the

end of the jet the turbulence occurs at the gas flow rate of 8 l/min while the turbulence of the gas jet at the outlet of the plasma pencil occurs at the gas flow rate of 10 l/min. This result validates the theoretical prediction.
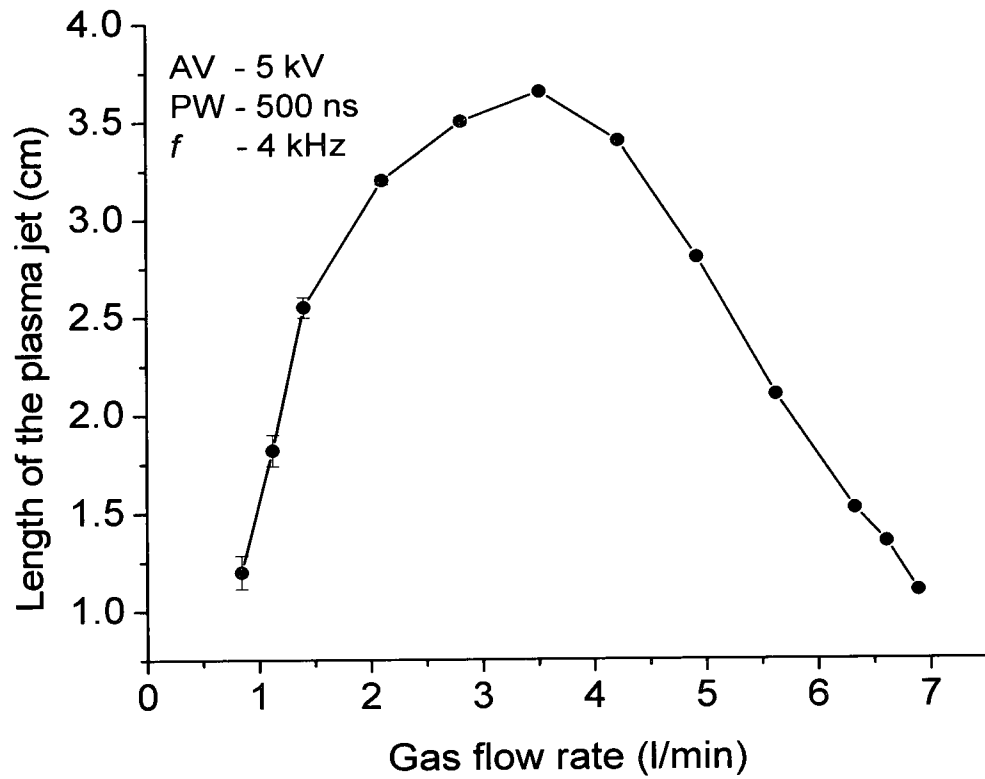
FIG. III.5. Dependence of the length of the plasma jet on the gas flow rate.
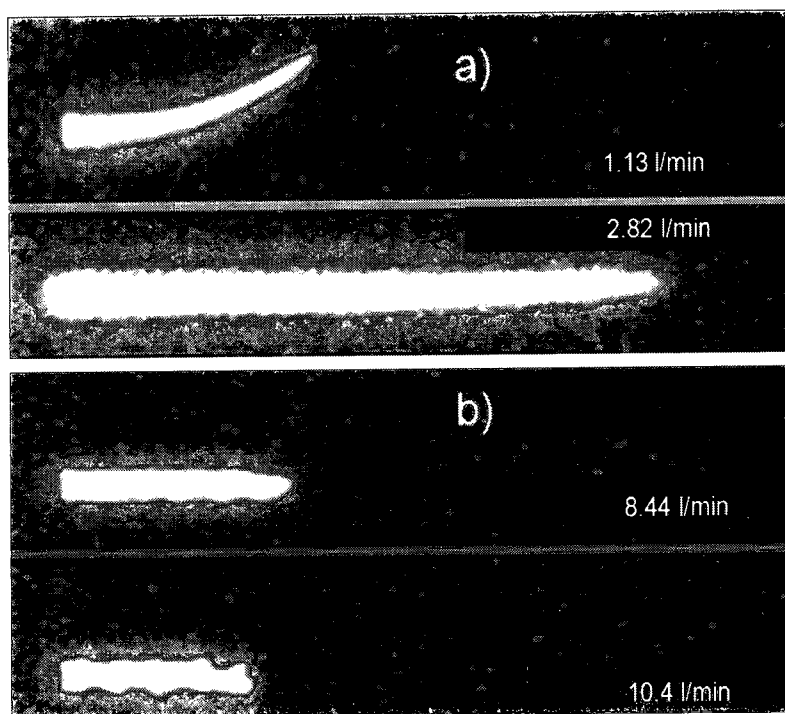
FIG. III.6. a) Shape of the plasma jet for different flow rates, and b) turbulence in the jet.

III.3.2. Effect of Applied Voltage Amplitude and Pulse Width on the Plasma Jet

It was found that the applied voltage amplitude and the width of the discharge sustaining pulse exert strong effects on the characteristics of the plasma jet. Figure III.7 shows the change of the jet length and shape with applied voltage amplitude and pulse width. Figure III.7a shows the change of the length with applied voltage for two different gas flow rates. The length of the plasma jet increases almost linearly with the applied voltage amplitude. Although the jet length increases almost linearly, the rate of the increments is not constant. For the GFR of 2.8 l/min and pulse width of 500 ns the length of the jet reaches to the optimum when the applied voltage is over 6.5 kV. This optimum length is around 5.7 cm. By increasing the GFR; the length of the plasma jet can be increased by operating the plasma pencil in higher applied voltage. At the gas flow rate of 5.5 l/min and applied voltage of 7.5 kV the optimum length of the plasma jet is 7 cm. For the GFR of 2.8 l/min and 5.8 l/min the gas channel is diffused after 6 cm and 7.5 cm, respectively on its propagation axis (Fig. III.3). So, a laminar gas flow is important in the plasma jet propagation. The increased air diffusion in the helium gas channel increases the oxygen and nitrogen percentages and leads to greater volumetric recombination, which ultimately stops the jet propagation. Fig. III.7b shows the change of length of the plasma jet and the bending of the jet's tip with applied voltage for the GFR of 2.8 l/min. The bending at end happens because of the buoyancy force on the gas jet. The length of the plasma jet reaches an optimum value at the applied voltage of 6.5 kV. At the optimum jet's length, increasing the applied voltage elevates the electric field strength at the tip of the plasma jet which creates plasma along the diffuse gas channel, called the branching of the plasma jet.

The length of the plasma jet also increases with the pulse width (Fig. III.8). For the gas flow rate of 2.8 l/min and the applied voltage of 5 kV, the jet length reaches at the optimum for a pulse width above 800 ns. In this case the optimum jet's length is 5.8 cm. It also shows that for the gas flow rate of 2.8 l/min plasma jet can not propagate beyond the distance of 5.8 cm. This is due to the high percentage of air diffusion into the feed gas channel. A higher applied voltage and a longer pulse width translate to higher energy deposition into the plasma, which lead to longer jet under laminar gas flow conditions.
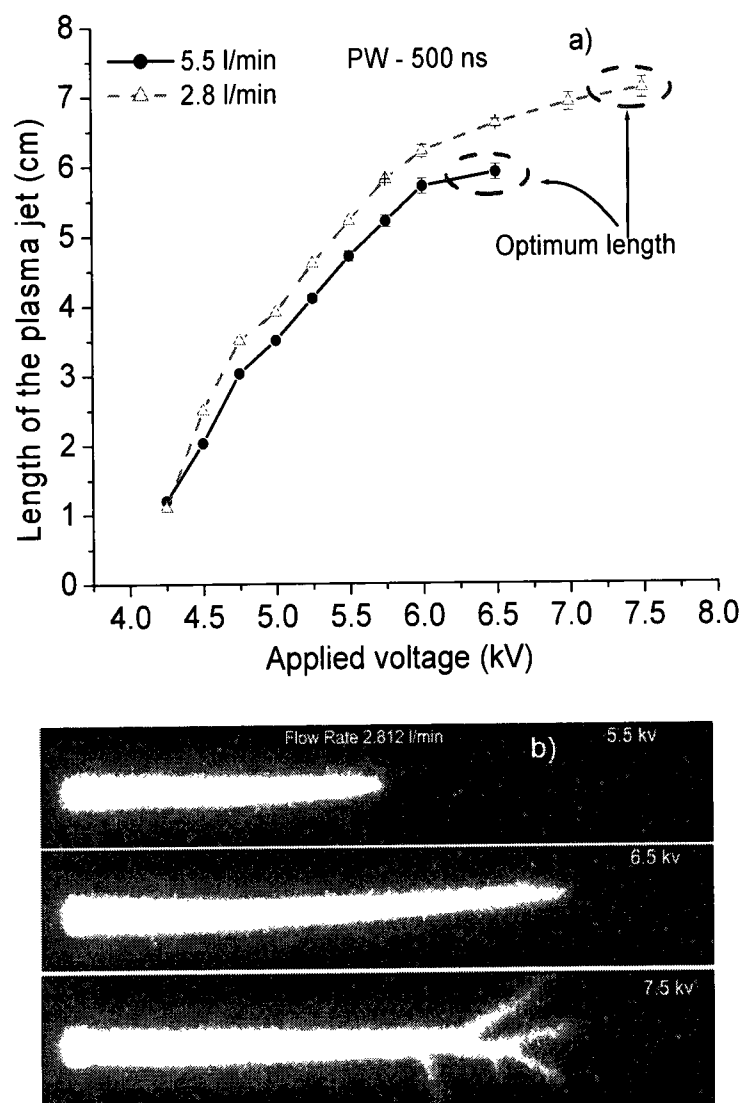
FIG. III.7. Effect of applied voltage on plasma jet: a) length of the plasma jet increases with applied voltage (PW = 500 ns), and b) bending and branching at the end of the plasma jet.
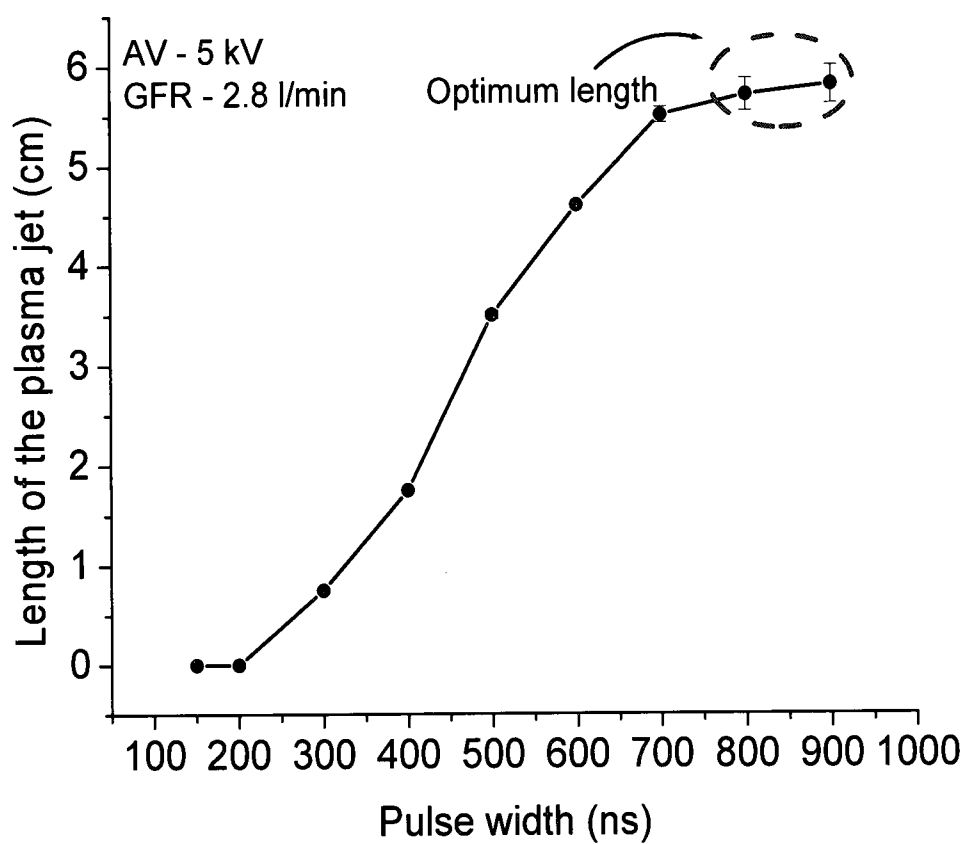
FIG. III.8. Effect of pulse width on the length of plasma jet.

III.3.3. Jet's Temperature Measurement

The temperature of the plasma jet as measured by using mercury thermometer is shown in Fig. III.9. As a result of collision, the energy gained by the electron from the applied voltage is transferred to the gas. The heat transfer from the discharge to the neutral gas is given by, $Nc_{p1}(T - T_0)\upsilon_F$ [41]; where N is the neutral number density, c_{p1} is the specific heat at constant pressure per molecule, T is the temperature of the discharge and T_0 is the temperature of the input gas and υ_F is the required time for the feed gas to travel the discharge zone. From the energy balance equation, $Nc_{p1}(T - T_0)\upsilon_F = jE$, j is the current density and E is the electric field. Higher gas flow rate means higher number of the feed gas mole in the discharge chamber. The maximum power in the discharge for different gas flow rates is shown in Fig. III.10. It shows that for a constant input voltage the maximum power decreases with the GFR. So the plasma jet temperature decreases with the increase of the GFR. If the gas molecules spend less time (gas velocity increases) near the discharge zone it can not accumulate enough energy from the input voltage and the temperature decreases. As the ambipolar diffusion is much higher than the gas flow diffusion, gas flow diffusion plays a minor role in the bulk energy losses. For a constant GFR the temperature of the jet increases with applied voltage (Fig. III.9). This temperature was measured at 2 cm from the initial position along the jet axis. More input energy increases the thermal energy in the discharge and consequently the plasma temperature increases. The rotational temperature of the helium plasma jet measured from the rotational band of the nitrogen also gives the same results [45].
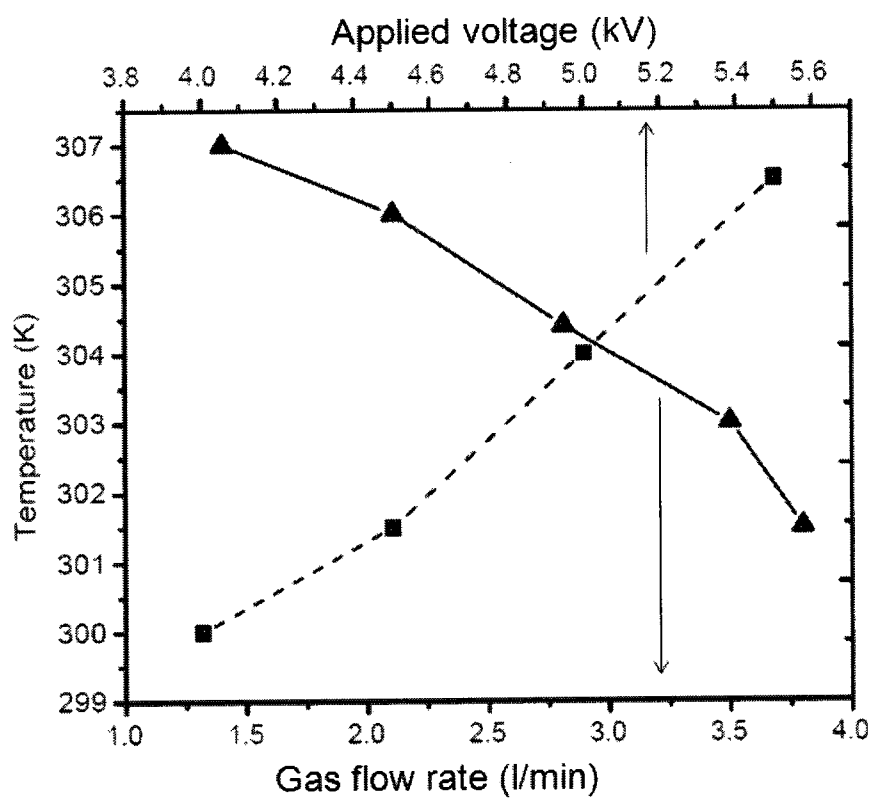
FIG. III.9. Temperature measurement for different flow rates (AV - 5kV, PW - 500ns), and different applied voltages (GFR - 2.812 l/min, PW - 500ns).
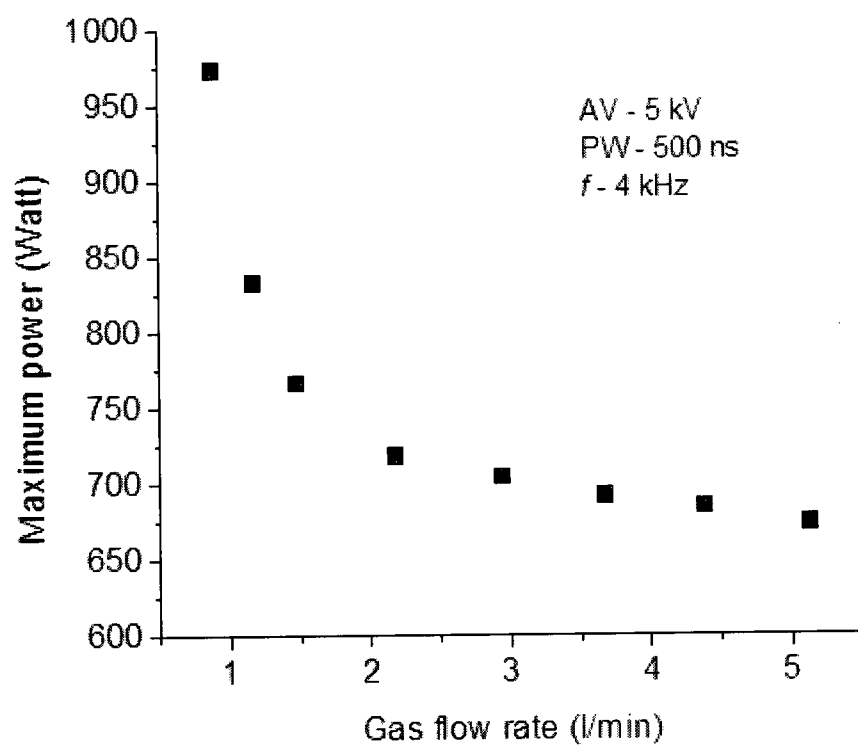
FIG. III.10. Change of the maximum input power in the gas discharge with gas flow rate.

III.3.4. Emission Spectra of the Plasma Jet

Since the plasma jet propagates along a helium channel in the ambient air, oxygen and nitrogen species mix into the flow. The emission spectra of the jet are shown in Fig. III.11. All the emission lines were identified by using National Institute of Standards and Technology (NIST) [46] database. The emission spectra show that the prominent emission peaks are for the excited nitrogen and helium. Atomic oxygen is also present in these spectra, moreover there is atomic oxygen too. The most prominent emission lines are N_2 (337 nm), N_2^+ (391 nm), He (706 nm), O (777 nm) and OH⁻ (309 nm).
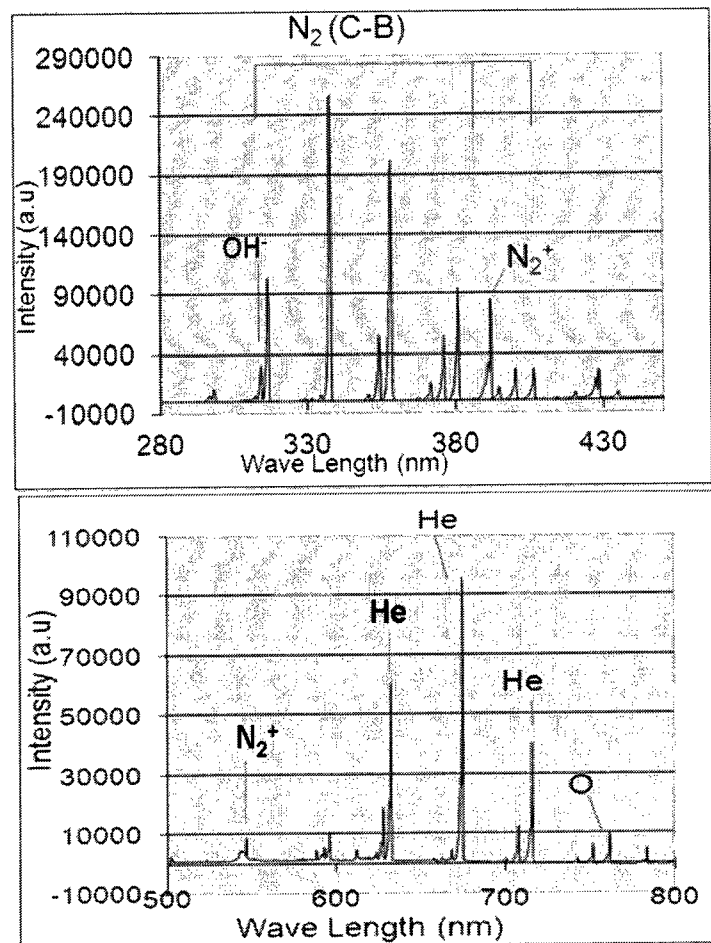
FIG. III.11. Emission spectra of plasma jet.

The emission line at 309 nm is found generally when water vapor is present in the gas mixture. In open air, there is some water vapor and through dissociation of water molecules OH⁻ radicals were formed. The emission line at 309 nm is that of the excited hydroxil radical. The emission line at 337 nm is from the transition of excited nitrogen, from the C to the B state.

$$N_2 \ (C^3\Pi_u, \ v_c=0) \rightarrow N_2 \ (B^3\Pi_g, \ v_b=0) + 337 \ nm$$
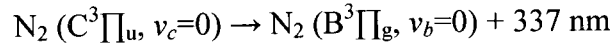
The emission at 328 nm is from the band head of the 0-3 transition and the emission of 394.5 nm is from the band head of the 2-5 transition. The excitation energy of ground state nitrogen to $N_2 \ (C^3\Pi_u, \ v_c=0)$ is 11.03 eV. This excitation can happen due to energetic electrons or metastable helium collisions with neutral nitrogen. The emission line at 391 nm is ascribed to the transition of nitrogen ion from the B state to the ground state.

$$N_2^+ \ (B^2\Sigma_u^+, \ v_b=0) \rightarrow N_2 \ (X^2\Sigma_g^+, \ v_x=0) \ + 391 \ nm$$
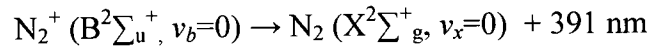
The generation of $N_2^+ \ (B^2\Sigma_u^+, \ v_b=0)$ can happen in two different ways; i) direct electron collision and ii) penning ionization. The ionization energy of nitrogen is less than the excitation energy of helium metastable (2^3S). So the main generation process of N_2^+ $(B^2\Sigma_u^+, \ v_b=0)$ is due to the direct collision of high energy electron with the neutral nitrogen. On the other hand, because of the long lived metastable helium the penning ionization creates $N_2^+ \ (B^2\Sigma_u^+, \ v_b=0)$. The state $N_2^+ \ (B^2\Sigma_u^+, \ v_b=0)$ can be populated by:

$$N_2 + e \rightarrow N_2^+ \ (B^2\Sigma_u^+, \ v_b=0) \ + 2e \ , \quad E_e = 18.7 \ eV$$

$$He \ (2^3S) + He+N_2 \rightarrow 2He + N_2^+ \ (B^2\Sigma_u^+, \ v_b=0)+e$$
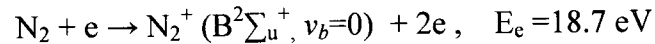
In the emission spectrum, the prominent helium emission lines are at 706 nm and 648 nm. The 706 nm line is produced by the following reactions [47]:

$$He + e \rightarrow He \ (3^3S) + e, \qquad\qquad E_e = 22.72 \ eV$$

$$He^* + 2 \ He \rightarrow He_2^* + He$$

$$He_2^* +e \rightarrow He^+_2 + 2e$$

$$He^+ + 2 \ He \rightarrow \ He^+_2 + He$$

$$He^+_2 + e \rightarrow He_2 \rightarrow He \ (3^3S) + He$$

$$He \ (3^3S) \rightarrow He \ (2^3P_0) + hv \qquad\qquad \lambda = 706 \ nm$$
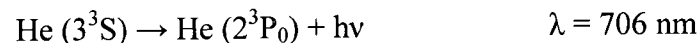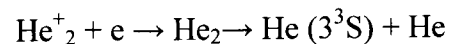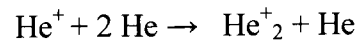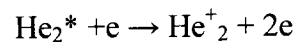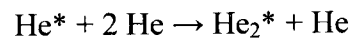
The spectral line at 777 nm is from the transition of excited atomic oxygen. The generation of atomic oxygen is due to the high energy electron collision with molecular oxygen. It can also be generated through penning reaction because of the metastable helium.

III.4. SUMMARY

The fundamental properties of the plasma jet are discussed in this chapter. It shows that the plasma jet always follows the feed gas stream line. The length and shape of the plasma jet strongly depend on the GFR, applied voltage amplitude, and its pulse width. At the optimum length of the plasma jet, high input energy in a diffuse gas channel splits the head of the plasma jet into branches. The bending of the plasma jet is due to bouncy force on the gas channel. Turbulence in the gas channel happens at the GFR of 10 l/min and leads to an unstable jet. Two parameters can stop further propagation of the plasma jet; i) low feed gas mole fraction, and ii) low input energy. For this reason, for a constant operating condition, a plasma jet has an optimum length. The maximum power consumed by the plasma decreases with GFR, so the temperature of the plasma jet decreases. The plasma jet temperature increases with applied voltage. The emission spectrum of the plasma jet is dominated by the emission lines from excited nitrogen and helium.

CHAPTER IV

FORMATION OF PLASMA BULLET

IV.1. INTRODUCTION

Generally plasma bullets are generated from a Dielectric Barrier Discharge (DBD) configured plasma pencil, single electrode plasma jet, plasma needle, and pin electrode plasma jet in an ambient atmosphere. To get a general idea about the formation and propagation of the plasma bullet, experimental investigations of the plasma jet generated by four different plasma jets were conducted, which are shown in Appendix A. It was found that the dielectric barrier has a great influence in the plasma bullet formation, propagation, and its chemistry. It is shown that the discharge always takes place in all directions from the high voltage electrode, but if there is any dielectric nearby, it expands towards the closest dielectric and the discharge grows along the dielectric surface. The plasma pencil is a dielectric barrier configured jet reactor and the plasma bullets form from the discharge chamber of the device. To understand the formation of the plasma bullet, the plasma inside the discharge chamber needs to be studied. The gap discharge of the plasma pencil is investigated in this chapter to understand the formation of plasma plume/bullet. This chapter is comprised of three parts: i) observation of plasma bullet formation, ii) plasma bullet formation time; and iii) plasma bullet formation criteria. Electrical, optical, and imaging techniques were used to carry out the investigations of the formation of plasma bullet at the outlet of the plasma pencil.

IV.2. EXPERIMENTAL SET-UP

To understand the formation and expansion process of the plasma bullet from the discharge chamber, the plasma pencil, made of a plexi glass half-cylinder, was used to take the side view image of the discharge chamber and the outlet by using ICCD (Fig. IV.1a) camera with the exposure time of 10 ns - 20 ns and 20 ns delay. To make this transparent half-cylinder plasma pencil, two semi-circular disks made of plexi glass

attached with two semi-circular ring electrodes were placed 5 mm apart in a hollow half-cylinder. The schematic of this plasma pencil is shown in Fig. IV.1a. The front view of the plasma bullet was taken by setting the ICCD camera at the head-on view of the plasma pencil as shown in Fig. IV.1b. The front view image of the plasma bullet at the outlet of the plasma pencil was taken. The electrical investigation of the discharge chamber was done by analyzing the discharge current and gap potential of the plasma pencil. Unipolar square-wave voltage pulses were applied to one of the electrodes while the other electrode was grounded through a resistor "R". The repetition frequency (f) of the voltage pulse was 4 kHz. The total current of the plasma pencil was measured across the resistor (Fig. IV.2) when the plasma is on. The discharge current of the plasma pencil was measured by subtracting the capacitive current (current measured when there is no discharge) from the total current. The Applied Voltage (AV) was measured at the high voltage end of the plasma pencil by using a high voltage probe. The potential across the gap determines the plasma characteristics inside the chamber. The gap potential of the discharge chamber was measured to calculate the dissipated energy per pulse to the feed gas inside the chamber.
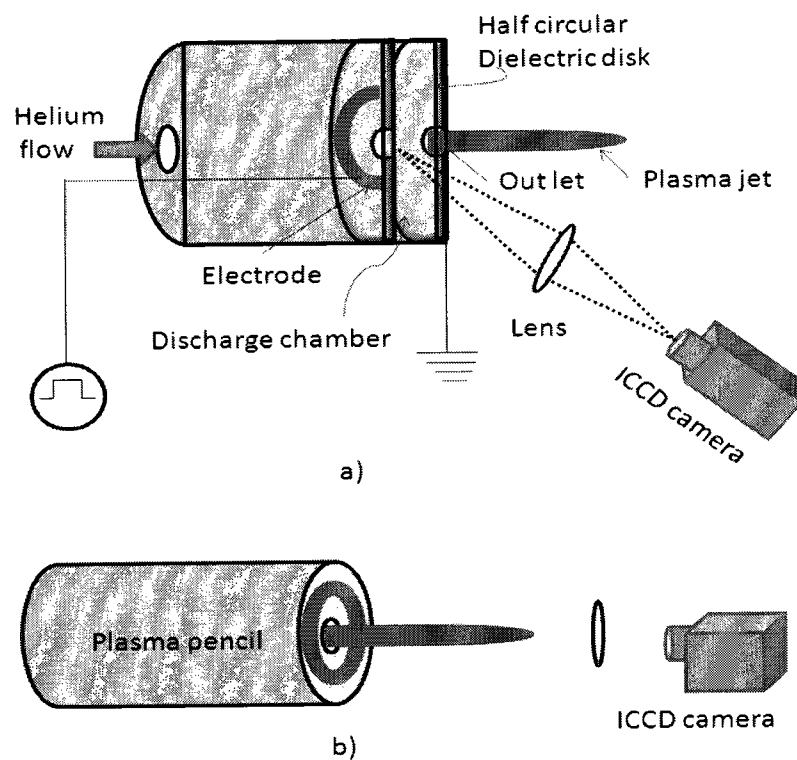
FIG. IV.1. Observation of plasma bullet formation: a) experimental setup for side view of the discharge chamber, and b) experimental setup for head-on view of the plasma pencil.
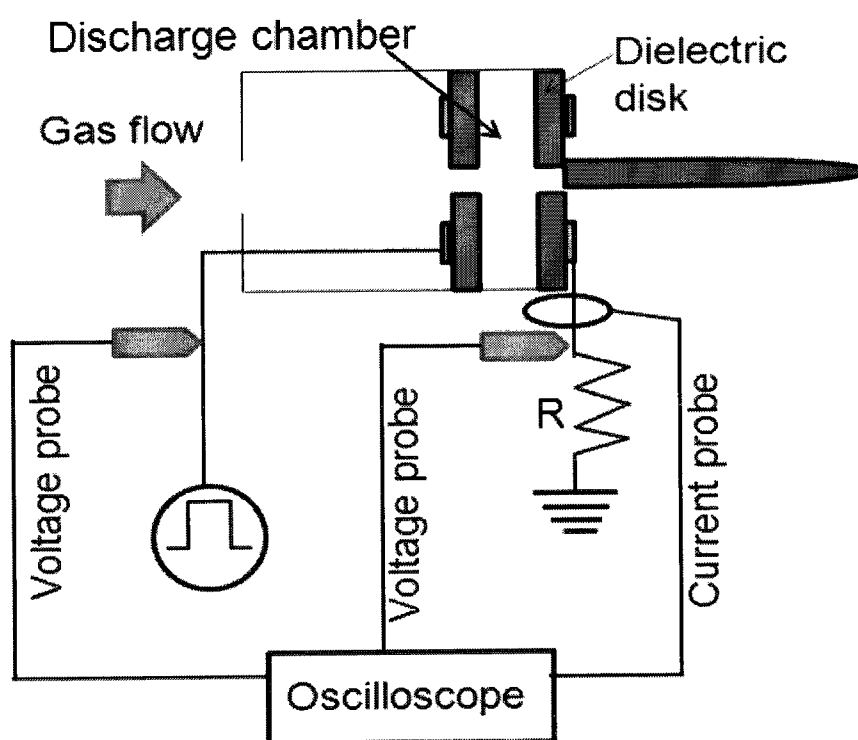
FIG. IV.2. Experimental setup for the electric measurement of discharge chamber.

IV.3. RESULTS

IV.3.1. Observation of the Plasma Bullet Formation

The side view image of the half-cylinder plasma pencil is shown in Fig. IV.3a. It shows that the discharge starts at the high voltage electrode (anode) and expands along the gas gap. The ionized gas creates an ion channel from the high voltage electrode to the grounded dielectric. Afterwards, the discharge inside the chamber decreases and a comparatively more intense discharge is observed at the surface of the grounded dielectric. This surface discharge propagates along the outlet surface and comes out in the ambient air. Figure IV.3a shows that the plasma bullet at the outside of the half-cylinder plasma pencil forms at 350 ns. The head of the cathode directed streamer is positively charged and it always forms close to the cathode [48]. It was found that the head of the plasma jet is positively charged [38]. So this cathode-directed streamer or the positive discharge front forms at the outlet on the grounded dielectric of the plasma pencil. The front view of the plasma pencil's outlet shows that the plasma formed from the surface of the outlet has a donut shaped cross-section (Fig. IV.3b). This primary plasma bullet shows up because of the expanded discharge along the dielectric surface. The plasma bullet generated by pin electrode jet does not exhibit a donut-shape (Appendix A). If we consider the grounded dielectric as a capacitor, the electric field lines will be along the outlet surface. The accumulated surface charge on the dielectric, which expands along the outlet's surface, follows the electric field line and forms a donut shaped plasma bullet/plume.
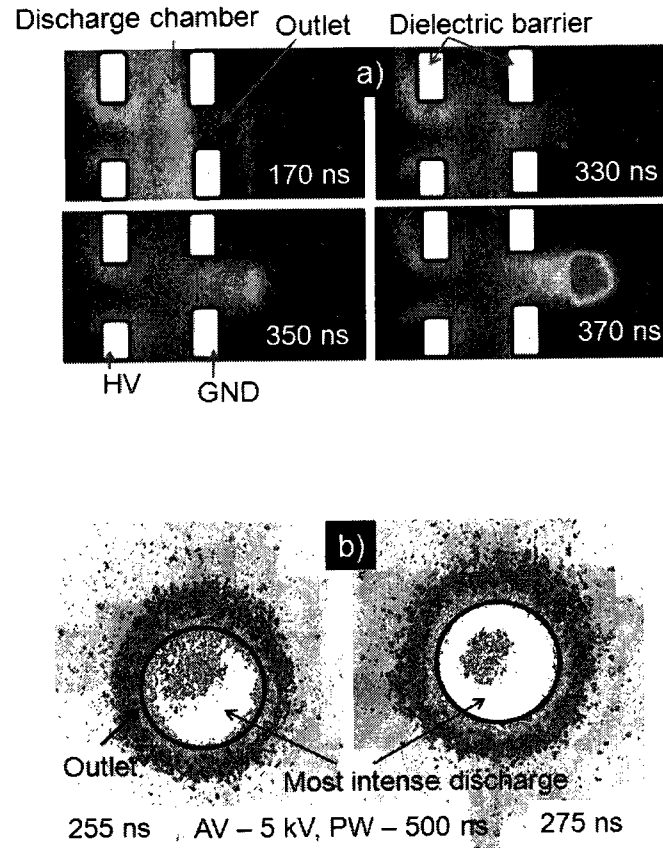
FIG. IV.3. Side view and front view of the plasma bullet formation process: a) side view of the half-cylinder plasma pencil's discharge chamber, and b) head-on view of the plasma pencil's outlet.

IV.3.2. Plasma Bullet Formation Time

There are two positive discharge current peaks per voltage pulse; one is due to the discharge inside the chamber and the second occurs during the discharge expansion through the outlet hole. The correlation between the images of the discharge chamber at different times with the discharge current waveform of the plasma pencil shows that the jet comes out from the discharge chamber when the second positive current peak starts to increase [18]. The discharge current waveform for different input voltages, shown in Fig. IV.4, also confirms that the second positive current peak corresponds to the jet formation. At the applied voltage of 3.5 kV, there is no second positive current peak and no jet shows up at the outlet of the plasma pencil. The second positive current peak shows up with the increment of the applied voltage from 3.5 kV and the current peak shifts to the left (shorter time) with the increment of the voltage amplitude, which shows that the plasma bullet formation time depends on the applied voltage. For a specific feed gas, the average electron/ion drift velocity increases with applied voltage and the plasma bullet formation time decreases.

Figure IV.5 shows the plasma bullet velocity outside the discharge chamber as measured from ICCD images for different input voltages. The red circle on Fig. IV.5 indicates that the plasma bullets take less time to come out from the discharge chamber for higher applied voltages. The plasma bullet comes out from the discharge chamber at 275 ns, 350 ns, and 420 ns of the pulse for the applied voltage of 6 kV, 5.5 kV, and 4.5 kV, respectively. The emission spectrum at the outlet of the plasma pencil taken in the transverse direction to the jet axis for different applied voltages is shown in Fig. IV.6. The temporal evolution of the emission spectrum of the plasma bullet at the outlet of the plasma pencil shows that the emission intensity increases with applied voltage and the plasma bullet takes less time to come out from the discharge chamber when the applied voltage is higher. At the applied voltage of 5 kV, the emission from excited N_2 and N_2^+ starts at 250 ns, where at the applied voltage of 4 kV the emission starts at 360 ns. The emission from excited N_2 and N_2^+ starts almost at the same time for the applied voltage of 5 kV, where as for the applied voltage of 4 kV the emission from excited N_2 starts earlier then the N_2^+. This is because the excitation energy of N_2 is less than the excitation energy of N_2^+. The temporal evolution of N_2 (337 nm) emission at the beginning of the jet for

different pulse widths is shown in Fig. IV.7. The intensity and the initial onset time of the 337 nm emission line does not change with pulse width.

In the plasma pencil, the gap width is 0.5 cm, the diameter is 3 cm and the operating voltage is 3-10 kV. Assuming that the electric field is uniform inside the chamber, the average electric field is $\bar{E}\alpha V$. Therefore, the average drift velocity of the electron/ion is $\bar{v} = \dfrac{d}{t_g} = \dfrac{\mu V}{d}$, where, d is the gap width, V is the amplitude of the applied voltage, t_g is the time required for electron/ion to travels across the gap, and μ is the mobility. So the average discharge expansion velocity increases with applied voltage leading to an earlier formation of the plasma bullet.
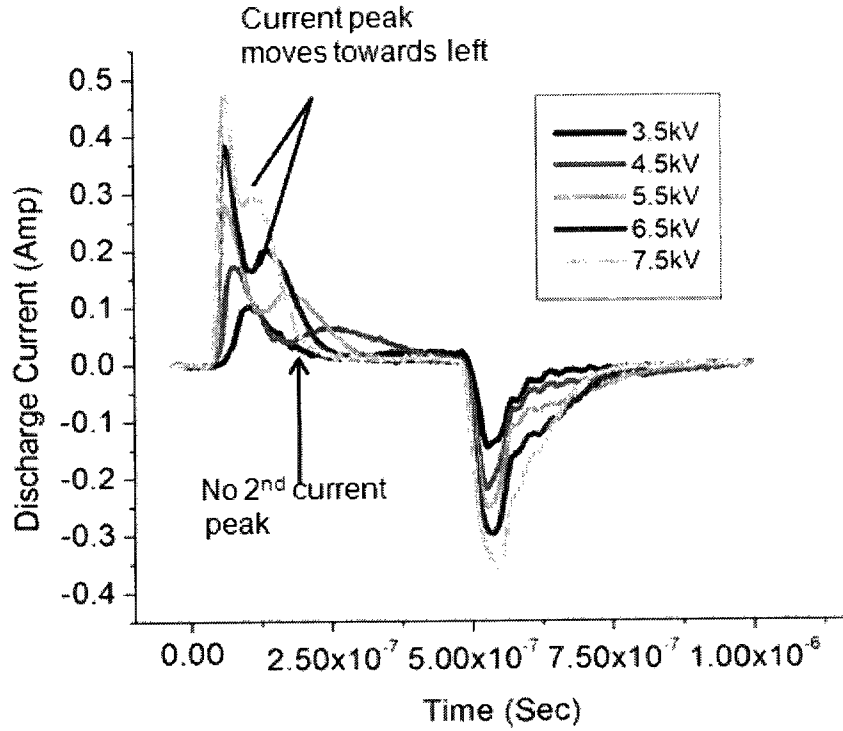
FIG. IV.4. Discharge current waveform for different applied voltages.
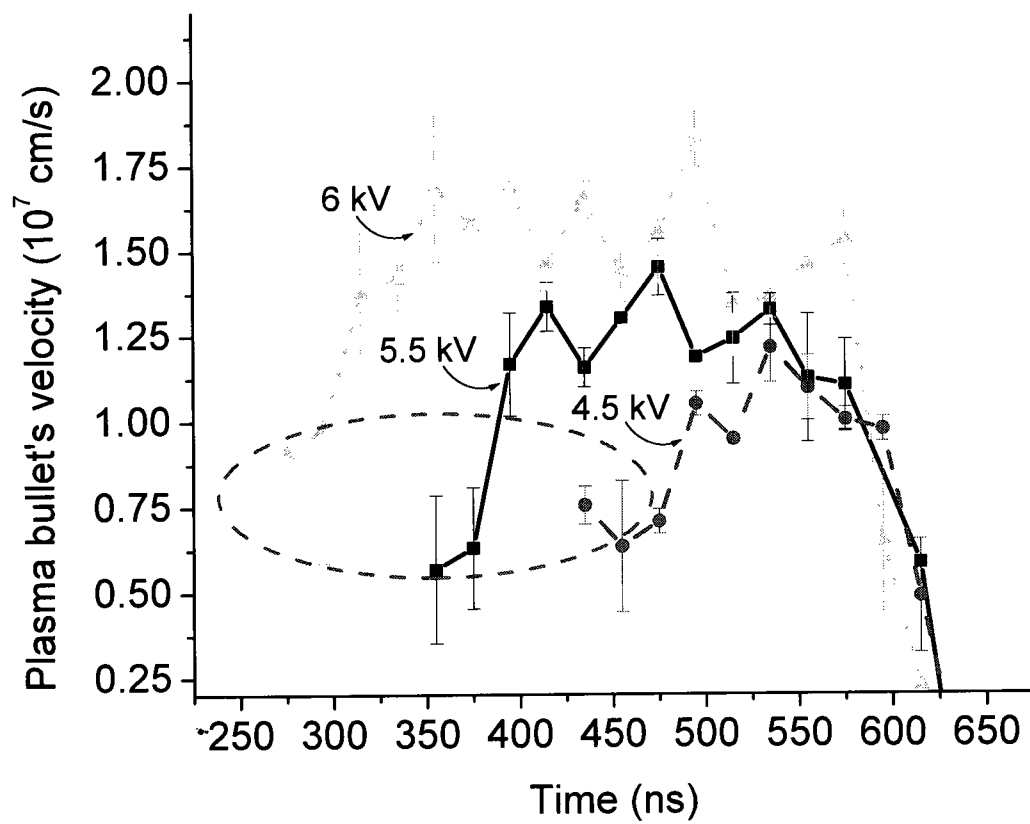
FIG. IV.5. Plasma jet propagation velocity with different applied voltages.
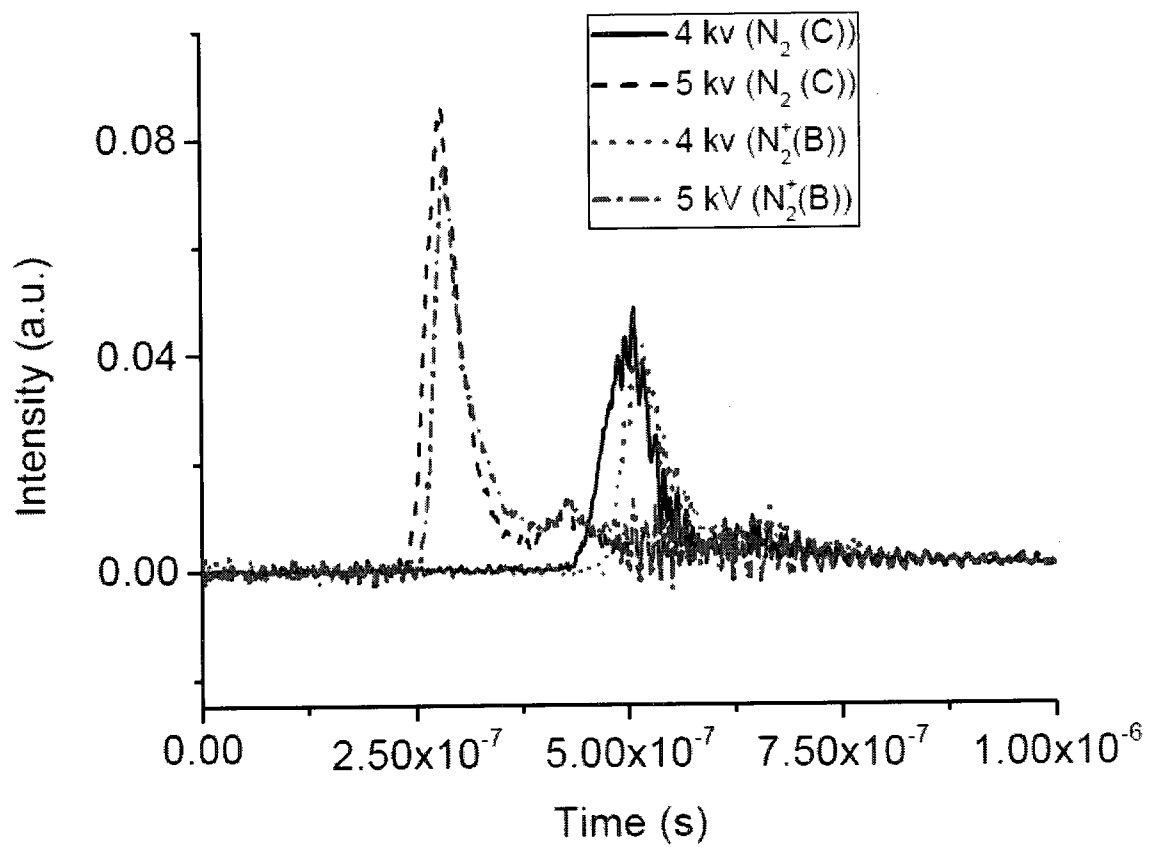
FIG. IV.6. Temporal evolution of the emission line of nitrogen at 337 nm and 390.5 nm wavelengths measured at the beginning (z = 0) of the plasma bullet.
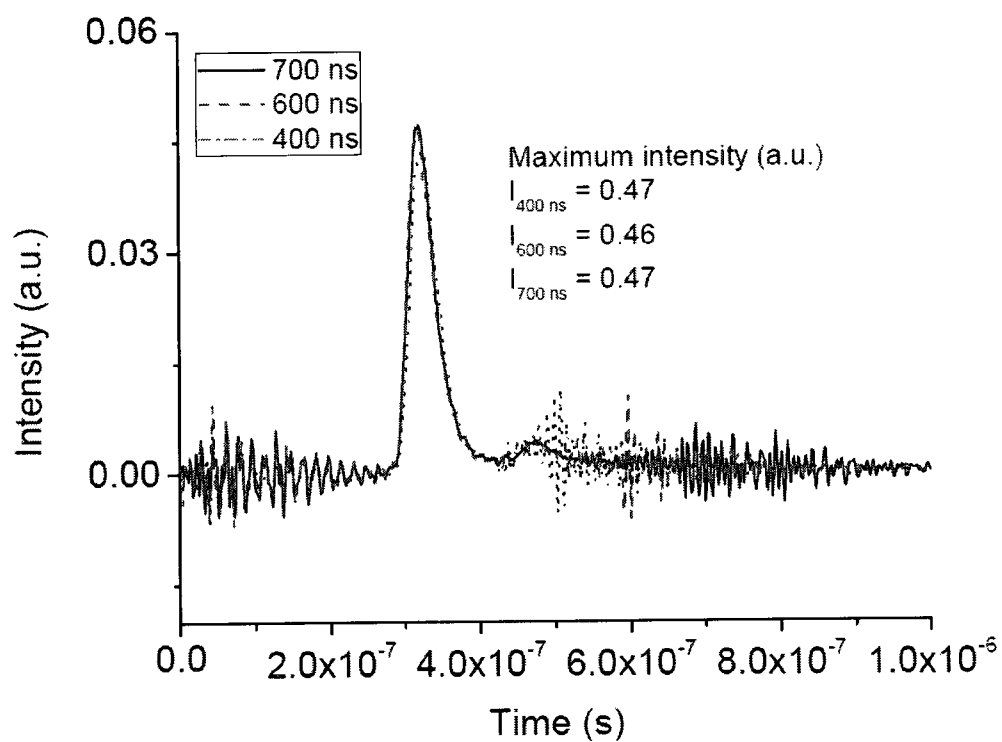
FIG. IV.7. Temporal evolusion of the 337 nm emission line at the beginning of the plasma bullet (z = 0) for different pulse widths.

IV.3.3. Formation Criteria of Plasma Bullet

IV.3.3a. Characterization of the gap discharge

The discharge phenomenon inside the discharge chamber is complex, especially when the electrodes are attached or close to a dielectric. A dielectric covered electrode makes a significant difference in the discharge because of its highly reduced conductivity. This dielectric retains a charge on its surface. The magnitude and the spatial distribution of the accumulated charge determine the characteristics of the resultant electric field at the dielectric surface. The electric field produced by the surface charge modifies the external electric field and influences the discharge in the gap [49-52]. The accumulated charge produced field is in the opposite direction to the applied electric field (normal to the dielectric surface). So the resultant electric field on the dielectric surface decreases with the charging process. The schematic of the electric field line normal to the dielectric surface is shown in Fig. IV.8. The capacitance of a dielectric disk is constant; so when the dielectric disk is fully charged the accumulated charge rearrange themselves along the electric field line on the surface of the dielectric. The expanded surface charge at the outlet of the grounded dielectric is the initial charge in the plasma bullet and it plays an important role in the formation of the plasma bullet. The gap potential was measured by using the following equation, $V_{gap} = V_{app} - \frac{1}{C_d} \int I_T \, dt$. Here C_d is the capacitance of the dielectric and I_T is the total current. Fig. III.9 shows the gap potential, input voltage, and the corresponding discharge current for the applied voltage of 5.5 kV. The applied voltage has three distinct phases: i) voltage rise time, ii) constant voltage phase, and iii) voltage fall time. The applied potential causes a rise of the gap voltage until the breakdown is started. The gap potential reaches its peak at the steady state phase of the applied voltage pulse. The discharge current starts to increase at the point when the gap potential is at its peak. The peak of the first positive discharge current (identified as 1) decreases to a low value; the second positive discharge current starts to increase from that point and reaches to the second positive peak (identified as 2). The whole positive discharge current waveform is spread over the first two phases of the applied voltage. At the outlet of the plasma pencil, the helium gas mixes with ambient air, and consequently, the nitrogen mole fraction in the helium channel increases. The excitation energy of

nitrogen is lower than the excitation energy of helium. The expanded charge through the outlet is exposed to the high input voltage and receives enough energy to ionize nitrogen molecules, which eventually creates an avalanche. The negative gap potential at the applied voltage fall time creates a negative discharge current (identified as 3), which generates a second discharge in the plasma pencil. This discharge expands along the pencil's outlet and it is identified as the second jet at the voltage fall time. The length of the second jet increases with the applied voltage. Fig. IV.10a shows the expansion of the discharge at the voltage fall time for different input voltages. This discharge also expands along the surface of the pencil's outlet. The front view of the outlet shows a hollow plasma jet (Fig. IV.10b).

The average input power per pulse to the whole system and to the discharge were calculated by using the following equations:

$$P_T = I_T x V \text{ and } P_d = I_d x V_g$$

$$P_{(average)} = \frac{\text{Total energy}}{\text{Total time}} = \frac{\int_0^\tau P dt}{\tau}$$

(Equ. IV.1)

where, P_T is the total input power, P_d is the consumed power by the discharge, I_T is the total measured current, I_d is the discharge current, V_g is the gap potential, V is the input voltage and τ is the total time (total duration of the two positive current pulses shown in Fig. IV. 9). The peak positive input power to the whole system was measured by taking the maximum of the power waveform which was found by multiplying the positive total current with the applied voltage. The total power waveform for different applied voltages is shown in Fig. IV.11a. In the same way, the peak positive input power to the discharge was measured by taking the maximum value of the power waveform found by multiplying the positive discharge current with the gap voltage. The input power to the discharge for different applied voltages is shown in Fig. IV.11b. Figure IV.12 shows the peak power to the whole system and to the discharge for different applied voltages. The average power was calculated by dividing the total energy for a specific duration of the pulse by that time interval. The average input power to the discharge and the total average input power in the whole system, only for the positive current waveform, are shown in Fig. IV.13. Almost 56% of the average total input power during the first two

phases of the applied voltage is used during the first gap discharge. For a constant gas flow rate, loss of energy is higher for the higher input voltage. In order to estimate the electron density in the discharge chamber, it was assumed that the plasma inside the chamber is uniform and electron density is uniform everywhere inside the plasma. The discharge current density can be expressed by, $j = \frac{I_d}{A} = n_e \mu_e e E = \frac{n_e \mu_e e V_g}{d}$. Here, A is the area of the electrode, d is the gap width, μ_e is the electron mobility, and n_e is the number density of electrons. The peak positive current and the peak positive gap potential were used to estimate the electron density. In this case $A = 0.75$ cm^2, $d = 0.5$ cm and the electron mobility in helium is 1.13×10^3 cm^2/V.s. The calculated peak electron density for different applied voltages is shown in Fig. IV.13. The estimated electron density in the discharge chamber is in the order of 10^{11} cm^{-3}.
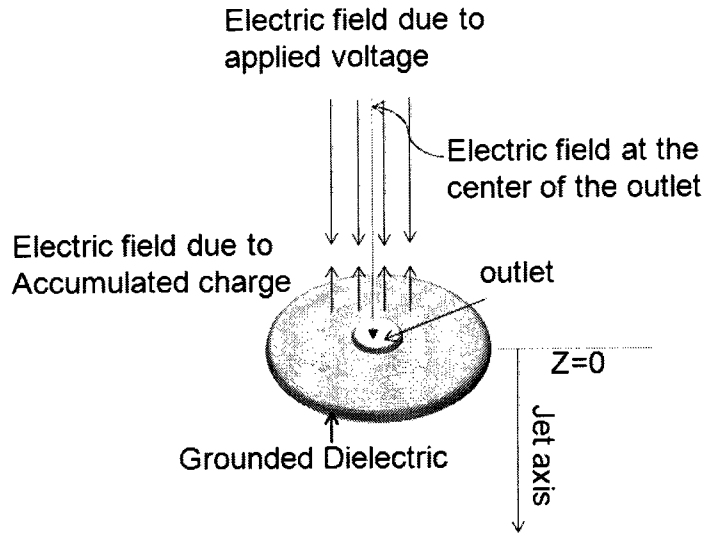
FIG. IV.8. Electric field line normal to the dielectric surface.
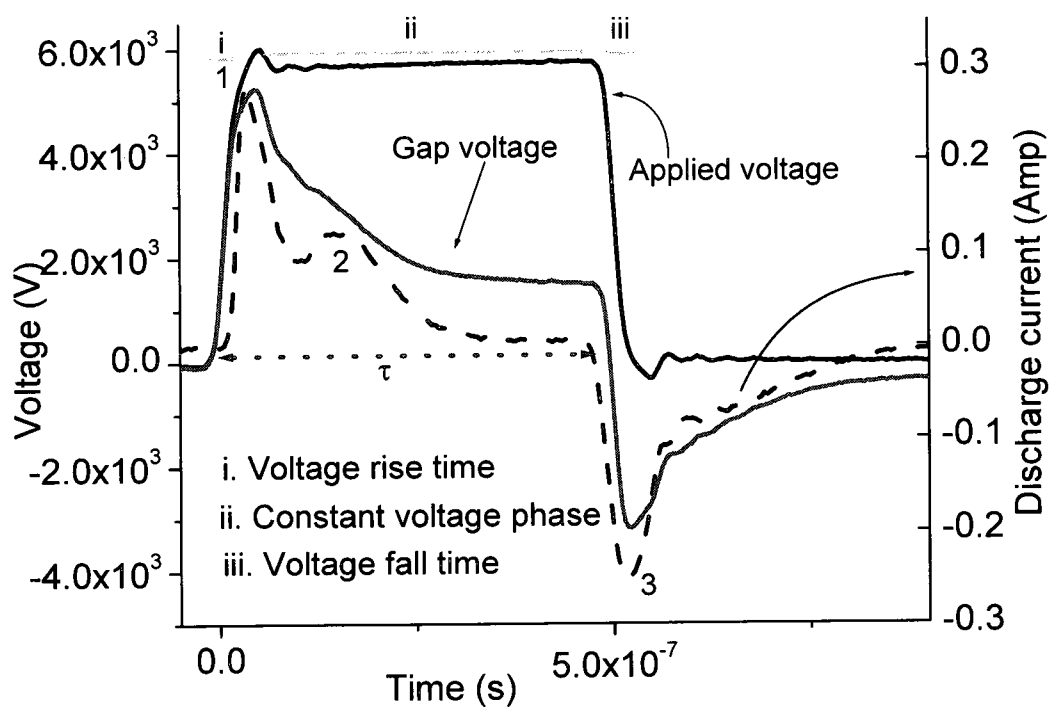
FIG. IV.9. Applied voltage, discharge current, and gap potential of the plasma pencil.
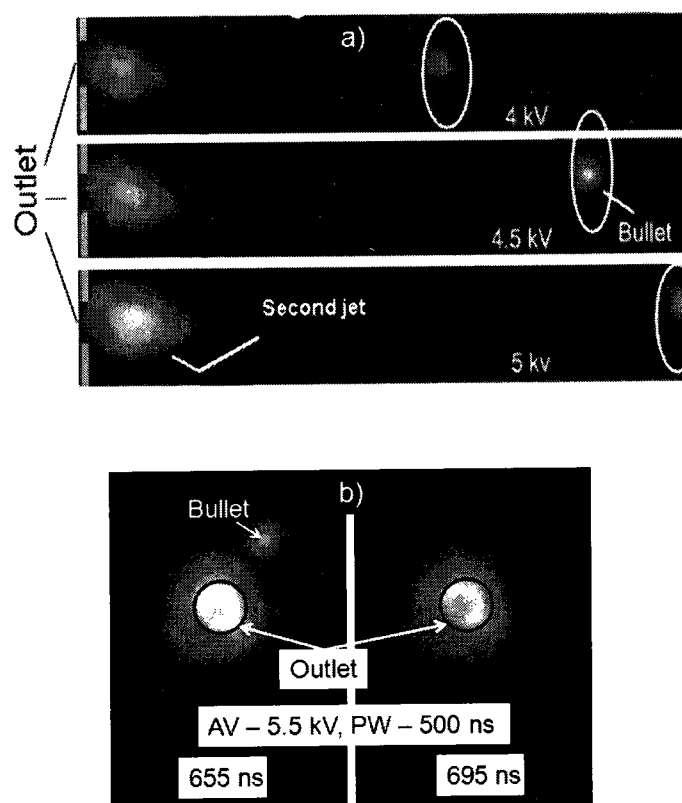
FIG. IV.10. Formation of second jet at the voltage fall time: a) side view of the second jet for different applied voltages, and b) front view of the pencil's outlet at the voltage fall time.
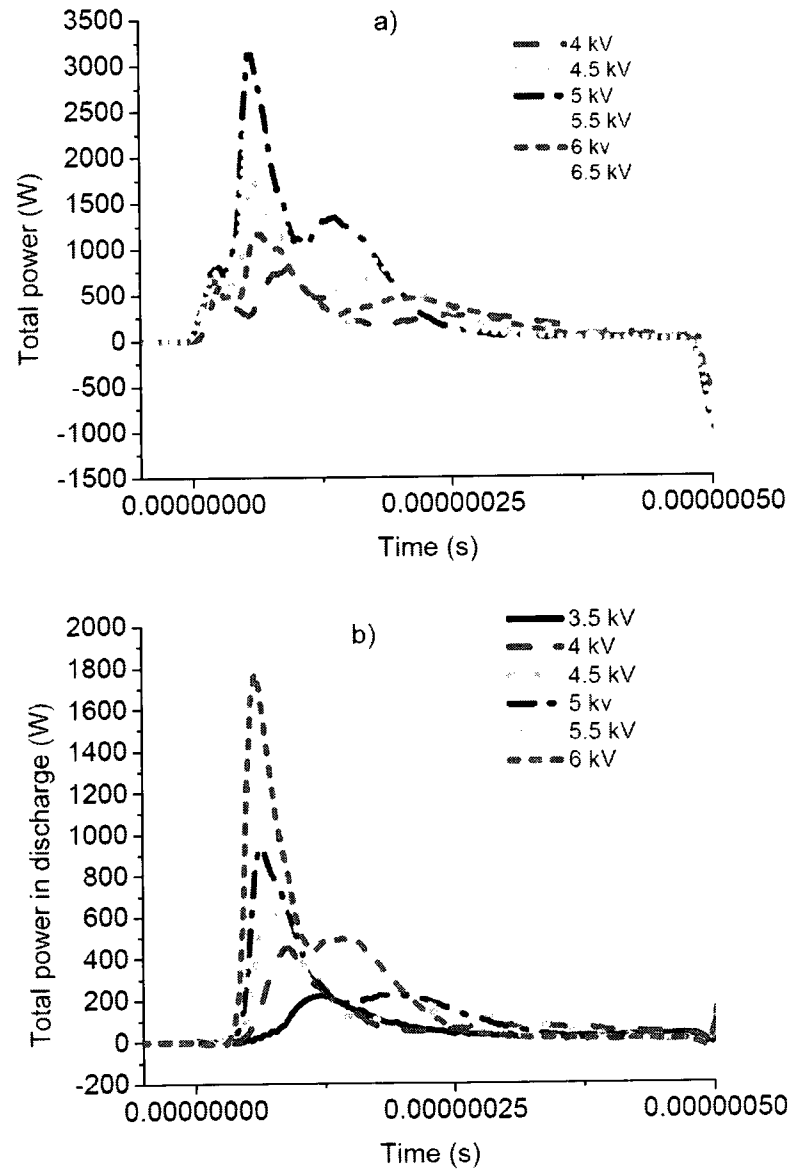
FIG. IV.11. Calculated power to the system during the positive current waveform: a) total power calculated from the applied voltage and total current, and b) total power calculated from the discharge current and gap voltage.
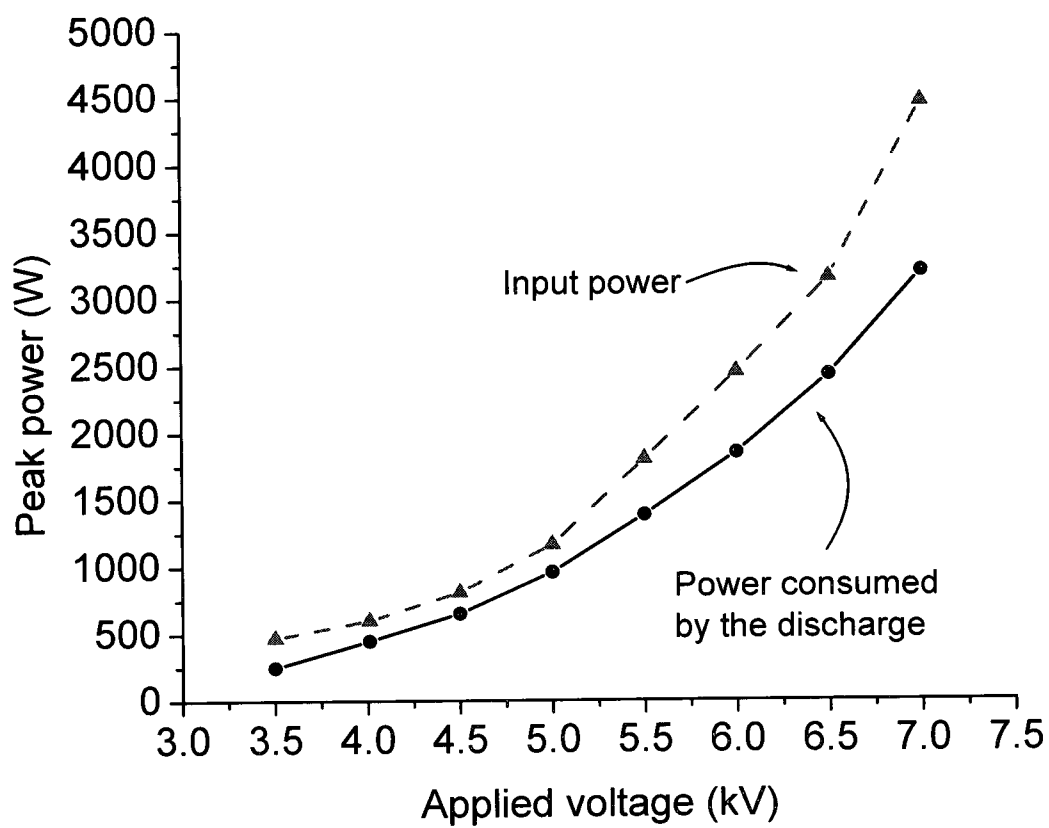
FIG. IV.12. Peak positive input power for different input voltages.
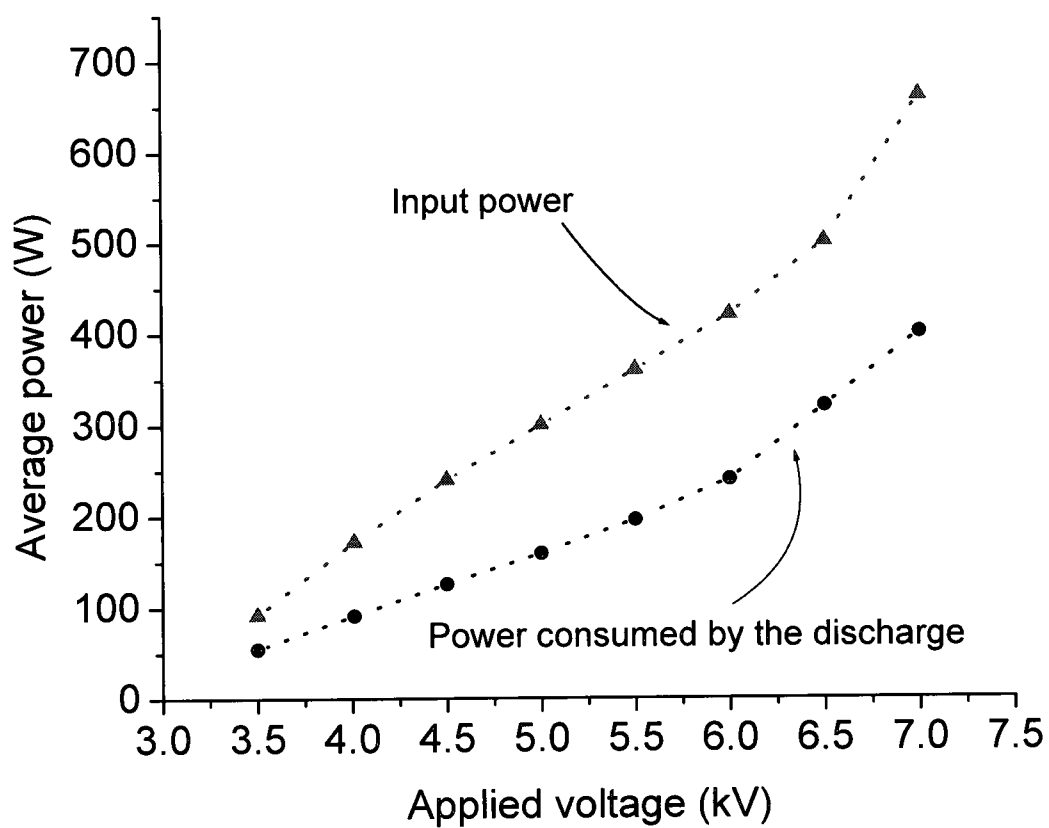
FIG. IV.13. Average power for a single pulse calculated for different input voltages in the operation of the plasma pencil.
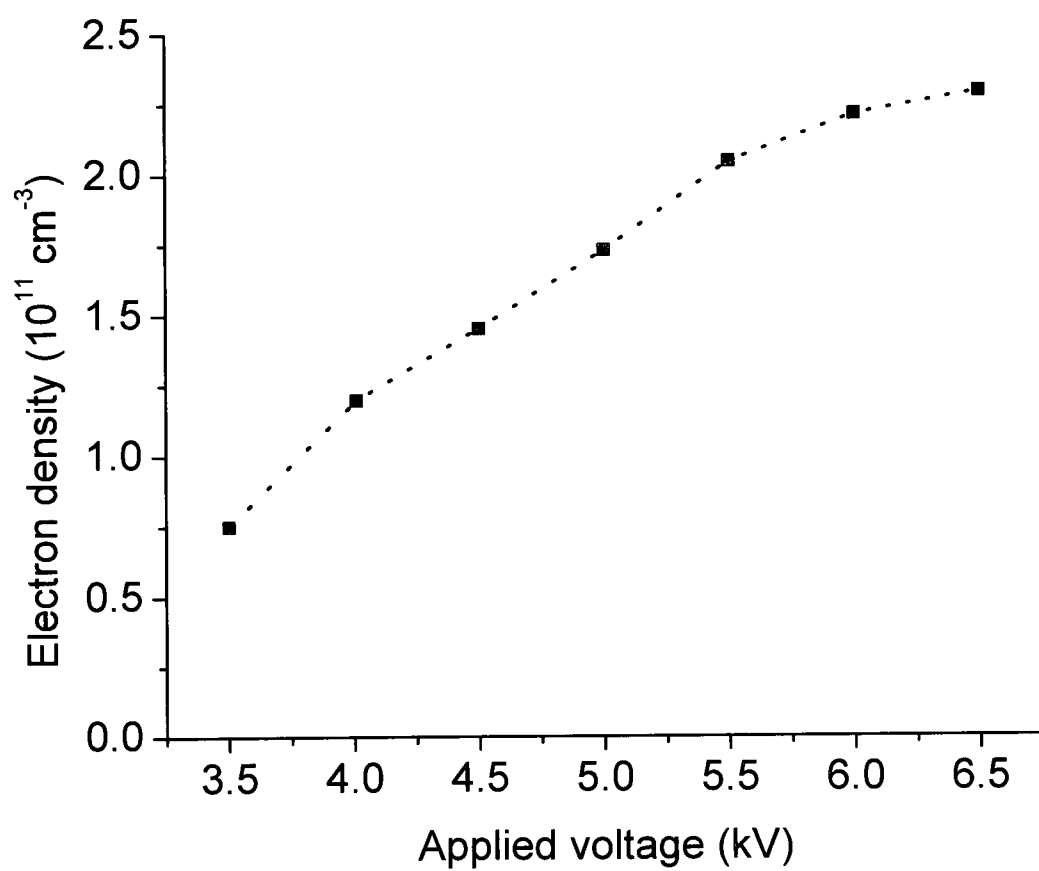
FIG. IV.14. Maximum electron density in the gap plasma for different applied voltages.

IV.3.3.b. Formation of plasma bullet

It was found in the previous sections that the plasma bullet forms during the constant phase of the applied voltage. To understand the formation of the primary plasma bullet, only the positive discharge current waveform was considered for further investigation. The stored charge in the discharge was calculated from the positive phase of the discharge current waveform. The total charge (Q) during the discharge on time was calculated by integrating the discharge current (I_d) with time, $Q = \int_0^t I_d(t)dt$. The charge (Q) calculated from the positive current pulse for different input voltages is shown in Fig. IV.15. The calculated total charge increases with applied voltage. The charge increment rate shows a transition at the applied voltage of 5 kV. The energy calculated for the gap discharge for different input voltages is shown in Fig. IV.16. The input energy to the discharge increases with applied voltage. No plasma comes out the discharge chamber for applied voltage magnitudes up to 3.5 kV. When the voltage reaches 3.5 kV, the calculated charge for the positive discharge current is 1.45×10^{-8} C and the input energy per pulse to the discharge is 2.75×10^{-5} J. It is under these conditions that we observe a bullet start emerging out of the discharge.

To investigate the effect of pulse width on the bullet formation, the total charge was calculated from the positive discharge current waveform for different pulse widths. The applied voltage was kept at 3.5 kV and the pulse width was increased from 500 ns to 850 ns in 50 ns increments. Figure IV.17 shows the discharge current wave form with a 3.5 kV AV pulse, for different pulse widths within 500-850 ns. It shows that the second positive current peak shifts towards the right with the increase of the pulse width. The initial point of the 2nd positive current pulse does not show a prominent shift within this pulse width range. The first positive discharge current peak does not show a prominent change with the pulse width; only the duration of the discharge current becomes longer for wider pulses. There is a little fluctuation in the peak positive current for different pulse widths. Figure IV.18 shows the calculated charge for the positive discharge current pulse for different pulse widths. The jet does not show for pulse widths up to 650 ns, but increasing the pulse width further can create enough charge to generate a plasma bullet. The calculated input energy per pulse to the discharge for different pulse widths is shown

in Fig. IV.19. The calculated charge and the energy for the pulse width of 700 ns are 1.5 x 10^{-8} C and 2.78 x 10^{-5} J, respectively. Similar experiments were conducted for applied voltages of 4.5 kV, 5kV and 5.5 kV, GFR of 3.6 l/min and pulse widths from 150 ns to 400 ns in 20 ns step. Table IV.1 shows the calculated charge per pulse for the specific pulse width (critical pulse width) at which the plasma bullet comes out. The plasma bullet shows up on the outlet of the plasma pencil at lower pulse widths for higher AV. The calculated charge for these applied voltages at the critical pulse width is 1.48 x 10^{-8} C. The rate of change of input energy with applied voltage is high. So, in the formation of the plasma bullet, the impact of the applied voltage is much more prominent than the impact of the pulse width.
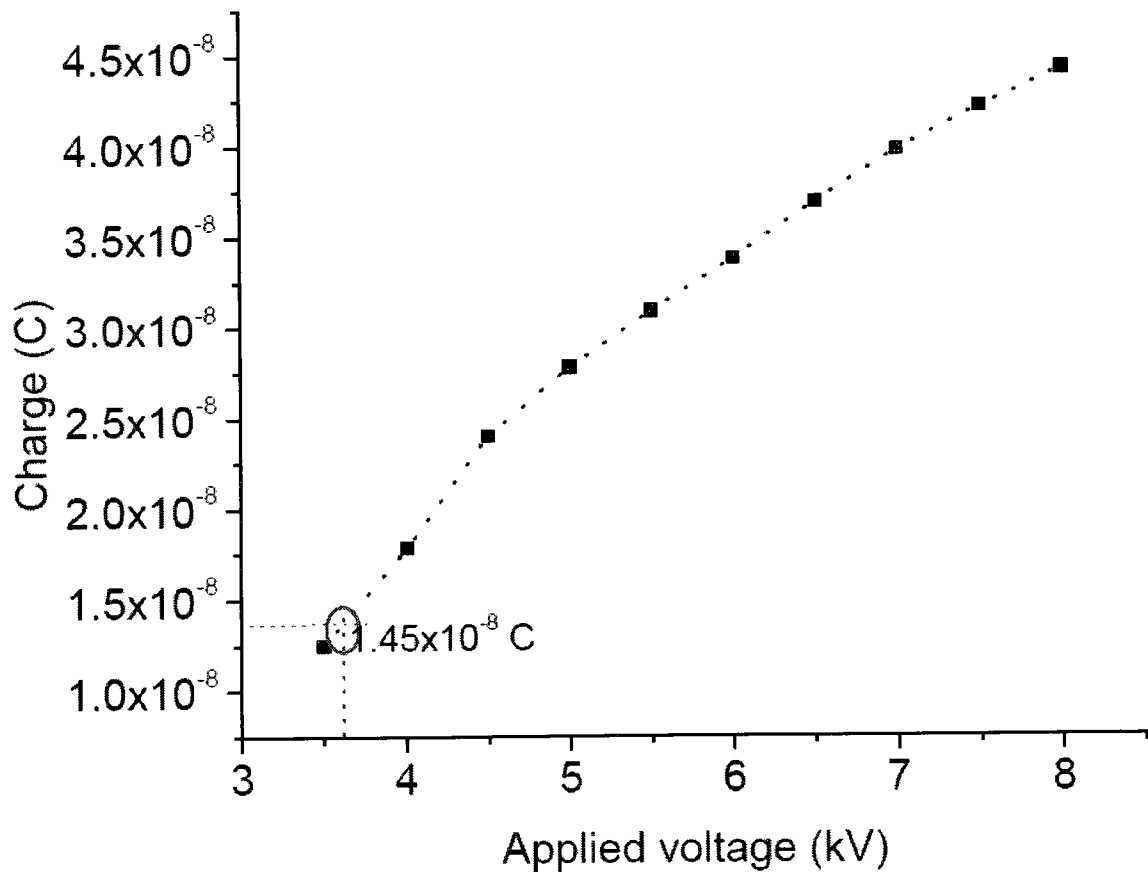
FIG. IV.15. Total charge calculated from the positive discharge current waveform for different input voltages at an operating pulse width of 500 ns.
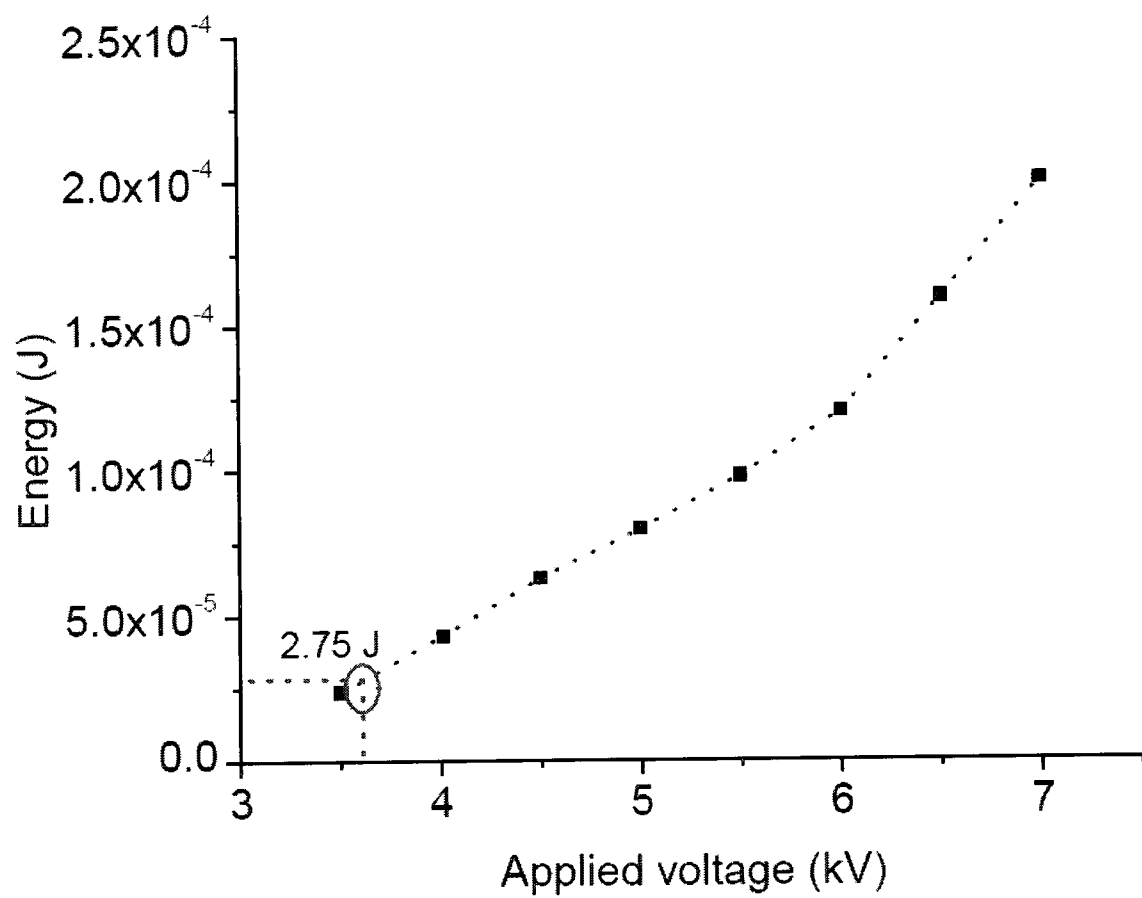
FIG. IV.16. Input energy to the discharge for different input voltages at an operating pulse width of 500 ns.
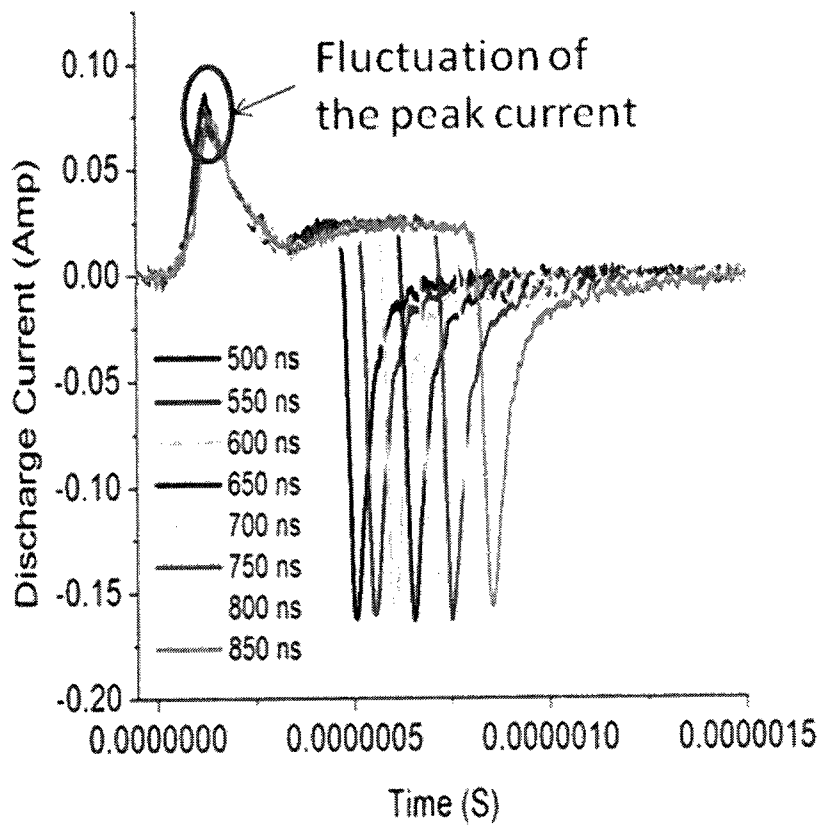
FIG. IV.17. Discharge current waveform for different pulse widths at the operating voltage of 3.5 kV and GFR of 3.6 l/min.
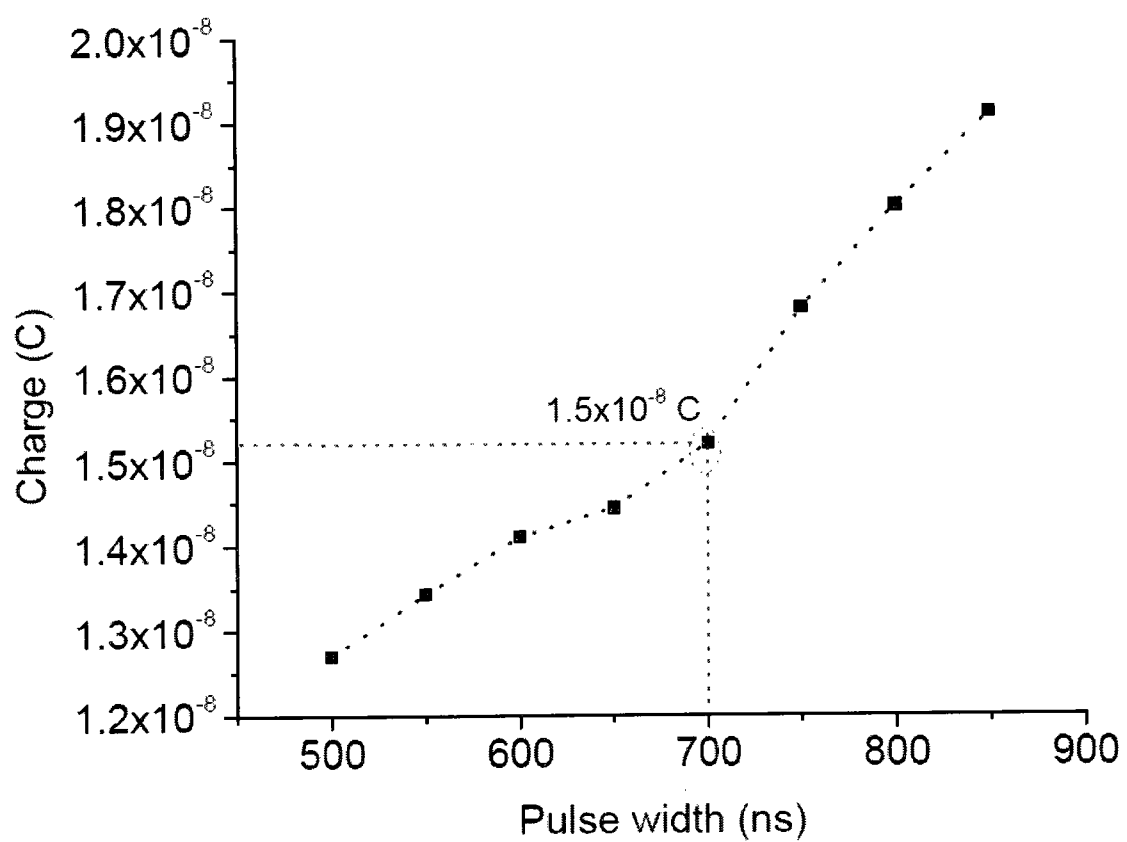
Fig. IV.18. Total charge calculated from the positive discharge current waveform for different pulse widths at the applied voltage of 3.5 kV.
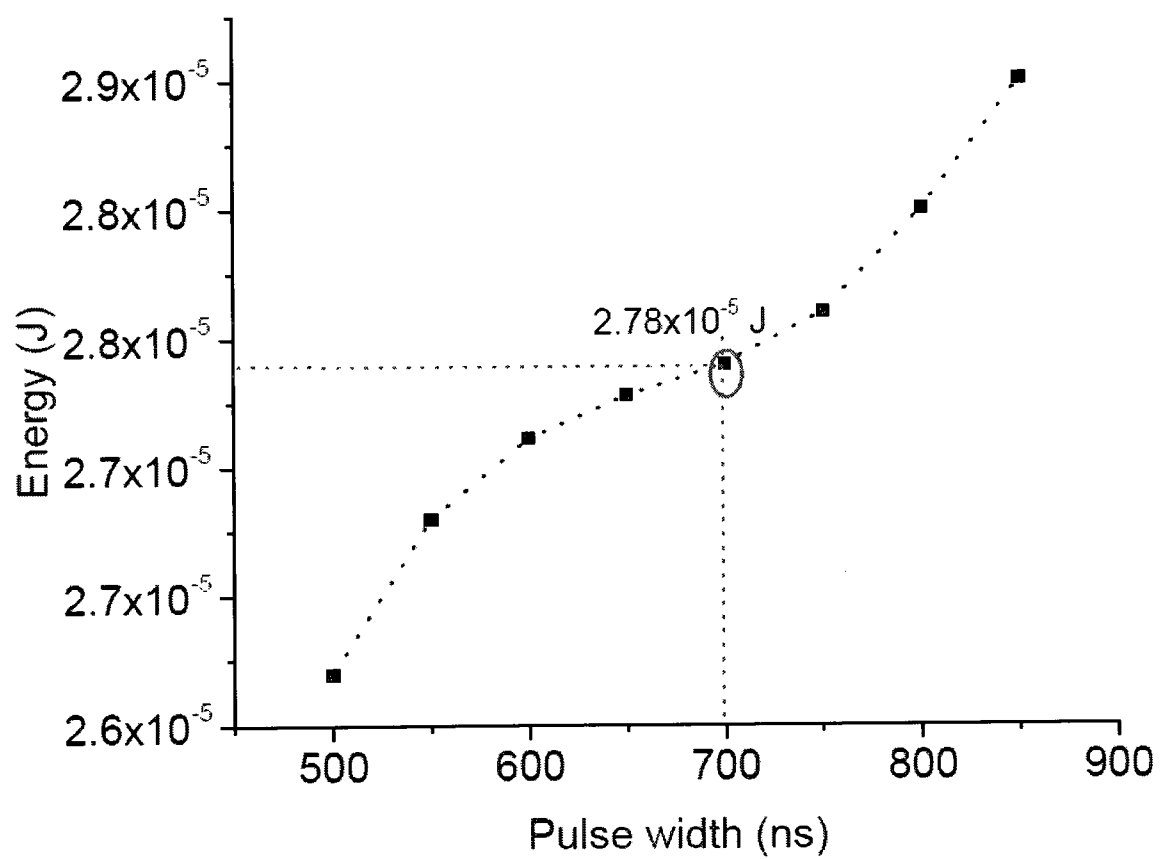
FIG. IV.19. Input energy to the discharge for different pulse widths at the applied voltage of 3.5 kV.

Table IV.1. Calculated charge for different applied voltages at critical pulse width.

AV (kV)	Measured PW (ns)	Calculated charge
3.5	>650	1.50×10^{-8} C
4.5	>250	1.48×10^{-8} C
5.0	>200	1.52×10^{-8} C
5.5	>170	1.45×10^{-8} C

IV.4. SUMMARY

The experimental investigation of the plasma bullet/plume formation from the plasma pencil was studied by using imaging techniques and electrical measurements. Experimental results show that the jet forms from the outlet surface of the plasma pencil as donut shaped. This donut-shaped initial plasma bullet is because of the surface charge on the grounded dielectric and its expansion following the electric field line. The formation time of the plasma bullet in an ambient atmosphere depends on the applied voltage. The increased applied voltage provides more energy to the discharge and the bullet formation time decreases. There is a second plasma jet at the outlet of the plasma pencil during the voltage fall time. The estimated electron density inside the discharge chamber is in the order of 10^{11} cm^{-3}. The average power per pulse shows that almost 44% of the input power is lost during the experiment. The formation criterion of the plasma bullet was investigated by calculating the total charge and total energy during the first gap discharge for different applied voltages and pulse widths. It shows that it requires minimum 2.8×10^{-5} J energy and 1.5×10^{-8} C charge per pulse to the first gap discharge to generate a plasma bullet for the applied voltage of 3.5 kV. The required minimum charge in the first discharge to generate a plasma bullet is 1.48×10^{-8} C. The change of the energy and the total charge in the discharge shows that the effect of the amplitude of the applied voltage is more efficient then the effect of the applied voltage pulse width on the characteristics of the plasma bullet.

CHAPTER V

PROPAGATION OF PLASMA BULLET

V.1. INTRODUCTION

To understand the propagation of the plasma bullet in the ambient atmosphere the characteristics of the plasma bullet should be properly understood. The plasma bullet velocity is an important parameter in the understanding of the plasma bullet's expansion/propagation phenomenon. Considering its high velocity, investigators explained the jet's propagation phenomenon by invoking streamer models [31], ionization wave model [33], or a surface solitary wave model [38]. The length of the plasma jet changes with Applied Voltage (AV), feed Gas Flow Rate (GFR) and Pulse Width (PW). It was found that the velocity of the plasma bullet also changes with applied voltage. The plasma properties in the plasma bullet vary with the operating parameters of the plasma pencil. In this chapter the characteristics of the plasma bullet along its propagation pathway for different operating conditions are investigated. The main diagnostic tools currently used for the characterization of the plasma bullet are the ICCD camera and spectrometer. The ultra fast image of the plasma jet was captured by using an ICCD camera to investigate the size, shape, and position of the plasma bullet. The temporal and the spatial evolution of the plasma bullet can be traced from the image of the plasma bullet. In this chapter, experiments employing an ICCD camera and a dielectric probe were carried out to understand the plasma bullet propagation in the ambient air. The spatially resolved jets' current measurements by using a dielectric probe/capacitive probe show delay between the consecutive positions of the probe. The plasma bullet velocity was investigated from the ICCD image of the plasma bullet and the delay between the consecutive jet current peaks due to the spatial movement of the probe along the jet axis for different applied voltages, pulse widths, and feed gas flow rates. One of the main objectives of this chapter is to determine the propagation velocity of the plasma bullet by using the ICCD and the dielectric probe. The shape of the plasma bullet changes during its propagation in the ambient air from the outlet of the plasma pencil to the end of the plasma jet. The decrease of the plasma bullet's diameter along its

propagation pathway is called the contraction of the plasma jet/bullet. There have been many theoretical and experimental investigations [53-58] of constricted discharges in inert gases that have shown that the contraction arises above a certain critical pressure. The general discussion of the contraction can be found in [41]. The contraction can occur, because of increased discharge current [58, 59] too. All these experiment are done inside the tube to see the contraction of the plasma column. Kabouzi [59] performed a detailed and in-depth work to explain the contraction of the plasma column in atmospheric pressure microwave discharge inside a tube. In this chapter, the gradual change of the shape of the plasma bullet in the ambient atmosphere with time and position is investigated. To understand the propagation of the plasma bullet in the ambient atmosphere, the plasma characteristics in the plasma bullet along its propagation axis are estimated by using a dielectric probe. From the spatially resolved jet current and the current density, the Reduced Electric Field (REF) and the Electron Density (ED) of the plasma bullet for 0.3 cm of the plasma jet are measured along the jet axis for different applied voltages.

V.2. EXPERIMENTAL SET-UP

To measure the jet velocity, an ICCD camera was placed in the tangential position to the jet axis and the image of the plasma bullet is taken by operating the camera with 20 ns delay and 20 ns exposure time. The plasma bullet velocity from the image of the plasma jet was measured as shown in Chapter II. To measure the plasma bullet velocity from the plasma jet current along the axis, a dielectric probe was placed at different positions along the bullet propagation axis starting from 1.0 cm of the jet axis and measured the jet current at that position across a resistor (R). The experimental set-up for the electrical diagnostic of the plasma bullet propagation along the jet axis is shown in Fig. V.1. The front view of the plasma bullet was taken by placing the ICCD camera at the head-on view of the plasma pencil as shown in Fig. IV.1b. The diameter of the plasma jet was measured from the side-view image of the plasma jet. The plasma pencil was operated with different high voltage pulses with magnitude in the 5 - 7 kV range. The operating pulse widths were set within the range from 400 ns to 800 ns and the frequency was set to 4 kHz. The outer hole at the grounded dielectric barrier was used as

the reference position of the plasma bullet (z=0). All the results presented in this chapter are the average of five measurements.
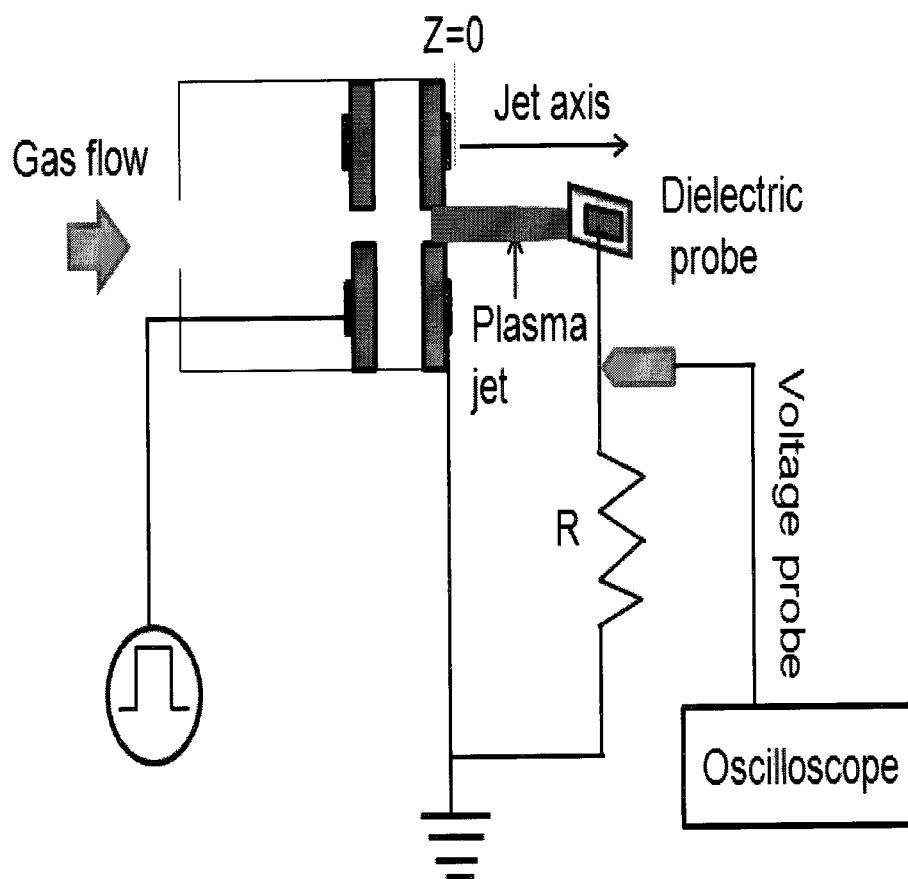
FIG. V.1. Experimental set-up for the electrical investigation of the plasma bullet along the jet axis.

V.3. RESULTS

V.3.1. Plasma Bullet's Velocity

It was observed in Chapter III that the length of the plasma jet changes with AV, PW, and GFR. In this section, the correlation between the length of the plasma jet and the velocity of the plasma bullet is discussed. The plasma bullet velocity for different AVs, GFRs, and PWs was measured by using two different methods: a) imaging technique (ICCD camera), and b) electrical technique (dielectric probe). The plasma bullet velocity curve for every 20 ns along the jet axis is shown in Fig. V.2. The velocity curve of the plasma bullet along the jet axis shows that there are three distinct phases of the plasma bullet: i) transition phase, ii) propagation phase, and ii) collapse of the plasma bullet. In the transition phase, the plasma bullet's velocity increases from the reference point (z = 0 cm) to a distance approximately 1.45 cm from the outlet. The propagation phase in the plasma bullet's velocity curve is due to the self-sustained propagation of the plasma bullet in the ambient atmosphere along the jet axis. This phase starts from the end point of the transition phase. The velocity of the plasma bullet is strongly unsteady along the propagation phase. For this reason, the average plasma bullet velocity for every 40 ns along the jet axis is plotted in further investigations. At the end of the pulse width, the jet velocity decreases rapidly and the bullet dies away. This abrupt decay of the plasma bullet's velocity is due to the collapse of the plasma bullet. All three phases of the plasma bullet velocity curve are explained in this section.
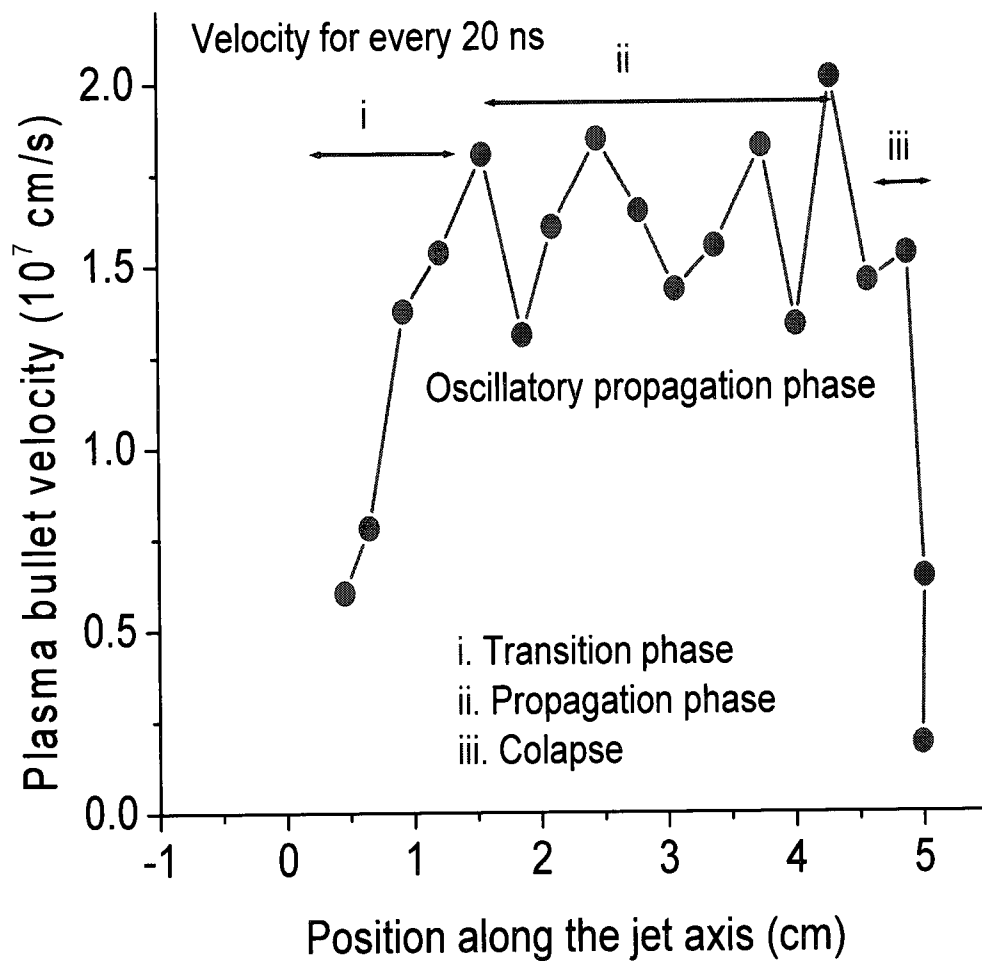
FIG. V.2. Plasma bullet velocity measured from the ICCD image of the plasma jet for every 20 ns.

V.3.1.a. Velocity Measurement by Using ICCD Camera

The plasma bullet velocity for different applied voltages (PW = 500 ns, GFR = 3.2 l/min) along the jet axis in the ambient atmosphere measured from the ICCD images of the plasma bullet for every 40 ns is shown in Fig. V.3. At the beginning, it shows that the plasma bullet velocity for different applied voltages is almost the same; it increases with applied voltage along the transition phase up to 1.5 cm of the jet axis. The plasma bullet velocity reaches its peak within 0.85 cm and 1.5 cm of the jet axis for the operating applied voltage within 5 kV to 6.25 kV. The end point of the transition phase moves towards the left with the increase of the applied voltage. It gives the notion that the propagation phase of the plasma bullet starts closer to the outlet for a higher applied voltage. The length of the propagation phase and the velocity of the plasma bullet along this phase increases with the applied voltage. The collapse of the plasma bullet starts at the end of the propagation phase.

Whereas the plasma bullet collapses at different positions on the jet axis for different applied voltages, for a constant pulse width it collapses at the same time independently on the magnitude of the applied voltage [38]. If there is a correlation between the length of the plasma jet and the pulse duration, there must be a correlation between the length of the plasma jet and the velocity of the plasma bullet. Fig. V.4 shows the correlation between the average plasma bullet velocity and the length of the plasma jet. The average plasma bullet velocity was calculated by taking the average of the velocity from the beginning of the plasma bullet to the end of the bullet's propagation phase. The average propagation velocity of the plasma bullet is the average plasma bullet velocity only along the propagation phase. The average propagation velocity is much higher than the average plasma bullet velocity (V_{av}). The average plasma bullet velocity and the average propagation velocity increase with the length of the plasma jet. The plasma jet length measured from the image of the plasma jet is also shown in Fig. V.4. This measured jet length was compared with the average plasma jet length (l_{cal}) calculated by multiplying the pulse width (τ_{pw}) and the average plasma bullet velocity

$(l_{cal} = \tau_{pw}.v_{av})$. It shows that the measured jet length is almost the same as the calculated average jet length.
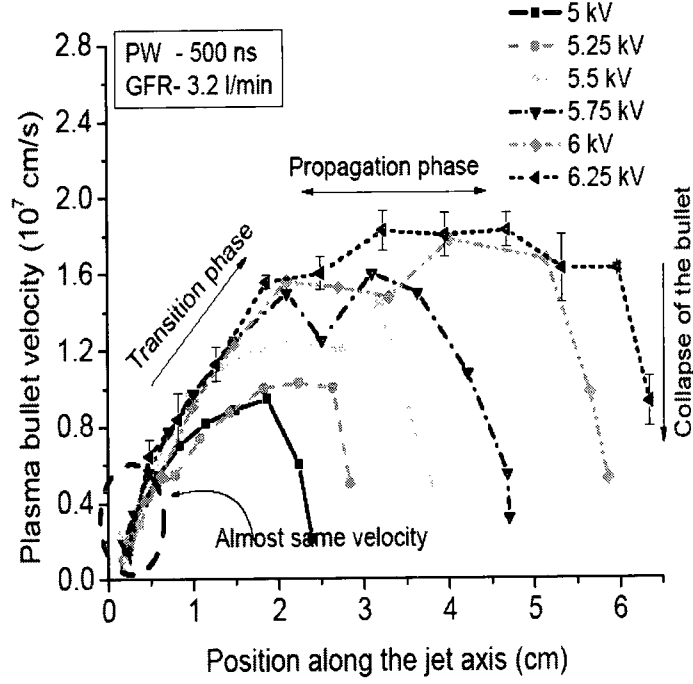
FIG. V.3. Plasma bullet velocity for different applied voltages along the jet axis measured from the ICCD image of the plasma jet for every 40 ns: i) transition phase, ii) propagation phase, and iii) collapse of the plasma bullet.
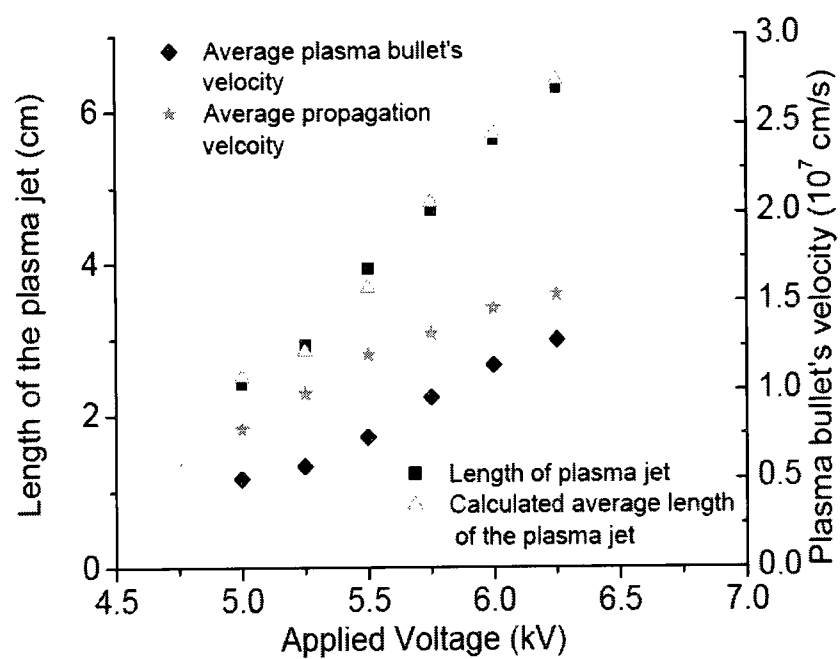
FIG. V.4. Correlation between the average bullet velocities, bullet's propagation velocity, measured and calculated plasma jet length for different applied voltages and the GFR of 3.2 l/min and pulse width of 500 ns.

Figure V.5 shows the plasma bullet velocity for different operating pulse widths from 550 ns to 700 ns in 50 ns increments. The plasma bullet's velocity change is almost the same along the transition phase for the change of the pulse width from 550 ns to 650 ns. As the plasma bullet moves towards the end of the transition phase, the fluctuation in the velocity increases. At the end of the transition phase, the plasma bullet's velocity is the same for all five pulse widths. The length of the propagation phase increases with pulse width and at the end of the propagation phase, the plasma bullet's velocity shows an abrupt decay like previous velocity curves. Figure V.6 shows the length of the plasma jet and the average velocity of the plasma bullet for different pulse widths. The plasma jet's length increases almost linearly within the pulse width range from 400 ns to 700 ns. The average plasma bullet velocity curve follows the same trend as the length of the plasma jet for different pulse widths. The average propagation velocity increases with pulse width and is higher than the average plasma bullet velocity. The measured plasma jet length was compared with the calculated average jet length and it was found that within the low pulse width range (400-450 ns), the measured jet length is almost the same as the calculated average jet length (Fig. V.6). Further increase of the pulse width shows a prominent difference between the measured and the calculated average plasma jet length. In this case, the calculated average plasma-jet length is higher than the measured plasma-jet length.
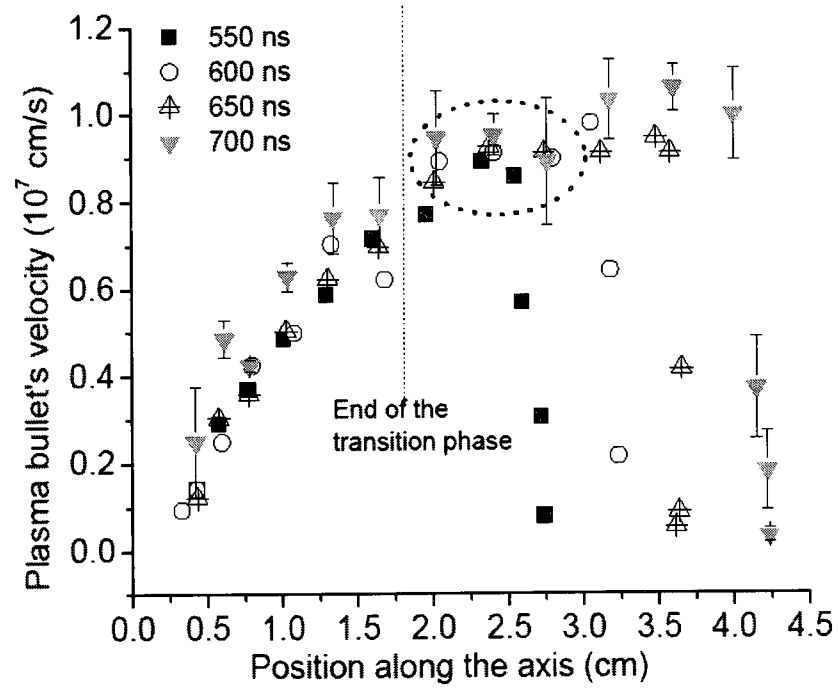
FIG. V.5. Plasma bullet velocity along the axis for different pulse widths measured from the ICCD image of the plasma jet for every 40 ns.
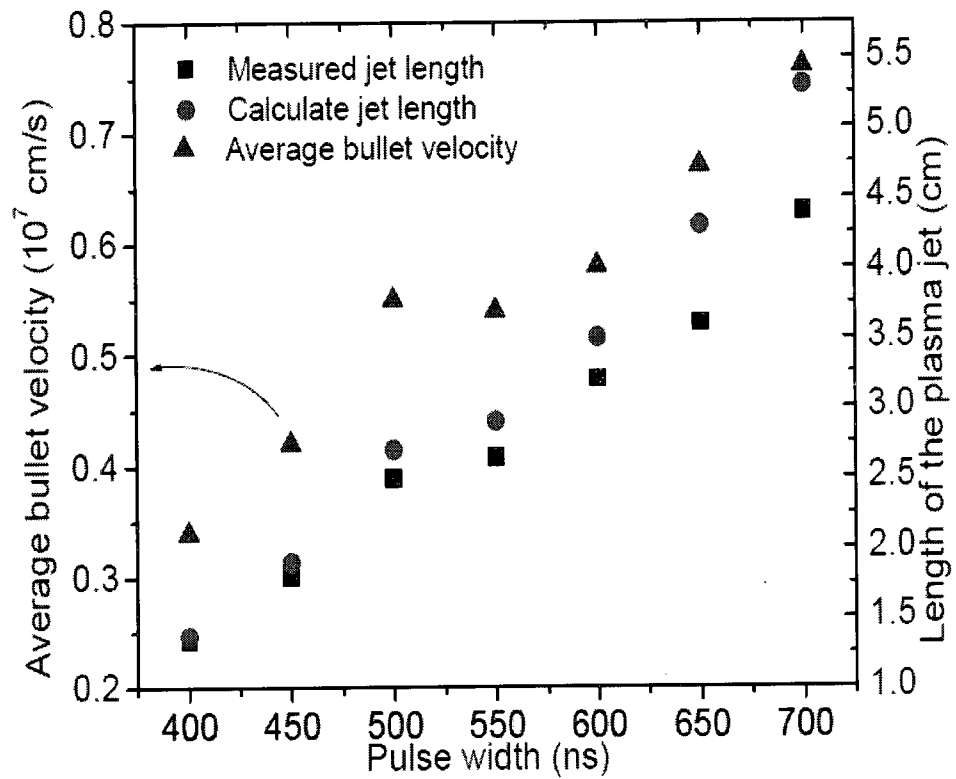
FIG. V.6. Correlation between the average plasma bullet velocity and the measured and calculated jet length for different pulse widths: average plasma bullet velocity and calculated and measured length of the plasma jet follow the same trend.

The change of the plasma bullet velocity with a GFR (AV - 5 kV, PW - 500 ns) along the jet axis is shown in Fig. V.7. Along the transition phase, the plasma bullet velocity is height for the gas flow rate of 2.36 l/min. The plasma bullet velocity along this phase is decreasing for the GFR above 2.36 l/min. The transition phase of the plasma bullet velocity curve ends within 1.0 cm and 1.75 cm of the jet axis for all GFRs (within 2.36-8.0 l/min). The length of the propagation phase for the GFR of 2.36 l/min is long compared to the length of the propagation phase for the feed GFR above 2.36 l/min. As the length of this propagation phase is decreasing the propagation velocity is also decreasing. Figure V.8 shows the average plasma bullet velocity and the length of the plasma jet for different GFRs (within 1.04-8.0 l/min). The average plasma bullet velocity and the average propagation velocity increase from the GFR of 1.04 l/min to the GFR of 2.36 l/min. Similar to the average velocity curve of the plasma bullet, the length of the plasma jet also increases from the GFR of 1.04 l/min to the GFR of 2.36 l/min. The measured plasma-jet length, the average plasma bullet velocity, and the average propagation velocity are decreased for the feed GFR above 2.36 l/min. The calculated plasma-jet length curve also shows the same trend as the measured plasma-jet length curve. For the GFR above 2.36 l/min, it does not show prominent difference between the calculated plasma-jet length and the measured plasma-jet length. The difference between the calculated jet length and the measured jet length decreases with the increase of the GFR.
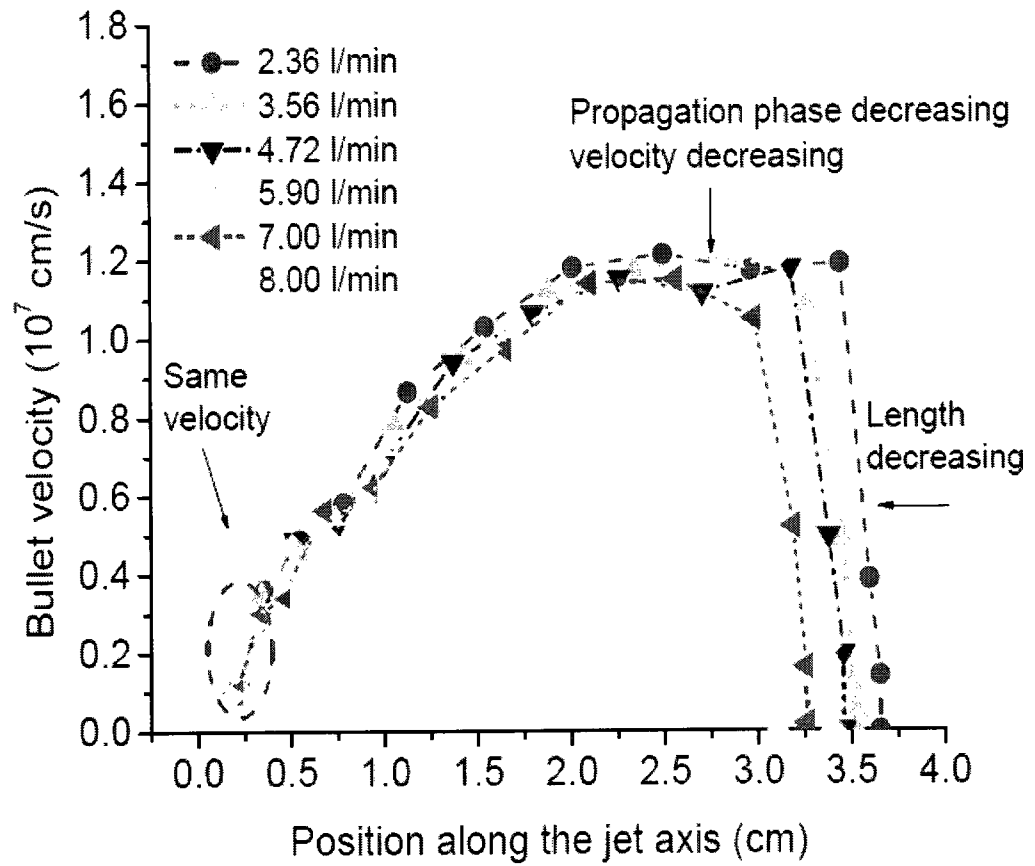
FIG. V.7. Plasma bullet velocity along the axis for different GFRs measured from the ICCD image of the plasma jet for every 40 ns for the operating applied voltage of 5 kV and pulse width of 500 ns.
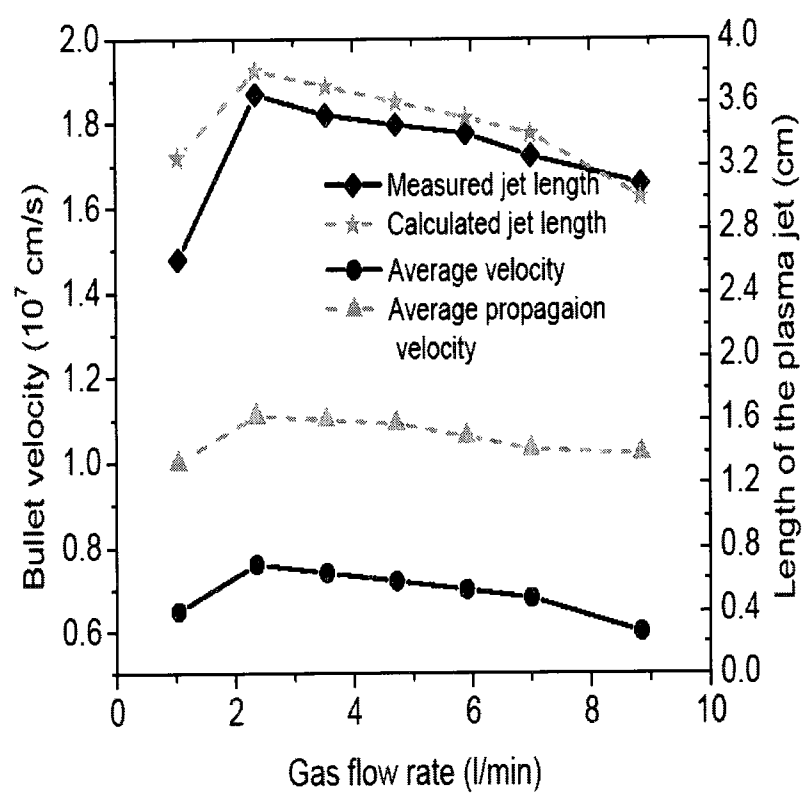
FIG. V.8. Comparison between the measured and calculated jet length, and the measurement of the average velocity and average propagation velocity of the plasma bullet for different GFRs.

V.3.1.b. Velocity Measurement by Using a Dielectric Probe

A Langmuir probe is not suitable at high pressure for plasma diagnostics. For this reason, a small metal plate was covered with a dielectric sheet named 'dielectric probe' and exposed to the plasma jet. This "probe" was placed at different positions along the jet axis and the jet current was measured at that position across a resistor (R) (Fig. V.1). The jet current waveform in Fig. V.9a shows that there is a time delay between the consecutive positions of the probe on the plasma bullet propagation axis. When the plasma bullet reaches to the probe, the current starts to increase, reaches its peak, and slowly decreases with time from the peak value. This current does not decrease to zero until the pulse is over. This is evidence of the generation of a single bullet for every pulse and it also shows that there is a low density plasma channel behind the head of the plasma bullet. The current peaks as a function of the probe's position on the jet's axis and the required time for the plasma bullet to reach that position are shown in Fig. V.9b. The velocity of the electron is much higher than the velocity of the ion. The peak in the current curve is due to the propagation of electrons. The velocity of the plasma bullet is measured from the spatial difference between two consecutive positions of the probe and the time difference between the jet current peaks for those positions. The measured velocity calculated in this process for three different AVs, PWs and GFRs are shown in Fig. V.10, Fig. V.11, and Fig. V.12, respectively. The plasma bullet velocity curve measured by using both techniques shows a similar trend: an initial acceleration of the plasma bullet then a relatively constant velocity phase followed by a deceleration phase. The average plasma bullet velocity at 1.0 cm on the jet axis is calculated by diving the distance of 1.0 cm with the required time for the plasma bullet to travel this distance. As the outlet of the plasma pencil is taken as the initial position of the plasma bullet, the required travel time is calculated by subtracting the formation time of the plasma bullet from the required time for the plasma bullet to reach that position (1.0 cm) on the jet axis.
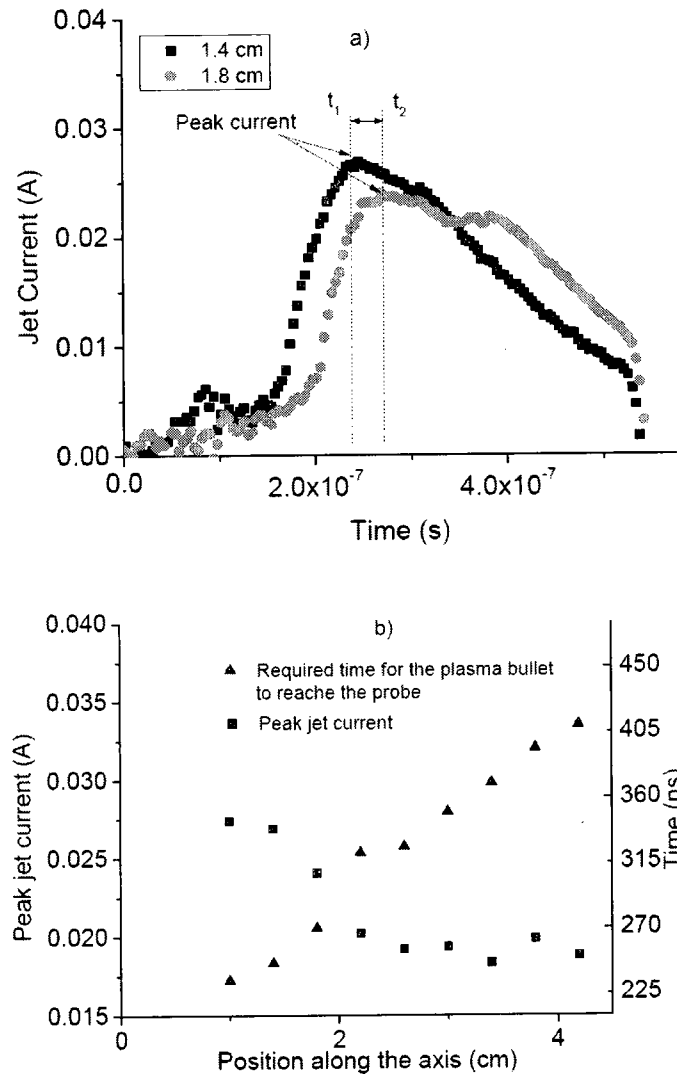
FIG. V.9. a) Jet current waveform at different positions along the axis, and b) position of the probe along the jet axis, time required for the plasma front to reach that position, and the corresponding current peaks at that position.

The plasma bullet velocity measured by using the dielectric probe for different applied voltages (5 kV, 6 kV and 6.5 kV) is shown in Fig. V.10. The plasma bullet velocity increases with applied voltage from its creation and reaches its peak at the end of the transition phase, which is the initial point of the propagation phase. The propagation phase of the plasma bullet starts approximately within 1.4cm and 1.85 cm on the jet axis. The initial point of the propagation phase on the jet axis in this applied voltage range agrees with the plasma bullet's velocity curve measured by using ICCD camera. The length of the propagation phase increases with applied voltage. The plasma bullet velocity along the propagation phase increases when the length of the propagation phase increases.

The plasma bullet velocity for three different pulse widths (550 ns, 650 ns and 750 ns) are shown in Fig. V.11. At the beginning, the plasma bullet velocity is the same for all three pulse widths. The propagation phase of the plasma bullet starts within 1.15 cm and 1.85 cm of the jet axis. The plasma bullet's propagation velocity decreases when the length of the propagation phase decreases.

The plasma bullet velocity for different GFRs is shown in Fig. V.12. Similar to the velocity curve for different applied voltages and pulse widths, the transition phase of the plasma bullet's velocity curve ends around 1.45 cm on the jet axis. Along the propagation phase, the plasma bullet propagation velocity is higher for the feed GFR of 3.8 l/min than the propagation velocity for the GFR of 3.0 l/min and 5.8 l/min. The length of the plasma jet is height for the gas flow rate of 3.8 l/min. It can be said that the average plasma bullet velocity is higher when the plasma bullet travels longer path.
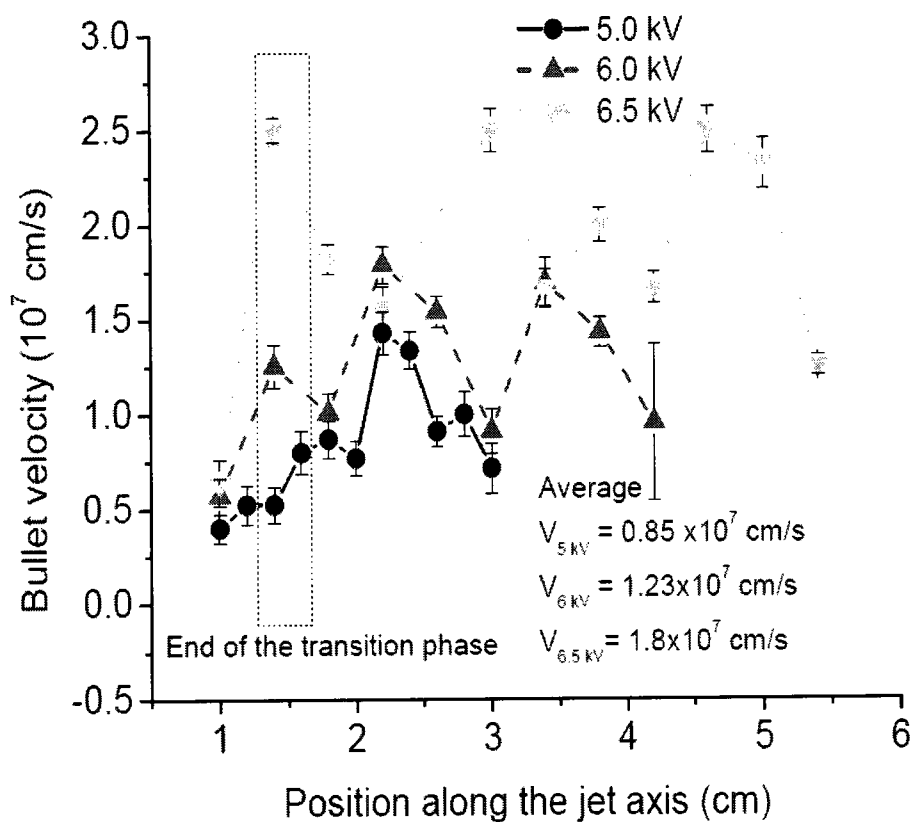
FIG. V.10. Plasma bullet velocity along the jet axis for different applied voltages measured by using a dielectric probe of the operating pulse width of 500 ns and gas flow rate of 3.6 l/min.
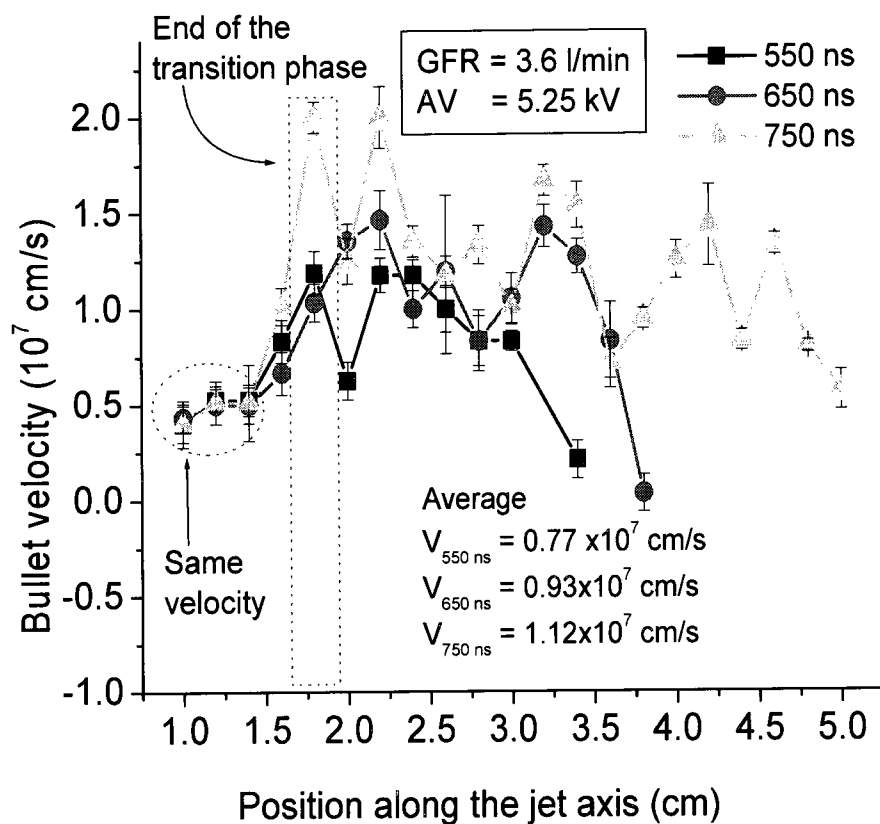
FIG. V.11. Plasma bullet velocity along the jet axis for different pulse widths measured by using a dielectric probe.
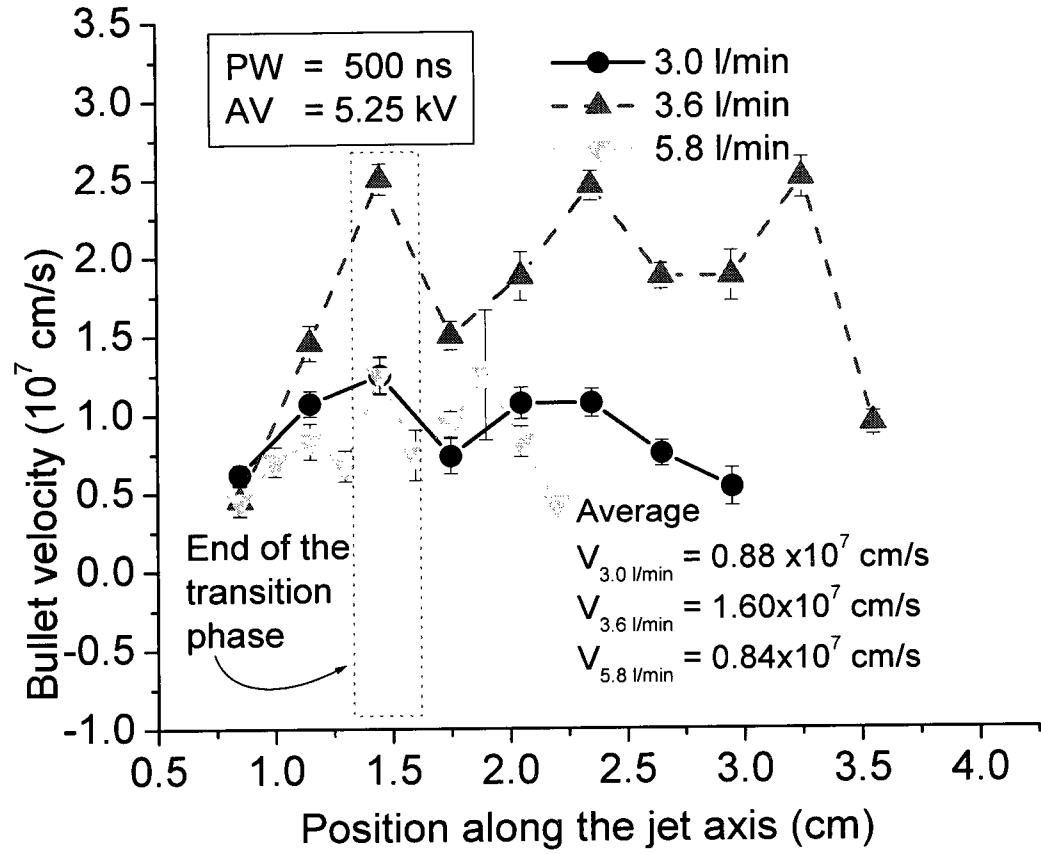
FIG. V.12. Plasma bullet velocity along the jet axis for different GFRs measured by using a dielectric probe.

The average plasma bullet velocity increases with applied voltage and pulse width (i.e. with the length of the plasma jet). It shows that the average plasma bullet velocity and the length of the plasma jet are the greatest for the feed GFR of 3.8 l/min. The calculated average jet length is a little higher than the measured plasma jet length. The average plasma bullet velocity measured by a dielectric probe is higher than the average plasma bullet velocity measured from the ICCD image of the plasma jet.

The measurements show that for longer jets the plasma bullet velocity reaches higher values. The plasma bullet velocity curve measured using two different methods shows a similar trend. The charged particles and the excited molecules come out from the discharge chamber and at the outlet of the plasma pencil; it ionizes and excites nitrogen and oxygen in air. As the ionization energy of nitrogen is lower than the ionization energy of helium, there will be enhanced plasma chemistry close to the outlet in the ambient air. The electric field at the outlet of the plasma pencil increases with applied voltage, so the ionization process increases and the plasma bullet expansion velocity increases along the transition phase. It was found that the avalanches to streamer transition take place earlier for higher applied voltages [60]. As was found in the previous chapter, the input energy to the gap discharge for different pulse widths does not increase linearly; the plasma bullet velocity along the transition phase is not consistent. The fluctuation of the plasma bullet velocity along the transition phase for different pulse widths indicates that there is an effect of gap discharge along the transition phase of the plasma bullet. The transition phase of the plasma bullet velocity curve for these operating conditions end almost at the same position and it is within 1.0 - 1.75 cm of the jet axis from the outlet of the plasma pencil.

The propagation phase of the plasma bullet is the quasi stationary velocity phase. Experimental investigation shows that, in general, the length of the propagation phase increases when the plasma bullet velocity is higher in the transition phase. It shows that the velocity along the propagation phase is higher for the longer length of this phase. This indicates that the plasma property of the bullet during the transition phase influences the further propagation of the plasma bullet. Higher input energy creates a more energetic plasma bullet in the transition phase, which can propagate a longer path along the jet axis. The higher rate of air diffusion in the feed gas channel enhances the attachment process

in the jet plasma and the plasma bullet velocity decreases. The required time scale to diffuse air in the helium gas channel's radius is $\dfrac{d^2}{D_{dif}}$, where d is the radius of the jet, and D_{diff} is the diffusion rate constant of air in helium. The diffusion time decreases with the decrease of the channel's diameter. In addition, the rate of diffusion is inversely proportional to the square root of the gas density. Air diffusion increases into the helium channel along the jet axis as the feed gas velocity decreases on the axis.

It was found that the velocity of the streamer increases linearly with length [61]. The transition from the non-stationary regime (transition phase) to the stationary regime (propagation phase) in the streamer have been also observed in Wagner's [62] work. For a fixed pressure and sufficiently high EF, the transition has been observed at a certain value within $z = 1.0$ cm to $z = 1.5$ cm of the jet axis for these operating conditions. In this region the acceleration of the plasma bullet greatly increases and it depends on the input voltage and the plasma chemistry.

The calculated length from the average velocity of the plasma bullet and the pulse width shows that there is a correlation between the length of the plasma jet and the operating pulse width of the applied voltage. The calculated average length of the plasma jet is little long compare to the measured length of the plasma jet. The actual calculated length of the plasma jet will be the product of the average plasma bullet's velocity and the pulse duration after subtracting the formation time of the plasma bullet, and this will be smaller than the calculated length of the plasma jet presented here.

V.3.2. Contraction of Plasma Bullet

The shape of the plasma jet, which is emerged in ambient air is close to conical then cylindrical, having a radius that decreases from its beginning to its tip. The plasma bullet forms from the outlet of the plasma pencil and contracts gradually along its propagation pathway. In general, the diameter of the plasma bullet decreases from the starting ($z = 0$ cm) to a distance on the jet axis around $z = 1.2$ cm. After $z = 1.2$ cm of the jet axis, the diameter of the plasma bullet is almost constant along its propagation pathway. At the end of the plasma jet the diameter of the plasma bullet decreases rapidly. Figure V.13 shows the change of the plasma bullet's diameter along the jet axis for

different applied voltages, GFRs, and pulse widths. The diameter of the plasma bullet decreases with applied voltage and pulse width and increases with GFR. Figure V.13a shows that for a constant gas flow rate of 2.812 l/min the diameter of the plasma bullet decreases from the beginning and it becomes constant when the plasma bullet is at 1.3 cm and 1.5 cm on the jet axis for the operating applied voltage of 5.5 kV and 6.5 kV, respectively. At the end of the jet, the diameter of the plasma bullet decreases. The plasma bullet in atmospheric air normally shows a radial contraction, but when the gas flow rate increases, the diameter of the plasma bullet increases (Fig. V.13b). Figure V.13c shows that the diameter of the plasma bullet at the beginning is same for all three pulse widths and it decreases at the same rate.

The head-on image of the plasma bullet shows that at the creation of the plasma bullet the plasma is hollow. This donut-shaped plasma bullet gradually contracts to a volume of plasma with no visible empty space in its center along the jet axis. Figure V.14 shows the contraction of the plasma bullet along the jet axis. Contraction of the plasma bullet depends on the gas flow rate and the applied voltage. The time when the contraction of the plasma bullet takes place is higher for increased gas flow rate but this contraction time decreases with the increase of the applied voltage. It shows that the contraction of the plasma bullet occurs at an earlier time (AV = 5 kV, t_{con} = 385 ns; AV = 5.5 kV, t_{con} = 365 ns) for higher AV and contraction happens at a later time for higher GFRs (GFR = 2.8 l/min, t_{con} = 385 ns; GFR = 5.62 kV, t_{con} = 465 ns). As the diameter of the plasma bullet decreases, the empty space inside the plasma bullet also decreases.
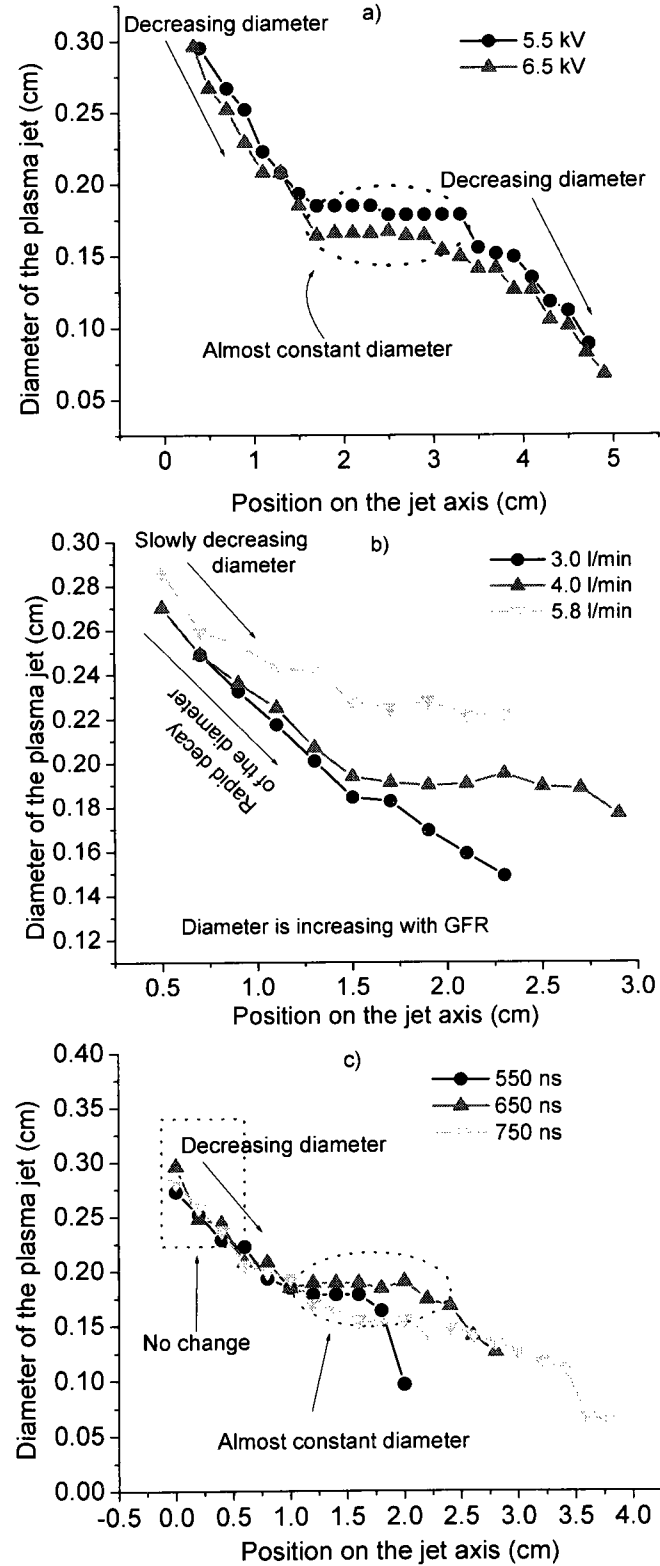
FIG. V.13. Change of the jet diameter along the axis for, a) different AVs, b) different GFRs, and c) different PWs.
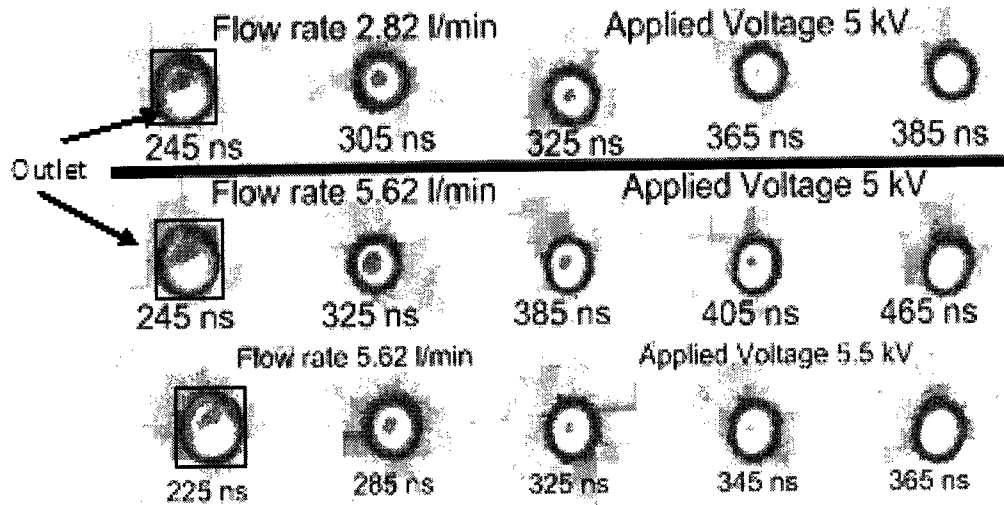
FIG. V.14. Effect of the gas flow rate and the applied voltage on the plasma bullet contraction: The image of the outlet hole (within the square) shows that the bullet form around the surface of the hole as donut shape (white color is the most intense and the blue color is the least intense) and contracted to a volume of plasma bullet. The contraction of the bullet for different flow rates and for different voltages is shown.

To explain the contraction of the plasma bullet, the EF line in the space due to the charge in the donut-shaped plasma bullet was calculated. Consider the initial plasma bullet as a charged ring of radius 'a'. The ring is cylindrically symmetric as in Fig. V.15. The center of the ring is at the center of the XY plane. Let the source point be at r' making an angle α with the X-axis and the observation point is at r distance from the center making an angle θ with Z-axis. A detailed calculation for the EF component in the space due to the ring charge is shown in Appendix B.
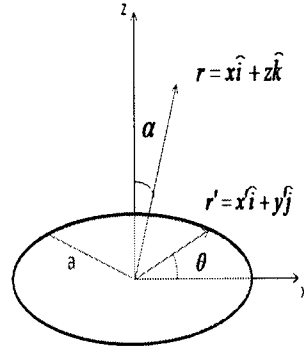
FIG. V.15. Schematic of the EF measurement for a charged ring at any position in the space.

The x and z components of the electric field in the space due to the ring charge are:

$$E_x = \frac{1}{4\pi\varepsilon_0}\frac{Q}{\pi d^2}\left\{\frac{\eta\sin\theta}{(1+\eta^2)^{3/2}}\frac{\pi - \frac{2(\pi-\sqrt{2})\eta}{1+\eta^2}\sin\theta}{1-\frac{2\eta}{1+\eta^2}\sin\theta} - \frac{1}{(1+\eta^2)^{3/2}}\frac{\frac{2\sqrt{2}\eta}{1+\eta^2}\sin\theta}{1-\frac{2\eta}{1+\eta^2}\sin\theta}\right\} \quad \text{(Equ. V.1)}$$

$$E_z = \frac{1}{4\pi\varepsilon_0}\frac{Q}{\pi d^2}\left\{\frac{\eta\cos\theta}{(1+\eta^2)^{3/2}}\frac{\pi - \frac{2(\pi-\sqrt{2})\eta}{1+\eta^2}\sin\theta}{1-\frac{2\eta}{1+\eta^2}\sin\theta}\right\} \quad \text{(Equ. V.2)}$$

At a = 0 and $\theta = 0$

$$E_z = \frac{1}{4\pi\varepsilon_0}\frac{Q}{\pi d^2}\left\{\frac{\eta\pi}{(1+\eta^2)^{3/2}}\right\} = \frac{1}{4\pi\varepsilon_0}\frac{Qr}{(d^2+r^2)^{3/2}} \quad \text{(Equ. V.3)}$$

The maximum EF will be near the charged ring. The EF due to the ring charge in the space close to the ring is shown in Fig. V.16. The EF line inside the ring is towards the center of the ring. The radial EF in the X-Y plane (x > d) is outwards (Fig. V.16a), and the diffusion of air into the helium channel is high along the radial direction. The EF line in the X-Z plane close to the ring (z < d) is towards the jet axis as in Fig. V.16b. The ionization reaction process is high along the center of the plasma bullet and the recombination reaction process is high in the outward direction of the plasma bullet. Because of this cone shaped EF line, the hollow donut-shaped plasma bullet contracts to a volume of plasma and its contraction happens earlier for higher applied voltage. In higher rate of laminar feed gas flow, the number of moles is high in the center of the gas channel and the diffusion of air into the channel is low, so the diameter of the plasma jet does not show a prominent change. Massery and Cannon [54, 55] examined this contraction in low temperature plasma channel in a tube generated by pulsed power, and described the contraction because of the formation of ions in the core and recombination towards the surface.
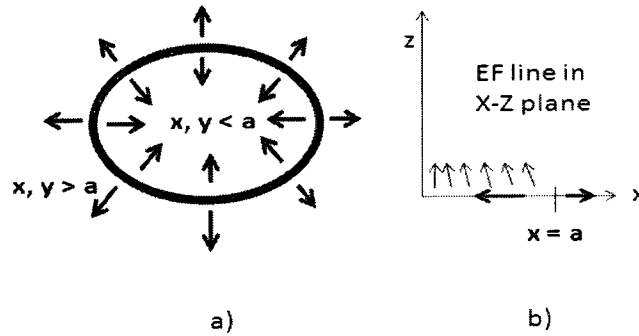
FIG. V.16. EF line due to a charged ring: a) on the X-Y plane and b) on the X-Z plane.

V. 3.3. Electrical Characterization of the Plasma Bullet

The jet current at different positions along the jet axis is measured by using the dielectric probe as in the previous section (V.3.1b) of this chapter. The current density is calculated from the peak jet current and the cross-sectional area of the plasma bullet at that position. These measurements are conducted from 1 cm of the axis until the end of the jet in increments of 0.4 cm. In section V.3.1b it is shown that the jet current peak appears with delay for the different positions of the probe on the jet axis. By using a simple model *(Time delay = linear capacitance x linear resistance x z^2)*, the linear resistance (*r*) of the plasma jet for every jet segment is calculated. Here, z is the distance between the two consecutive positions of the probe. The linear capacitance of the plasma jet is calculated for a specific length of the jet assuming that it is exposed in a uniform electric field [41, 63]. It is considered that the charge is uniform along this specific segment of the plasma channel, which is only an approximation. The linear capacitance of the channel is, $c = \dfrac{\lambda}{U}$. Here, λ is the line charge density and U is the effective voltage due to the charge. The linear capacitance of the plasma jet segment is $c = \dfrac{2\pi\varepsilon_0}{\ln\left(\dfrac{d}{l}\right)}$.

Where *d* is the radius of the jet, *l* is the length of the jet segment and $\varepsilon_0 = 8.54x10^{-14}$ F/cm. The detail calculation of the linear capacitance of a line charge is shown in Appendix B. The estimated linear capacitance of 0.4 cm long plasma jet is 4.2 x 10^{-13} F. This linear capacitance is used in the model to calculate the linear resistance of the plasma jet. The power density (*p*) at different positions along the jet axis is calculated from the jet current by using the following equation:

$$p = \frac{4I^2 r}{\pi D^2} \quad \left(\frac{A^2}{cm^2}\frac{\Omega}{cm}\right) = jE \text{ and } \frac{p}{j} = E \quad \left(\frac{V}{cm}\right) \tag{Equ. V.4}$$

Here, *D* is the diameter of the jet, *j* is the current density, *r* is the linear plasma resistance and *E* is the electric field due to the jet segment.

When the plasma bullet is far from the outlet of the plasma pencil, the effect of applied voltage is insignificant. From the velocity curve, it is found that the propagation phase of the plasma bullet starts around 1.45 cm of the jet axis. Consider that the applied

voltage effect is insignificant and the electric field far from the bullet front is negligible when the plasma bullet propagates further from 1.4 cm of the jet axis. Using Equ. V.4, the average EF of the 0.4 cm long plasma bullet is calculated.

The drift velocity of the electrons is calculated from the following equation, $v_d = \mu_e E$, here μ_e is the electron mobility. In the atmospheric pressure helium plasma, $P\mu_e = 0.86*10^6$ cm^2.Torr/V.s [41]. This estimated electric field is not the local electric field on the plasma bullet's head. The electric field at the head of the plasma bullet is higher than the electric field in the channel behind the plasma bullet. The electron drift velocity calculated for this electric field at atmospheric pressure air ($P\mu_e = 0.45*10^6$ cm^2.Torr/V.s) or in pure nitrogen ($P\mu_e = 0.42*10^6$ cm^2.Torr/V.s) will be half of the calculated drift velocity in atmospheric pressure pure helium but it will be in the same order of magnitude. The average electron density in the plasma bullet (n_e) is calculated from the equation:

$$n_e = \frac{j}{ev_d}$$

(Equ. V.5)

where, j is the current density, e is the electron charge and v_d is the drift velocity of the electron. The current density and the electron density presented in the following sections are only along the propagation phase of the plasma bullet. Even the jet current is measured at 1.0 cm of the jet axis, the power density, reduced electric field, and the electron density at this position are not calculated, because at 1.0 cm of the jet axis, the plasma bullet is still attached to the outlet of the plasma pencil. The jet current measurement at this position is taken to get the time delay between the current peaks at 1.0 cm and 1.4 cm of the jet axis, which is required to measure the plasma parameters at 1.4 cm of the jet axis.

Figure V.17 shows the current density of the plasma bullet along the jet axis for different applied voltages. The current density increases with applied voltage. From the emergence of the plasma bullet, the current density maintains almost a steady state value along the propagation phase of the plasma bullet. At the end of the plasma jet, the current density again increases. It happens because the radius of the plasma bullet decreases at the end of the jet. The average power density and the reduced electric field of the plasma

bullet along the jet axis are estimated by using the Equ. V.4. The average power density of the 0.4 cm long plasma bullet along the jet axis is shown in Fig. V.18. The power density slowly decreases from 1.4 cm of the jet axis and it maintains a steady state power density value along the propagation phase of the plasma bullet. The power density increases with applied voltage. The reduced electric field of the plasma bullet along the jet axis shown in Fig. V.19 follows the same trend as the power density of the plasma bullet. The reduced electric field is the maximum within 0 and 1.5 cm of the jet axis. The reduced electric field fluctuates along the propagation phase for a longer plasma jet. Otherwise it slowly decreases along the propagation phase of the plasma bullet. The estimated electron density along the propagation phase is calculated from the current density and the drift velocity of the electron. This drift velocity of the electron depends on the reduced EF in the plasma. From this experimental investigation, the electron density in the plasma bullet at $z < 1.4$ cm is not investigated because of the difficulties to place the probe close to the outlet. For this reason, it is not possible to measure the electron density along the transition phase of the plasma bullet. The estimated electron density in the plasma bullet shown in Fig. V.20 along the jet axis increases with applied voltage. For the applied voltage of 5 kV and 6 kV, the electron density reaches to the maximum at 1.4 cm of the jet axis. There is a little fluctuation in the electron density value along the propagation phase of the plasma bullet.

The fluctuation of the electron density in the plasma bullet is less when the length of the plasma jet is short. As the drift velocity of electron in the mixture of air in helium will be lower than the calculated drift velocity, the estimated electron density will be higher than this estimated electron density in the plasma bullet. On the other hand, the average electric field is not the local electric field at the tip of the plasma bullet. The local electric field is higher than the average electric field, so the drift velocity of electrons will be higher than the measured electron drift velocity. The drift velocity of the electrons in the plasma bullet is calculated from the average EF and the effect of this EF on the electrons in atmospheric pressure pure helium. This drift velocity depends on the collision frequency of electrons with other species in the plasma. Depending on the electron drift velocity, the electron density in the plasma bullet also changes. To measure the electron density in the plasma bullet, one should know the local electric field and the

gas mixture exactly. Morrow [64] and Wu and Kunhardt [48] also observe a spatial oscillation of the electron density profile in streamer propagation in SF_6 and the mixture of N_2 - SF_6 gas, respectively. Still it does not have any well established explanation. It shows that the estimated average electron density higher when one generates a longer plasma jet. The streamer breakdown model done by Lozanskii [65] shows that at the end of the streamer, the curvature of the streamer front become sharp and the electric field increases at the tip, which increases the electron density and the streamer front velocity. The estimated electron density measured by using the dielectric probe is in the order of 10^{11} cm^{-3}. This result is the same as the measured electron density in atmospheric pressure helium non-thermal plasma jet by using a Rogowski coil [66] and a Langmuir probe [67]. The electron density calculated by using this model for different GFR is shown in Appendix B.
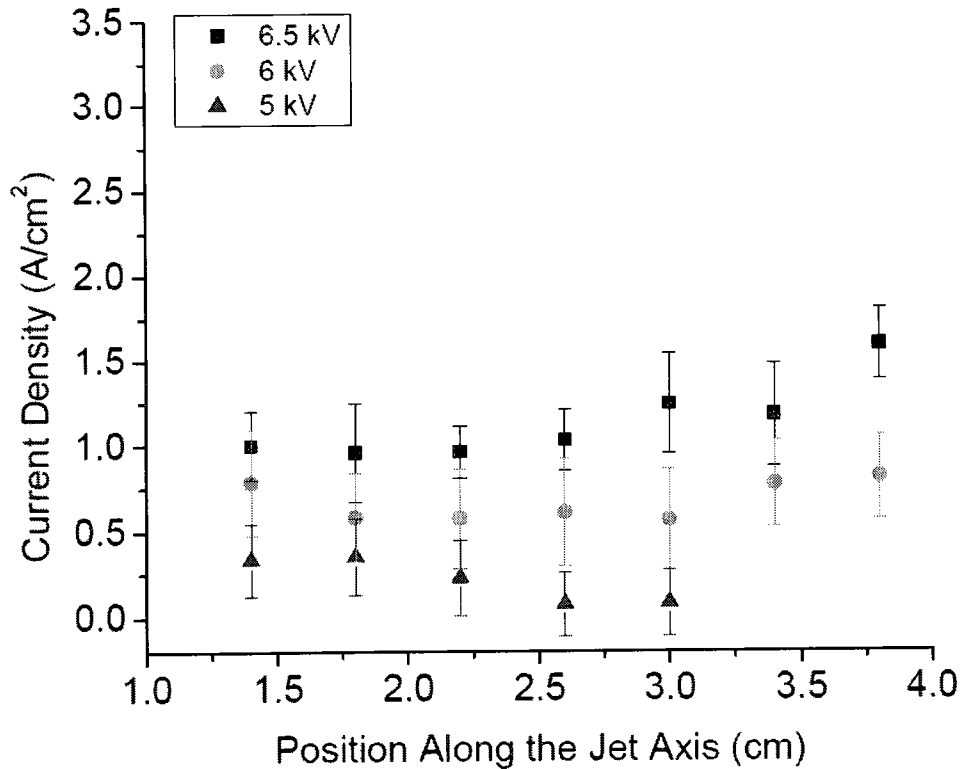
FIG. V.17. Jet current density along the jet axis for three different applied voltages with the pulse width of 550 ns and feed GFR of 3.0 l/min.
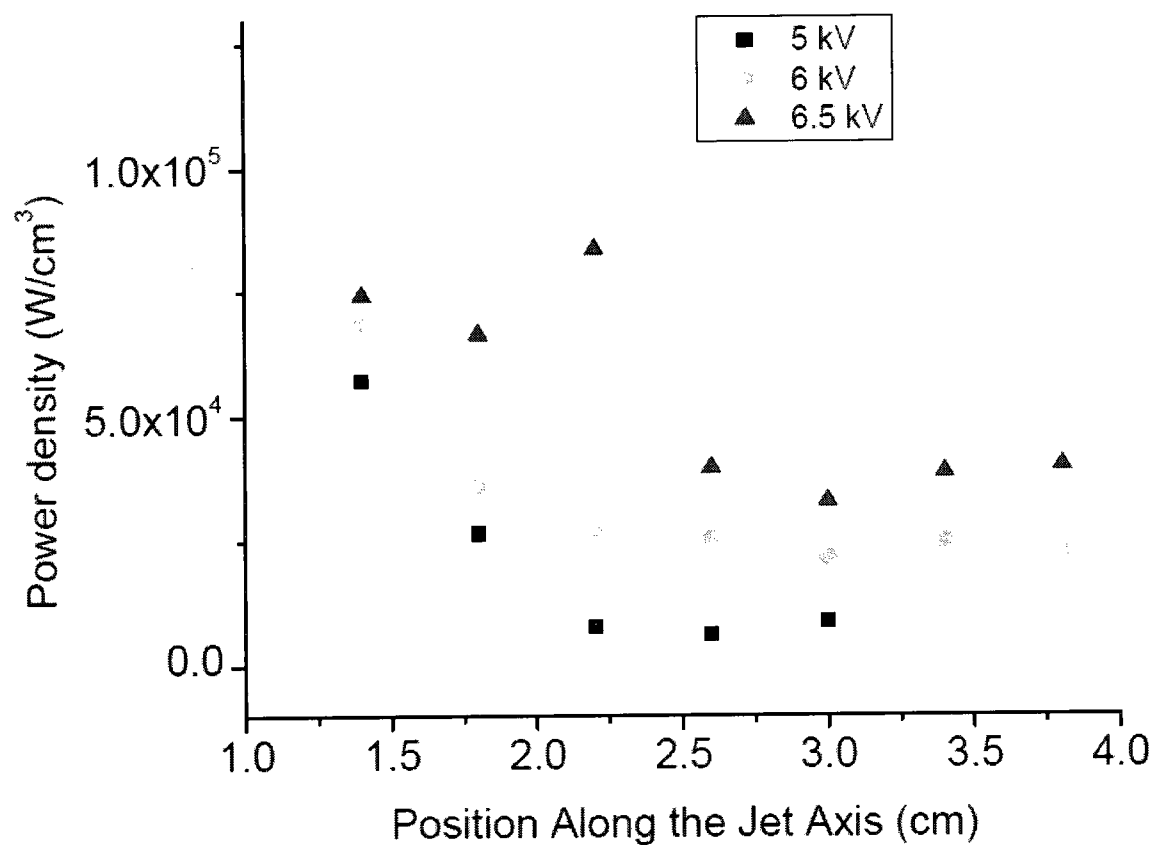
FIG. V.18. Power density of the 0.4 cm long plasma bullet along the propagation phase of the plasma jet.
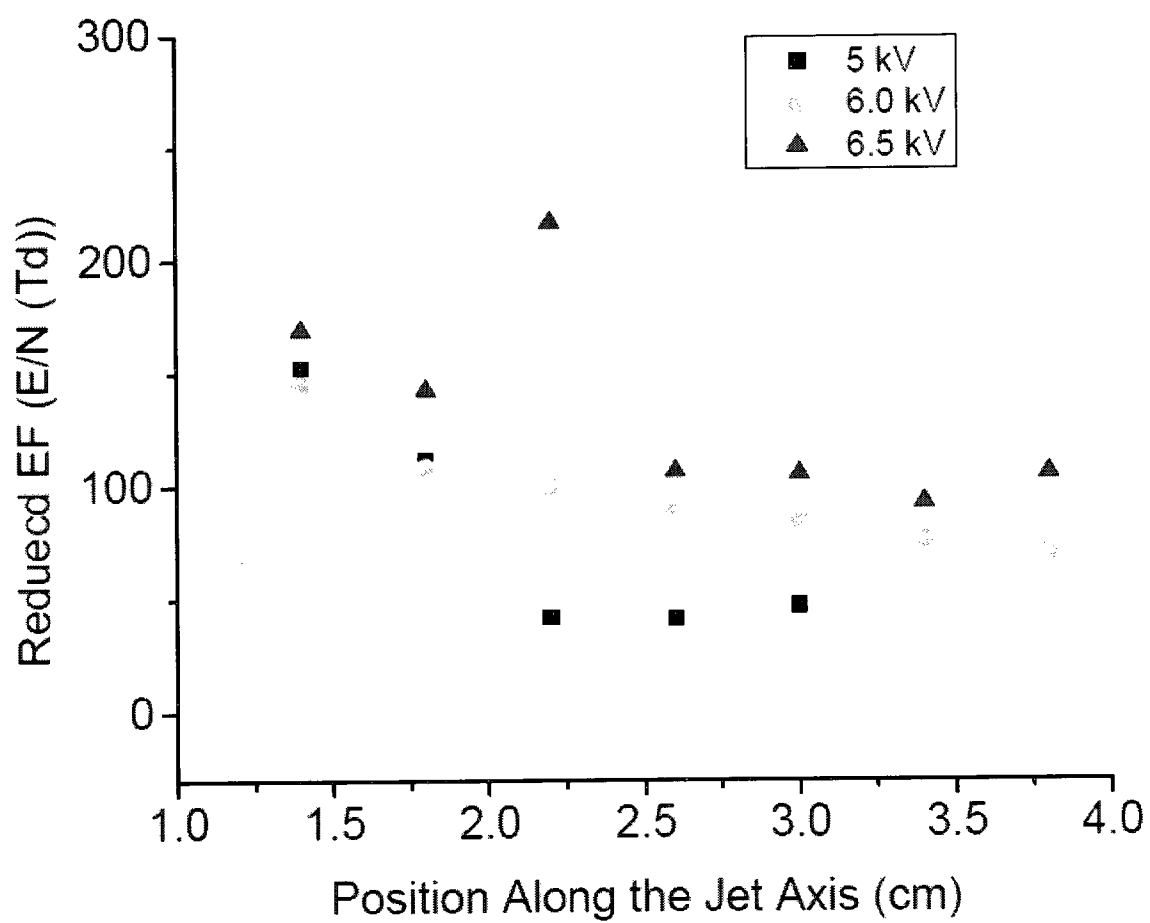
FIG. V.19. Estimated average reduced electric field of 0.4 cm long plasma bullet along the jet's propagation phase.
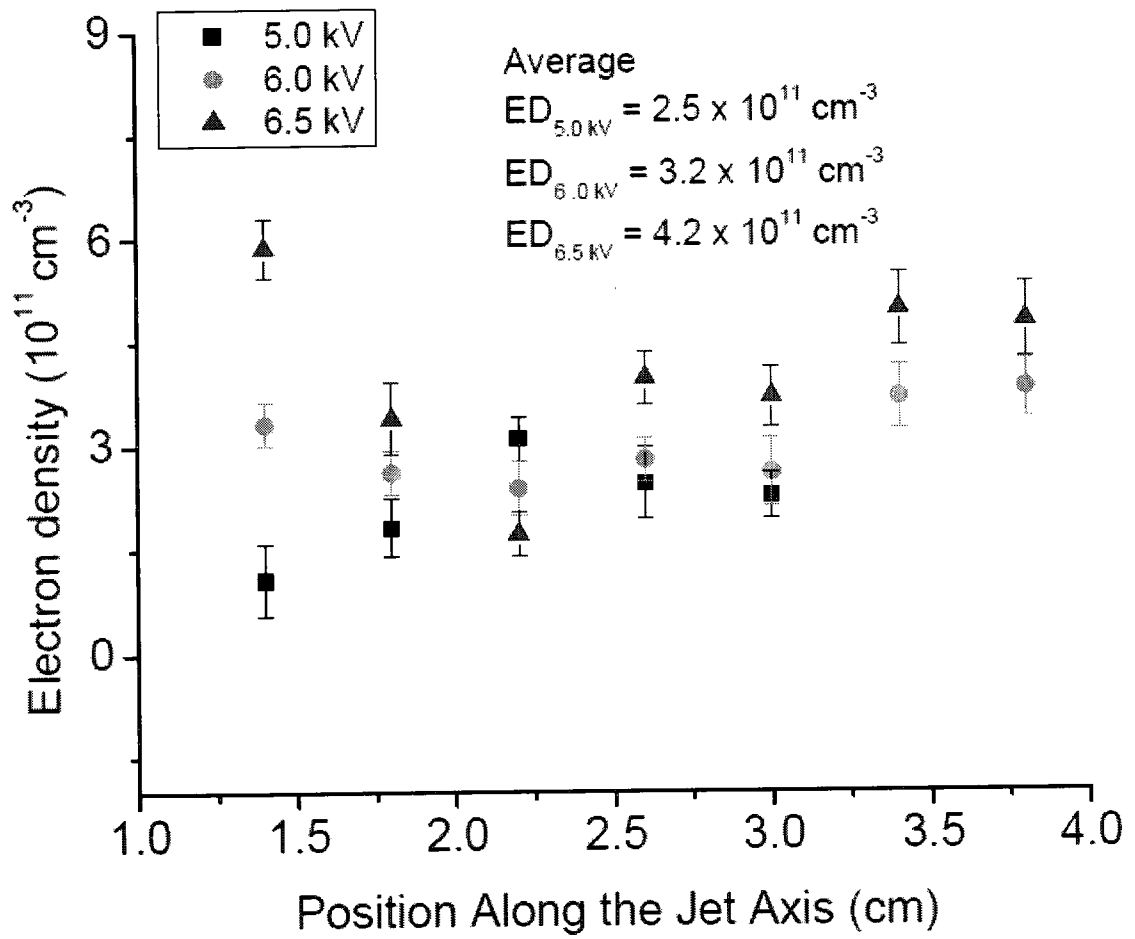
FIG. V.20. Estimated Electron Density (ED) of the plasma bullet along the jet axis for different applied voltages.

V.4. SUMMARY

To understand the propagation of a plasma bullet, the plasma bullet's velocity, size and shape, and the plasma properties in the plasma bullet along the propagation axis for different applied voltages, pulse widths, and feed gas flow rates were investigated. It was found that the plasma bullet velocity changes with the operating conditions of the plasma pencil. The plasma bullet velocity has three distinct phases. These phases in the velocity curve are common in streamer dynamics. For these operating conditions, the transition phase of the plasma bullet ends around 1.45 cm of the jet axis. The plasma bullet's velocity increases with the applied voltage and pulse width. The velocity of the plasma bullet is higher for the longer plasma jets. The length of the propagation phase increases with the plasma bullet's propagation velocity. There is a correlation between the length of the plasma jet, average plasma bullet velocity, and the operating pulse width. All these observations were justified for the plasma bullet velocity measured by two different tools: an ICCD camera and a dielectric probe. The error in the plasma bullet velocity measurement by using a dielectric probe is higher than the plasma bullet velocity measured by using an ICCD camera. The shape and size of the plasma bullet along its propagation pathway changes with applied voltage, pulse width, and gas flow rate. The diameter of the plasma bullet exhibits a constant diameter along the propagation phase. The diameter of the plasma bullet decreases with the increase of the applied voltage. For different pulse widths, the diameter of the plasma bullet is the same along the transition phase. It decreases along the propagation phase for a higher pulse width. The diameter of the plasma bullet increases with gas flow rate. The cone-shape electric field line due to the donut-shaped plasma bullet is responsible for the contraction of the plasma bullet along the jet axis, for which the hollow plasma bullet becomes a volume of plasma. The characterization of the plasma bullet along the jet axis is done by using a dielectric probe. As the investigation of the plasma bullet before 1.4 cm of the axis is not possible with a dielectric probe, the plasma bullet's characteristics in the transition phase is not properly understood by using a dielectric probe. The measured current density and the electron density of the plasma bullet are basically along its propagation phase. The maximum estimated average reduced electric field for the operating applied voltage of 6.5 kV and 6.0 kV is 225 Td and 186 Td, respectively. The maximum reduced electric field is at the

end of the transition phase. It shows a little fluctuation of the electron density value of the plasma bullet, which is propagating in pure helium along the jet axis. The average electron density increases with applied voltage. It was found that the estimated electron density is higher in the longer plasma jets. The plasma bullet has an inconsistent electron density value along the propagation phase, and it is in order of 10^{11} cm^{-3}. At the decay phase of the streamer, the reduced electric field decreases and the gradient of the electric field at the jet front increases, so the local electron density can increase along the decay phase of the plasma jet.

CHAPTER VI

OPTICAL INVESTIGATION OF THE PLASMA JET

VI.1. INTRODUCTION

In plasma applications and research, the observation of the emission spectrum and the estimation of the electric field strength is a common task. The emission spectrum from the excited species and the excitation process of the atoms and molecules in the plasma jet is shown in Chapter III. In this chapter, the spatial evolution of the intensity of different excited species for different operating conditions is presented. This is important to know for the application of the plasma jet. The electric field in the plasma determines the rate of many plasma–chemical reactions. The spatial evolution of the different excited species discloses the plasma chemistry along the jet axis, so the evolution of the energy in the plasma along the jet axis for a known gas mixture is also foreseeable.

VI.2. SPATIAL EVOLUTION OF DIFFERENT EXCITED SPECIES

It was found in Chapter III that the most intense emissions are from the excited nitrogen and helium. Beside that, atomic oxygen and hydroxyl ions are also present in the plasma. The intensity of the different excited species increases with applied voltage within the operating applied voltage (4 – 6.5 kV). The spatial evolution of the intensity of the excited nitrogen ($N_2(C)$ and $N_2^+(B)$) for two different applied voltages is shown in Fig. VI.1a. The intensity of the $N_2^+(390.8 \text{ nm})$ increases from the starting of the plasma bullet and reaches to its peak when the plasma bullet is within 0.6 cm and 1.5 cm of the jet axis. After this position, the intensity of $N_2^+(390.8 \text{ nm})$ decreases slowly. For the applied voltage of 5 kV, the intensity of the $N_2^*(336.6 \text{ nm})$ increases from the starting of the plasma bullet following the same trend as the intensity of $N_2^+(390.8 \text{ nm})$ until 0.9 cm of the jet axis and reaches to its peak at 2.2 cm of the jet axis. For the applied voltage of 6 kV, the intensity of $N_2^*(336.6 \text{ nm})$ reaches to the maximum around 0.6 cm of the jet axis and maintains an almost steady state intensity value until 3.0 cm of the jet axis. The

intensity of the metastable helium (He_m) and atomic oxygen (O) is shown in Fig. VI.1b. The intensity of He (706 nm) increases from the reference position and reaches to its peak around 1.2 cm of the jet axis. For the applied voltage of 5 kV, this intensity decreases linearly until the end of the plasma jet. For the applied voltage of 6 kV, the intensity is almost constant until 1.8 cm of the jet's axis and then decreases linearly. The intensity of O (777.4 nm) does not show prominent difference for these two applied voltages.

The spatial evolution of the intensity of the emission line from excited nitrogen, helium and atomic oxygen for two different pulse widths of the operating applied voltage of 6 kV is shown in Fig. VI.2a and in Fig. VI.2b. Figure VI.2a shows the intensity of the N_2^+ (390.8 nm) and N_2^* (336.6 nm) for the pulse width of 400 ns and 600 ns. The intensity of these species along the jet axis does not change with the pulse width. The maximum intensity of N_2^+ (390.8 nm) is within 0.9 cm and 1.5 cm of the jet axis. The intensity of N_2^* (336.6 nm) for both operating pulse widths shows a sharp increase until 0.6 cm of the jet axis from the beginning of the plasma bullet. This intensity starts to decrease at 2.4 cm and 3.3 cm of the jet axis for the pulse width of 400 ns and 600 ns, respectively. Figure VI.2b shows the intensity of He (706 nm) and O (777.4 nm). The intensities of these species also do not change with pulse widths of 400 ns and 600 ns.

Figure VI.3a and b show the emission intensity from the excited nitrogen, helium, and atomic oxygen for the gas flow rate of 3.0 l/min and 6.8 l/min. The choices of these gas flow rates are to observe the effect of laminar and turbulent gas flow in the plasma jet. At the gas flow rate of 6.8 l/min and applied voltage of 5 kV, there is turbulence in the feed gas channel. The intensity of the different excited species in the plasma bullet along the jet axis is higher for the gas flow rate of 3.0 l/min than the gas flow rate of 6.8 l/min. the intensity value for the turbulent gas flow fluctuates along the jet axis.

For a laminar feed gas flow rate, the intensity of N_2^+ (390.8 nm) and He (706 nm) reaches to its maximum within 0.9 cm and 1.5 cm of the jet axis. In Chapter V, it was found that the transition phase of the plasma bullet ends within 1.0 cm and 1.8 cm of the jet axis, and the plasma bullet velocity is the maximum within these positions. The

intensity of $N_2^*(336.6$ nm$)$ reaches its peak far from the maximum intensity of $N_2^+(390.8$ nm$)$. It is known that the excitation energy of N_2^+ (B) (18.5 eV) is higher than the excitation energy of N_2 (C) (11.0 eV). There is a correlation between the plasma bullet velocity curve along the transition phase and the intensity of He (706 nm), N_2^+ (B), and N_2 (C). The increament of these species along the transition phase is the evidence that the local reduced electric field in this region is increasing. Along the propagation phase of the plasma bullet the intensity of He (706 nm) and N_2^+ (B) decreases, and the intensity of N_2 (C) increases slowly. The plasma chemistry along the propagation phase is dominated by N_2^*. The change of the intensity of the different species along the jet axis depends on the gas mixture. For the gas flow rate of 6.8 l/min, the feed gas flow is turbulent and the mixing of air into the helium channel is nonuniform, so the intensity curve of the different species in the plasma bullet is not in the same shape as the the intensity curve for the gas flow rate of 3.0 l/min.
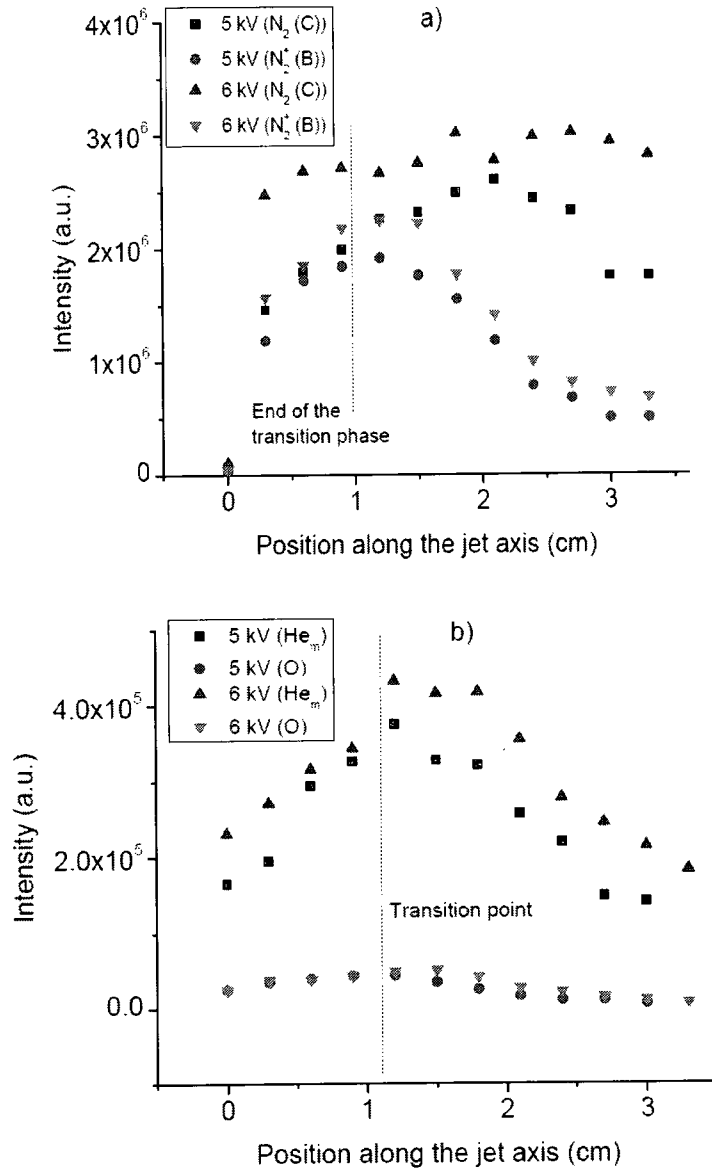
FIG. VI.1. a) Spatial evolution of the different excited species of nitrogen in the plasma bullet for different applied voltages, and b) spatial evolution of the excited helium and atomic oxygen for two different applied voltages (5 kV and 6 kV).
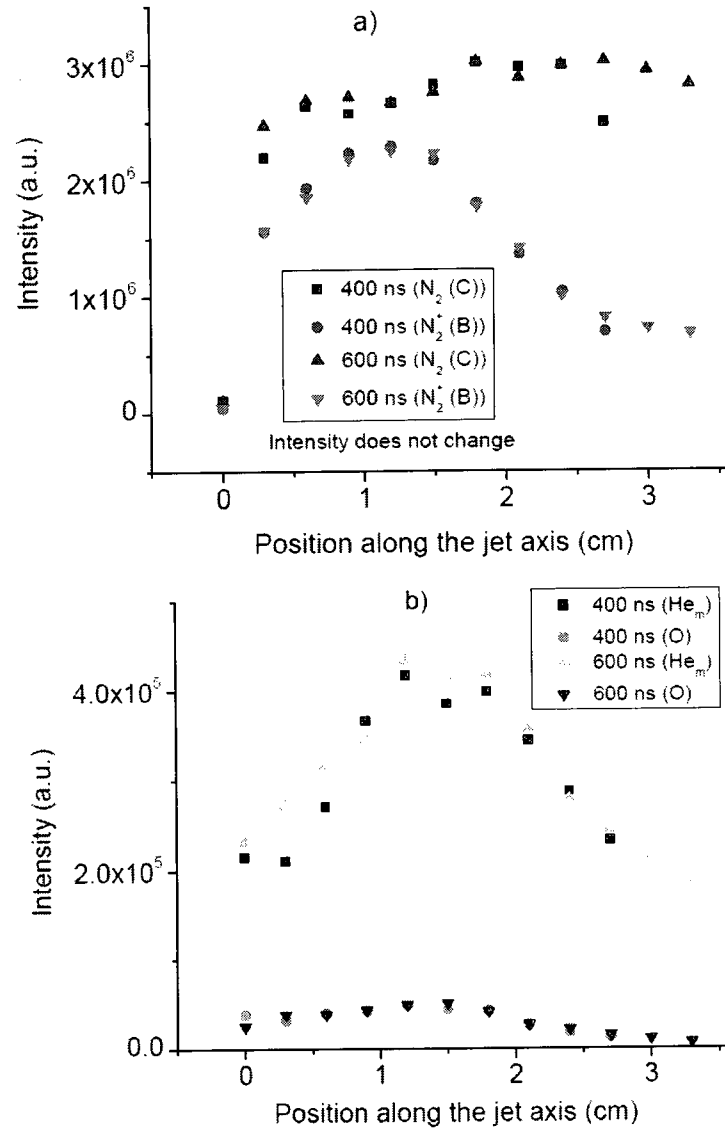
FIG. VI.2. a) Spatial evolution of the different excited nitrogen species in the plasma bullet, and b) spatial evolution of the excited helium and atomic oxygen species of the plasma bullet for two different pulse widths of 400 ns and 600 ns.
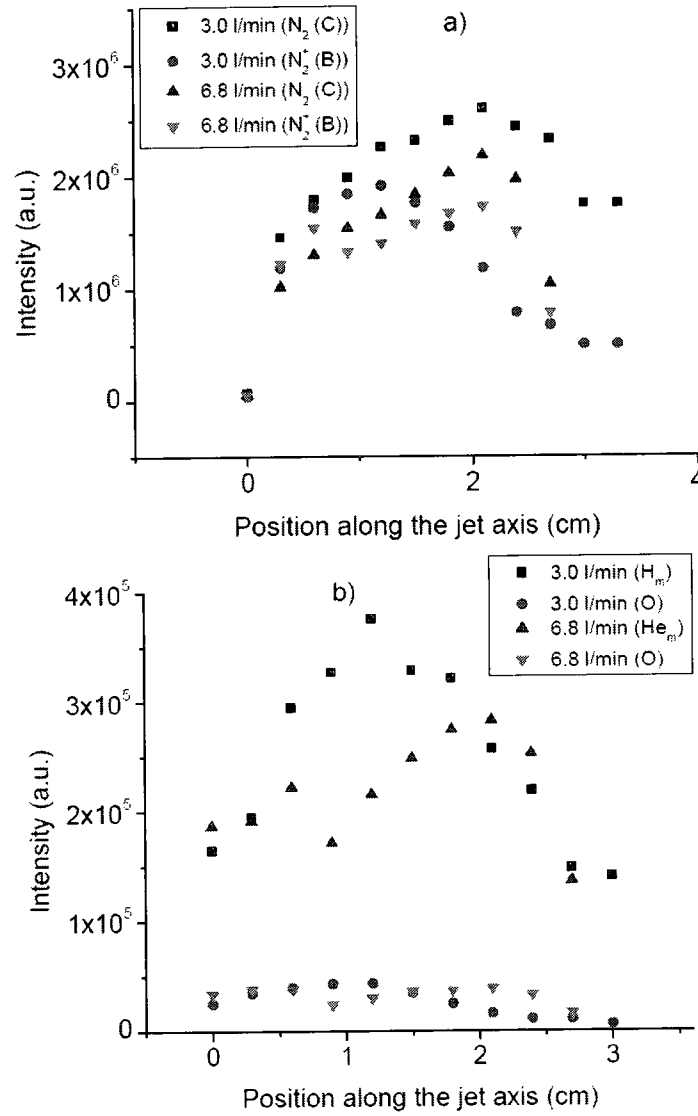
FIG. VI.3. a) Spatial evolution of the different excited nitrogen species in the plasma bullet, and b) spatial evolution of the excited helium and atomic oxygen species in the plasma bullet for two different gas flow rates of 3.0 l/min and 6.8 l/min.

CHAPTER VII

CONCLUSION

VII.1. CONTRIBUTION OF THIS WORK

An electrical discharge was employed to generate a plasma jet in a helium gas channel in the atmosphere pressure air. The physical properties of the plasma jet showed that the applied voltage, pulse width, and feed gas flow rate plays a crucial role in the shape and size of the plasma jet. It was found that two things can stop the propagation of the plasma bullet: one is the insufficient input energy and the other is the lack of a helium gas channel. There is a critical Reynolds number above which the helium gas turns from a laminar flow to a turbulent flow. The transition of the gas flow from laminar to turbulent for the plasma pencil's geometry is identified theoretically, and it is justified from the experimental results. For the plasma pencil's configuration, a helium gas flow rate above 10 l/min becomes turbulent at the beginning of the plasma jet. The plasma jet is bent upwards when the feed gas flow rate is low (<1.14 l/min). The length of the plasma jet increases with applied voltage and pulse width. At a constant gas flow rate, there is an optimum length of the plasma jet for a changing pulse width and applied voltage. An increased applied voltage at the optimum length of the plasma jet splits the head of the plasma bullet in branches. This occurs because of the high energy particles at the tip of the jet. The gas temperature of the plasma jet is in around room temperature and it increases with applied voltage and decreases with feed gas flow rate.

The formation of the plasma jet/bullet was investigated from the discharge properties inside the discharge chamber. The plasma bullet forms from the grounded cathode of the plasma pencil. It is similar to the formation of the positive discharge front. The donut-shaped plasma bullet is due to the surface charge on the grounded dielectric, which expands along the surface of the outlet on the plasma pencil. The estimated electron density inside the gap discharge is in order of 10^{11} cm^{-3}. The formation time of the plasma bullet decreases with applied voltage. With higher applied voltage, more energy is given to the discharge, which accelerates the plasma bullet formation process.

The power and the energy calculation show that 56% of the total input power is used in the discharge. There are two discharges per pulse in the discharge chamber. The plasma bullet forms at the first discharge. The critical input energy and the charge generated in the discharge chamber per pulse to form a plasma bullet is 2.8×10^{-5} J and 1.5×10^{-8} C, respectively for the applied voltage of 3.5 kV. The required minimum charge in the first discharge to generate a plasma bullet is 1.48×10^{-8} C. It was also found that the effect of the amplitude of the applied voltage pulse is more efficient than the duration of the pulse in the plasma jet generation process. The optical/electrical investigation of the plasma bullet at the surface of the outlet of the plasma pencil is not possible, so the plasma at the outlet of the plasma pencil is not well understood.

The propagation velocity measurement by using two different methods for different applied voltages, pulse widths, and feed gas flow rates shows that the plasma bullet velocity is higher when the length of the plasma jet is longer and it is lower when the length of the plasma jet is shorter. The plasma bullet velocity has three distinct phases. The transition phase of the plasma bullet ends up around 1.5 cm of the jet axis for our operating conditions. The length of the propagation phase increases with applied voltage and pulse width that means with the length of the plasma jet. The characteristics of the plasma bullet's velocity curves are similar to the velocity curve of a streamer break down. The collapse of the plasma bullet occurs because of higher air mole fractions in the helium channel, which enhances the attachment reaction process. A correlation between the pulse width and the length of the plasma jet is established from the velocity curve. Even the effect of applied voltage on the plasma jet is more efficient than the pulse width, and the plasma bullet velocity is not constant over its propagation pathway; for a constant pulse width, the length of the plasma jet can be expressed as the multiplication of the average plasma bullet velocity and the pulse duration. This correlation will be useful in the modeling of the plasma bullet's propagation.

Theoretical and experimental investigations have been done to explain the radial contraction of the hollow plasma bullet. It was found that the cone-shaped electric field close to the plasma bullet on the jet axis increases the ionization of the gas on the axis compared to the surface of the plasma bullet, where the recombination reaction process is dominant. This non-uniform ionization process is responsible for the contraction of the

plasma bullet. This contraction of the plasma bullet accelerates with the increase of the input energy. The increased amount of feed gas mole fraction retains the contraction of the plasma bullet. In this case, the reduced electric field decreases with the increase of the feed gas mole fraction, and the ionization process decreases.

The electrical characterization of the plasma bullet along the jet axis for different applied voltages shows that the current density of the plasma jet increases with applied voltage. The estimated average power density and the reduced electric field is the maximum around 1.5 cm of the jet axis. The maximum reduced electric field is within 100 – 350 Td for this work's operating conditions. The estimated average electron density of the plasma bullet along the propagation phase increases with applied voltage. The electron density measurement for different gas flow rates shows that the average electron density is higher when the length of the plasma jet is longer. The estimated electron density, considering that the electron is moving in pure helium, is at the order of 10^{11} cm^{-3}. The electron density curve measured from the intensity ratio of the excited nitrogen also shows the same shape as the electron density curve measured by a dielectric probe.

The emission spectra of the plasma jet show that the most prominent emission lines are from the excited nitrogen, helium, and oxygen. The spatial evolution of the different species in the plasma jet shows that the plasma chemistry is dominated by the excited nitrogen molecules, molecular ion of nitrogen, and helium metastable along the transition phase of the plasma bullet. Along the propagation phase, the plasma chemistry is dominated by the excited nitrogen molecules. The air mixing plays an important role in the plasma chemistry. The collapse of the plasma bullet is due to presence of the electro negative gas oxygen in the gas jet. The estimated reduced electric field from the intensity ratio of the first negative system of nitrogen and second positive system of nitrogen shows that it increases along the transition phase of the plasma bullet and at the end of the transition phase the reduced electric field is at its maximum, so the intensity of the different species is the maximum at that point. The maximum local reduced electric field is 350 Td for the applied voltage of 6 kV. For the same operating conditions, the maximum reduced electric field measured at the end of the transition phase measured by a dielectric probe is 186 Td.

VII.2. RECOMMENDATION FOR FUTURE WORK

Based on the findings from this work, further investigation can be planned for future work. The investigation of the plasma bullet formation has been done only by using the voltage and the current curve of the plasma pencil. The optical investigation of the plasma bullet formation needs to be done to find the specific formation time and formation position. The temporal evolution of the plasma species at the formation position will give the better idea of plasma bullet formation. The temporal and spatial evolution of the absolute number of different species explains the plasma bullet's chemistry and its propagation phenomenon. A complete radial profile of the plasma bullet at different position along the jet axis is required for further investigation.

As the propagation of the positive front is due to the ionization by photoionization process, a collisional radiative model will allow accurate results for a plasma bullet's propagation along the jet axis. It will consider the potoionization in the plasma bullet, which is required for the propagation of the positive front. The experiments need to be conducted in a controlled environment, like inside a chamber, where one can have control on the gas composition.

LITERATURE CITED

[1]   E. Neagu, Matt. Letter **21**, 119 (1994).

[2]   J. Salge, Surf. Coat. Technol. **80**, 1 (1996).

[3]   B. Eliasson and U. Kogelschatg, IEEE Trans. Plas. Sci. **19**, 1063 (1991).

[4]   M. P. Freeman, J. Quant. Spectrosc. Radiat. Transf., **8**, 435 (1968).

[5]   J. Y. Jeong, S. E. Babayan, V. J. Tu, J. Park, R. F. Hicks, and G. S. Selwyn, Plasma Source Sci. Technol., **7**, 282 (1998).

[6]   H. Koinuma, H. Ohkubo, T. Hashimoto, K. Inomata, T. Shiraishi, A. Miyanaga, and S. Hayashi, Appl. Phys. Lett., **60**, 816 (1992).

[7]   A. Schütze, J. Y. Jeong, S. E. Babayan, J. Park, G. S. Selwyn, and R. F. Hicks, IEEE Trans. Plasma Sci., **26**, 1685 (1998).

[8]   M. Teschke, J. Kedzierski, E. G. Finantu-Dinu, D. Korzec, and J. Engemann, IEEE Trans. Plasma Sci., **33**, 310 (2005).

[9]   J. Kedzierski, J. Engemann, M. Teschke, and D. Korzec, Solid State Phenom.,**107**, 119 (2005).

[10] J. L. Walsh, J. J. Shi, and M. G. Kong, Appl. Phys. Lett., **88**, 171501 (2006).

[11] S. Y. Moon, J. K. Rhee, D. B. Kim, and W. Choe, Phys.of Plasmas, **13**, 033502 (2006).

[12] X. Lu and M. Laroussi, J. Appl. Phys., **98**, 023301 (2005).

[13] M. Laroussi and T. Akan, Plasma Process. Polym., **4**, 777 (2007).

[14] M. Laroussi, IEEE Trans. Plasma Sci., **36**, 1612 (2008).

[15] M. Laroussi, A. Fridman, and R. M. Satava, Plasma Process. Polym., **5,** 6 (2008).

[16] E. Stoffels, I. E. Kieft, and R. E. J. Sladek, J. Phys. D: Appl. Phys., **36**, 2908 (2003).

[17] X. T. Deng, J. J. Shi, G. Shama, and M. G. Kong, Appl. Phys. Lett., **87**, 153901 (2005).

[18] C. Cheng, Z. Liye, R. Zhan, Surface Coat. Technol. **200**, 6659 (2006).

[19] G. Chen, S. Chen, M. Zhou, W. Feng, W. Gu, S. Yang, Plasma Sources Sci. Technol. **15**, 603 (2006).

[20] D. B. Kim, J. K. Rhee, S. Y. Moon, W. Choe, Appl. Phys. Lett. **89**, 061502 (2006).

[21] H. Ha, K. Inomata, H. Koinuma, J. Electrochem. Soc. **142**, 2726 (1995).

[22] H. Ha, M. Yoshimoto, H. Koinuma, B. K. Moon, H. Ishiwara, Appl. Phys. Lett. **68**, 2965 (1996).

[23] H. Ha, B. K. Moon, T. Horiuchi, T. Inushima, H. Ishiwara, H. Koinuma, Mater. Sci. Eng., B **41**, 143 (1996).

[24] B. Lee, Y. Kusano, N. Kato, K. Naito, T. Horiuchi, H. Koinuma, Jpn. J. Appl. Phys. **36**, 2888 (1997).

[25] E. Stoffels, A. J. Flikweert, W. W. Stoffels, G. M. W. Kroesen, Plasma Sources Sci. Technol. **11**, 383 (2002).

[26] Y. Duan, C. Huang, Q. Yu, IEEE Trans. Plasma Sci. **33**, 328 (2005).

[27] S. Forster, C. Mohr, W. Viol, Surface Coat. Technol. **200**, 827 (2005).

[28] J. Zhang, J. Sun, D. Wang, X. Wang, Thin Solid Films **506**, 404 (2006).

[29] M. Laroussi, C. Tendero, X. Lu, S. Alla, W. L. Hynes, Plasma Proc. Polym. **3**, 470 (2006).

[30] M. Laroussi and X. Lu, Appl. Phys. Lett., **87**, 113902 (2005).

[31] X. Lu and M. Laroussi, J. Appl. Phys., **100**, 063302 (2006).

[32] G. A. Dawson and W. P. Winn, J. Phys. **183**, 159 (1965).

[33] J. Shi, F. Zhong, J. Zhang, W. D. Liu and M. G. Kong, Phys. Plasmas **15**, 013504 (2008).

[34] E. Bloyet, P. Leprince, M. L. Blasco and J. Marec, Phys. Letters **83A**, 8 (1981).

[35] E. I. Asinovsky, A. N. Lagarkov, V. V. Markovets and I. M. Rutkevich, Plasma Source Sci. and Tech. **3**, 4 (1994).

[36] W. Pan, W. Zhang, W. Ma, and C. Wu, Plasma Chemistry and Plasma Processing **22**, 2 (2002).

[37] G. Arnoult, R. P. Cardoso, T. Belmonte, and G. Henrion, Appl. Phys. Lett., **93**, 191507 (2008).

[38] N. Mericam-Bourdet, M. Laroussi, A. Begum, and E. Karakas, J. Phys. D: Appl. Phys. **42**, 055207 (2009).

[39] Al-Shamma'a, A. I. Wylie, S. R. Lucas, and J. Jiu Dun Yan , IEEE Trans. of Plasma Sci. **30**, 1863 (2003).

[40] S. B. Yildrim and K. A. Agrawal, Exp. in Fluids **38**, 16 (2005).

[41] Y. P. Reizer, *Gas Discharge Physics*, Springer-verlag, 1991.

[42] J. J. Bloomer, *Practical Fluid Mechanics for Engineering Application.* Marcel Dekker, Inc. NY, 2000.

[43] A. Mesegure, Phys. Fluids **15**, 1203 (2003).

[44] J. A. Ratcliffe, *An introduction to the ionosphere and magnetosphere*, Cambridge University Press, Great Britain, 1972.

[45] C. O. Laux, T. G. Spence, C. H. Kruger, and R. N. Zare, Plasma Sources Sci. Technol. 12, 125 (2003).

[46] http://www.nist.gov/index.html (NIST)

[47] A. V. Ivanov, P. N. Penkin, and E. Yu Skoblo, Opt. Spectrosc. **54**, 552 (1983).

[48] C. Wu and E. E. Kundhardt, Phys. Rev. A-Gen. Phys. **37**, 11 (1988).

[49] A. Kara, Ö. Kalenderli, and K. Mardikyan, *Proceedings of the COMSOL Users Conference*, Prague, 2006.

[50] F. V. Topalis and I. A. Stathopulos, *IEEE 6th Int. Conf. Dielectric Materials, Measurements and Applications*, Manchester, 439 (1992).

[51] T. Martens, A. Bogaerts, W. Brok. and J. V. Dijk, Anal Bioanal Chem. **388**, 1583 (2007).

[52] M. Abdel-Salam, H. Singer, and A. Ahmed, J. Phys. D: Appl. Phys. **34** , 1974 (2001).

[53] C. Kenty, Phys. Rev. **126**, 1235 (1962).

[54] J. T. Massey and S. M. Cannon, J. Appl. Phys. **36**, 361 (1965).

[55] J. T. Massey, J. Appl. Phys. **36**, 373 (1965).

[56] I. E. Toader, J. Phys. D: Appl. Phys. **28**, 75 (1995).

[57] Yu B. Golubovskii, A. K. Zinchenko, and Yu M. Kagan, Sov.Phys.-Tech. Phys. **22**, 851 (1977).

[58] B. Yu Golubovskii and R. Sonneburg, Sov. Phys.-Tech.Phys. **24**, 173(1979).

[59] Y. Kabouzi, M. D. Calzada, M. Moisan, K. C. Tran, C. Trassy, J. of Appl. Phys. **91**, 3 (2002).

[60] M. I. Bortnik, I. I. Kochetov, and N. K. Ulyanov, High Teperature **20**, 2 (1982).

[61] A. V. Devidenko, A. B. Dolgoshein, and V. S. Somov, Sov. Phys.-JETP **28**, 2 (1968).

[62] H. K. Wagner, J. of Phys. **204**, 2 (1967).

[63] E. M. Bazelian, Y. P. Reizer, *Spark Discharge.* 1st Ed. CRC-Press, 1998.

[64] R. Morrow, Phys. Rev. A-Gen.Phys. **35**, 1778 (1987).

[65] E. D. Lozanskii, Sov. Phys-Uspekhi **18**, 893 (1975)

[66] A. Shashnurin, M. N. Shneider, A. Dogariu, R. B. Miles, and M. Keidar, Appl. Phys. Lett **94**, 231504 (2009).

[67] O. Sakai, Y. Kishimoto, and K. Tachibana, J. Phys. D: Appl. Phys. **38**, 431 (2005).

[68] J. D. Jackson, *Classical Electrodynamics.* 3rd Ed. Wiley: NY, 1999.

[69] D. J. Griffith, *Introduction to Electrodynamics.* 3rd Ed. Pearson. PLC, 1996.

[70] J. Schwinger, L. L. Deraad, K. A. Milton, W. Y. Tsai, J. Norton, *Classical Electrodynamics.* West view press,1998.

[71] U. V. Rienen, *Numerical methods in Computational Electrodynamics.* Springer, 2001.

[72] F. R. Zypman, Am. J. Phys. **74**, 4 (2006).

[73] S. V. Marshall and G. G. Skitek, *Electromagnetic Concepts and Applications.* Prentice Hall, 1987.

[74] J. R. Reitz, F. J. Milford, and R. W. Christy, *Foundations of Electromagnetic Theory.* Addison-Wesley, 1993.

[75] G. Hartmann, PhD Thesis, Universite de Paris-Sud, Orsay, France, 1977.

[76] Y. L. M. Creghton, *Pulsed positive corona discharge,* PhD Thesis, Eindhoven University of Technology, Netherland, 1994.

[77] K. V. Kozlov, H-E. Wagner, R. Brandenburg, and P. Michel, J. Phys. D: Appl. Phys. **34**, 3164 (2001).

[78] A. F. Djakov, Yu. K. Bobrov, L. N. Bobrova, and Yu V. yourguelenas, *Physics and Technology of Electric Power Transmission.* Moscow: MPEI, 1998.

[79] P. Paris, M. Aints, M/ Laan, and F. Valk, J. Phys. D: Appl. Phys. **37**, 1179 (2004).

[80] R. Brandenburg, V. A. Maiorov, Yu B. Golubovskii, H-E. Wagner, J. Behnke, and J. F. Behnke, J. Phys. D: Appl. Phys. **38**, 2187 (2005).

[81] S. V. Pancheshnyi, S. M. Starikovskaia, and Yu A. Starikovskii, Chem. Phys. Lett. **294**, 523 (1998).

[82] S. V. Pancheshnyi, S. M. Starikovskaia, and Yu A. Starikovskii, Chem. Phys. Lett. **262**, 349 (2000).

[82] D. J. Drake, *Characterization of Microwave Cavity Discharge in a Supersonic Flow*, Ph.D. Dissertation, Norfolk, VA. USA. 2009.

[83] http://www.siglo-kinema.com/database/index.htm (Siglo database).

[84] L.C. Pitchford, S. V. O'Neil, and J. R. Runble Jr., Phys. Rev. A. **23**, 294 (1980).

[85] V. Puech and L. Torchin, J. Phys. D **19**, 2309 (1986).

[86] E. Karakas, M. Koklu, A. Begum, J. Jarrige, and M. Laroussi, 36th *International Conference on Plasma Science (ICOPS),* San Diego, California (2009).

APPENDIX A

EFFECT OF DIELECTRIC BARRIER IN JET FORMATION

The plasma jet is a train of a plasma bullet/plume form from the outlet of a discharge chamber. At the beginning, the bullet is hollow-like donut. It is predicted that the surface wave discharge might play a major the role in bullet formation. Most of the non-thermal atmospheric pressure plasma jets discharge is in the dielectric barrier configuration, called the Dielectric Barrier Discharge (DBD) plasma jet. A plasma plume/bullet is not only generated from a DBD discharge, single electrode plasma pencils, plasma needles, and pin electrode plasma pencils can also generate a plasma jet. The gas discharge always takes place in all directions from the high voltage electrode, but if there is any dielectric nearby, it shows a fast growth towards the closest dielectric and the discharge grows along the dielectric surface [41]. If the dielectric surface is not close enough, the bulk gas discharge begins first. A dielectric barrier has an immense influence on the formation, propagation, and the chemistry of a plasma jet. A dielectric barrier has a strong influence on plasma jet formation but it is not essential to generate a plasma jet. Plasma jets can be generated from a bear electrode, which is powered by high voltage and is exposed in a gas flow.

To investigate the effect of dielectric barrier on the plasma jet, three different plasma pencils were used (Fig. A.1): i) single electrode plasma pencil, ii) pin electrode plasma pencil, and iii) single electrode plasma pencil with a dielectric barrier. All these plasma jets are configured with a pin electrode. In the single electrode plasma pencil, a pin electrode is placed inside a dielectric tube (Fig. A.1a) where, in the pin electrode plasma pencil, the tip of the electrode is exposed in the ambient atmosphere as in Fig. A.1b. A plasma jet generated from the single electrode plasma pencil was investigated and compared with the investigation result of the jet generated by single electrode plasma pencil with a dielectric barrier in front of its propagation axis. The only difference between these two pencils is the dielectric barrier on the jet propagation axis. All these plasma pencils are operated at high voltage pulse varied from 4-10 kV with the pulse width of 300-800ns and the frequency range of 3-10 kHz. The image of the plasma

discharge inside the pencil was taken with a Di-pro ICCD camera with an exposure time of 10ns-20ns and 20ns delay.

The camera is set at the tangential position to the jet axis to capture the axial expansion of the plasma bullet. The plasma bullet's velocity is measured from the image of the plasma bullet taken by ICCD camera with the exposure of 20 ns and 20 ns delay. The front view and side view image of the plasma bullet formation point are taken by placing the ICCD camera at head-on view and at the tangential position of the jet axis. The spatial evolution of the different species in the plasma jet along the jet propagation axis is observed by optical emission spectroscopy.
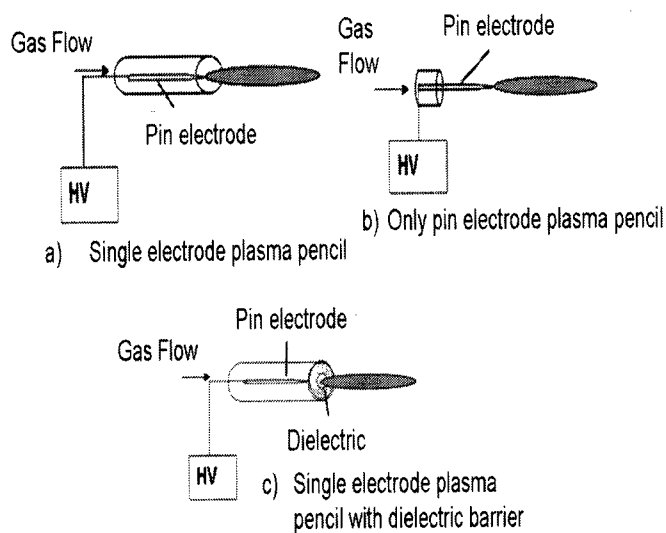

Figure A.1. Different kinds of plasma pencils: a) single electrode plasma pencil, b) pin electrode plasma pencil, and c) single electrode plasma pencil with a dielectric barrier.

The front view of the single electrode plasma pencil shows that the discharge starts from the tip of the pin, expands towards the nearby dielectric tube and propagates along the surface of the tube (Fig. A.2a). The side view of this plasma pencil shows that, when the plasma bullet comes out from the tube in the ambient atmosphere, the expanded bulk discharge from the tip of the pin and the surface discharge from the tube inner surface contracts to a single head. For a pin electrode configuration, discharge happens along the axis from the tip of the pin. As there is no nearby dielectric surface, no surface discharge is observed (Fig. A.2b). In this case the plasma bullet is not hollow in shape. It is known that in the presence of a dielectric barrier at the beginning of the plasma jet, the plasma bullet forms from the surface of the outlet hole. It is found that if there is a nearby dielectric, the discharge expands through the dielectric surface, so there is a possibility to have a donut-shaped plasma bullet. Otherwise the plasma bullet is a bulk of plasma. The dielectric barrier attached to the outlet is superfluous in the single electrode plasma pencil.
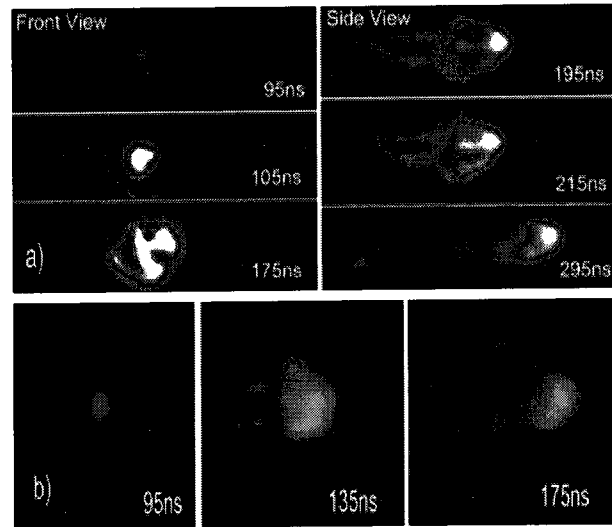

FIG. A.2. a) Front and side view of the single electrode plasma pencil, and b) side view of the pin electrode plasma pencil.

For a single electrode plasma pencil, plasma bullet velocity decreases along the jet axis (Fig. A.3a). An additional dielectric barrier in front of the single electrode plasma pencil changed the shape of the plasma bullet's velocity curve (Fig. A.3b). This dielectric barrier in the bullet's propagation axis increases its velocity from the beginning to 1.7 cm of the plume/bullet's propagation axis. Within 1.7 cm and 3.5 cm along the jet axis plasma bullet velocity is almost the constant and after that position it shows a fast decay of the velocity. The shape of this velocity curve is same as the velocity curve of the jet generated by a plasma pencil. The plasma bullet velocity generated from the single electrode plasma pencil is lower than the plasma bullet velocity generated by the single electrode plasma pencil with a dielectric barrier. The presence of the dielectric barrier changes the electric field for the similar electrode configuration. The non-uniformity of the electric field at the high voltage plays a pivotal role in the jet's propagation velocity.
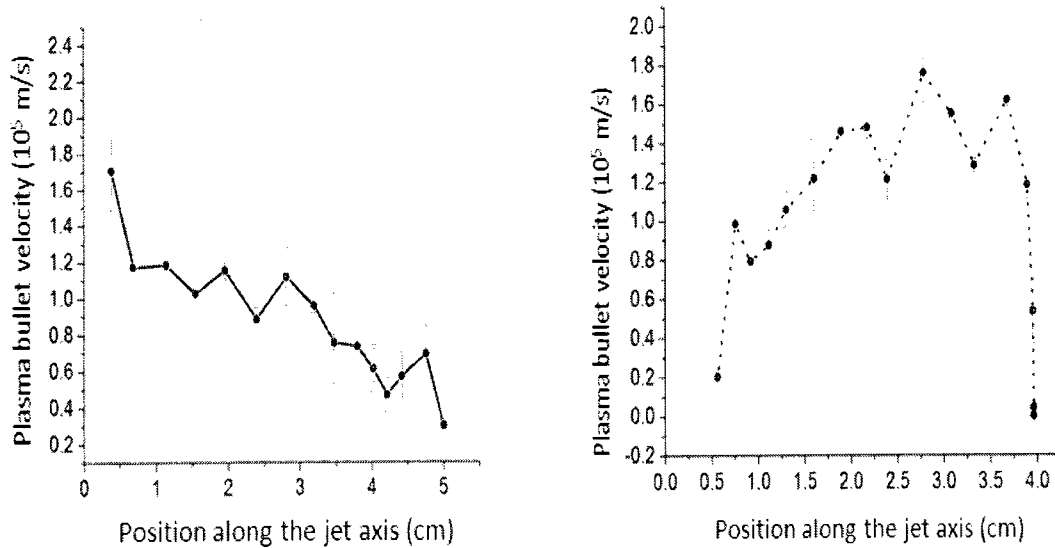
FIG. A.3.a) Plasma bullet velocity for single electrode configuration, and b) plasma bullet velocity for single electrode plasma pencil with a dielectric barrier [GFR = 4.2 l/m, f = 4 kHz, PW = 500ns, AV = 6 kV].

The spatial evolution of the emission spectrum of N_2^+ (B) always follows the similar shape as the plasma bullet's velocity curve. Beside the emission from excited N_2^+ (B), there is emission from different excited states of nitrogen, helium, atomic oxygen, and hydroxyl. For a single electrode pencil, the emission intensity of the different species along the jet's propagation axis shown in Fig. A.4a decreases as the velocity curve of this plasma jet decreases. Generally, the electric field of a pin electrode decreases along the axis, so the intensity of the different species also decreases. An extra perforated dielectric barrier in front of the pin electrode increases the intensity of the different species along the jet axis (Fig. A.4b), and the emission intensity of N_2^+ (B) is at its peak around 1.5-2.5 cm of the jet axis when the velocity is at its peak around 1.7-3 cm of the jet axis. The intensity of the emission from the metastable helium (706 nm) and the N_2^+ (B) changes in the same manner, i.e. penning ionization plays an important role in plume propagation. An external dielectric barrier changes the plasma jet's chemical properties. It changes the chemistry of the plasma jet along the jet axis.
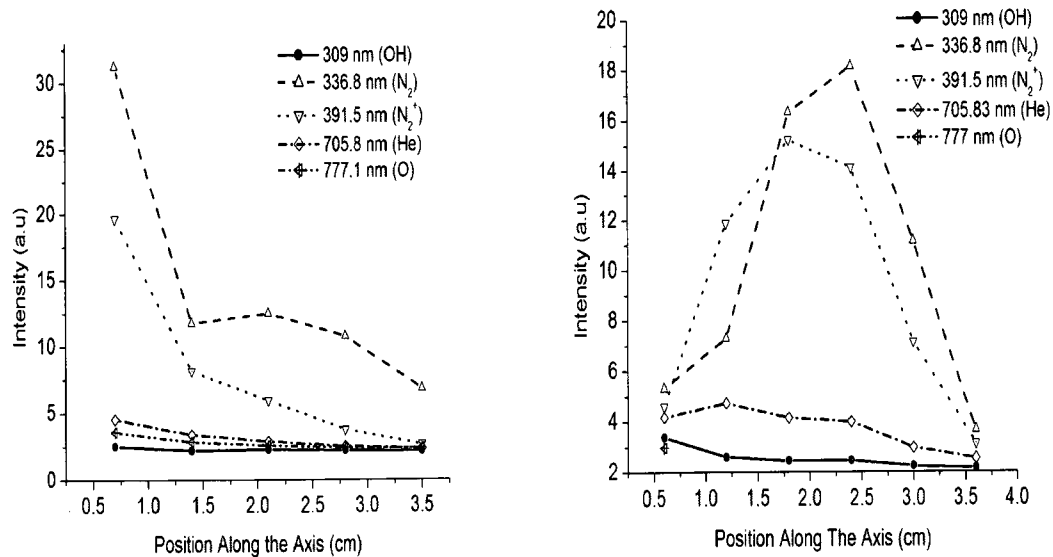

FIG. A.4. a) The emission spectra of the only single electrode plasma pencil along the jet's axis, and b) The emission spectra of the Pin with a dielectric barrier [GFR = 4.2 l/m, AV = 6 kV, PW = 500ns, f = 4 kHz].

In summary, it can be said that it is not necessary that the plasma jet will form in a donut shape. Only when it forms from the dielectric outlet, can there be a donut-shaped hollow plasma bullet. The dielectric barrier on the plasma jet's propagation axis plays an important role in a jet's propagation phenomenon. The dielectric barrier enhances the plasma chemistry. All the species' intensity increases when there is a dielectric barrier on the jet axis. The plasma jet velocity is related to the plasma chemistry, especially the intensity of the N_2^+ and N_2^*. The velocity of the plasma bullet increases with the excited species intensity. When the excited species starts to decrease the velocity of the bullet also decreases.

APPENDIX B

B.1. Linear Capacitance of the Plasma Jet

A streamer has a finite conductivity and one may consider a small segment of a plasma jet with a uniform charge distribution. There is no external electric field on the jet segment. So, the linear capacitance of the channel is, $c = \dfrac{\lambda}{U}$. Here, λ is the line charge density and U is the potential due to these charge. Figure B.1 shows the schematic of the plasma jet segment of l cm. In calculating the potential, $z = 0$ is taken at the middle of the jet's segment. In this way, the charge on the both direction contribute to the potential.
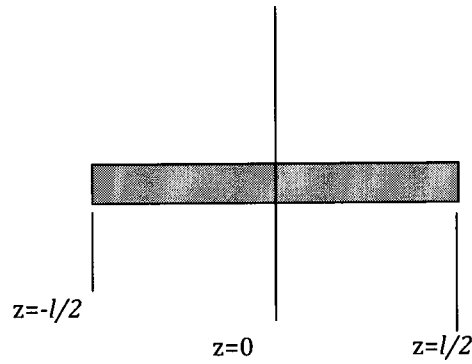
z=-l/2   z=0   z=l/2

FIG. B.1. Schematic of the jet segment.

$$U(l/2) = \frac{\lambda}{4\pi\varepsilon_0} \int_{-l/2}^{l/2} \frac{dz}{(z^2+r^2)^{1/2}} = \frac{\lambda}{4\pi\varepsilon_0} \ln\left(\frac{\{l/2 + ((l/2)^2+r^2)^{1/2}\}}{\{-l/2 + ((-l/2)^2+r^2)^{1/2}\}}\right)$$

$$= \frac{\lambda}{4\pi\varepsilon_0} \ln\left(\frac{\{l/2+((l/2)^2+r^2)^{1/2}\}^2}{r^2}\right) \qquad \text{(Equ. B.1)}$$

As the radius $r << l$, r^2 on the numerator can be neglected.

$$U(l/2) = \frac{\lambda}{2\pi\varepsilon_0} \ln\left(\frac{(l/2+l/2)}{r}\right)$$

$$\therefore U(l/2) = \frac{\lambda}{2\pi\varepsilon_0} \ln\left(\frac{l}{r}\right)$$

$$\text{Linear capacitance}, c = \frac{\lambda}{U} = \frac{2\pi\varepsilon_o}{\ln\left(\frac{l}{r}\right)} \qquad \text{(Equ. B.3)}$$

B.2. Electric Field Calculation for a charged Ring

Consider the initial plasma bullet as a charged ring of radius 'a'. The ring is cylindrically symmetric as in Fig. B.2. The center of the ring is at the center of the XY plane. Let the source point be at r ' making an angle α with the X-axis and the observation point is at r distance from the center making an angle θ with Z-axis. Due to axial symmetry, r is the function of z and x only. The distance of the observation point r was expressed in terms of the radius of the ring.
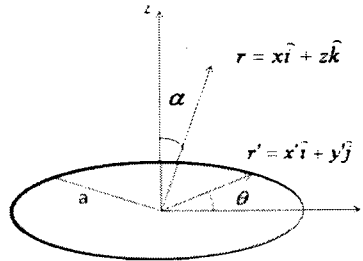

FIG. B.2. Schematic of the charged ring to calculate the electric field at any position in the space.

If the line charge in the ring is λ and the total charge is Q, the electric field due to the ring charge can be expressed as [68-70],

$$E = k\lambda \int \frac{(r - r')}{|r - r'|^3} dr'$$

(Equ. B.4)

Here $k = \dfrac{1}{4\pi\varepsilon_0}$

Express the distance of the observation point, $r = a\eta$. At the ring, $\eta = 1$

$$r' = aCos\theta \hat{i} + aSin\theta \hat{j}$$
$$r = a\eta Sin\alpha \hat{i} + a\eta Cos\alpha \hat{k}$$

$$r - r' = (a\eta Sin\alpha \hat{i} + a\eta Cos\alpha \hat{k}) - (aCos\theta \hat{i} + aSin\theta \hat{j})$$
$$= a[(\eta Sin\alpha - Cos\theta)\hat{i} + \eta Cos\alpha \hat{k} - aSin\theta \hat{j}]$$

(Equ. B.5)

$$Let, [(\eta Sin\alpha - Cos\theta)\hat{i} + \eta Cos\alpha \hat{k} - aSin\theta \hat{j}] = X$$

$$|r - r'|^3 = [a((\eta Sin\alpha - Cos\theta)\hat{i} + \eta Cos\alpha \hat{k} - Sin\theta \hat{j})]^3$$
$$= a^3[((\eta Sin\alpha - Cos\theta)\hat{i} + \eta Cos\alpha \hat{k} - Sin\theta \hat{j})^2]^{3/2}$$
$$= a^3[(\eta Sin\alpha - Cos\theta)^2 + \eta^2 Cos^2\alpha + Sin^2\theta]^{3/2}$$
$$= a^3[\eta^2 Sin^2\alpha + Cos^2\theta - 2\eta Sin\alpha Cos\theta + \eta^2 Cos^2\alpha + Sin^2\theta]^{3/2}$$
$$= a^3[\eta^2 + 1 - 2\eta Sin\alpha Cos\theta]^{3/2}$$

(Equ. B.6)

$$Let, [\eta^2 + 1 - 2\eta Sin\alpha Cos\theta]^{3/2} = Y$$

$$and, \chi = \frac{2\eta Sin\alpha}{\eta^2 + 1}$$

$$Y = (\eta^2 + 1)^{3/2}[1 - \chi Cos\theta]^{3/2}$$

$$dr' = ad\theta$$

In the ring charge, the radius is constant and there is no charge along the radial direction. Because of the axial symmetry, the integration on y-axis will be vanished. Integration only will be around the z-axis.

$$E = k\lambda \int \frac{(r - r')}{|r - r'|^3} dr'$$

$$E = k\frac{Q}{2\pi a} \int_0^{2\pi} \frac{a^2 X d\theta}{a^3 Y} = k\frac{2Q}{2\pi a} \int_0^{\pi} \frac{a^2 X d\theta}{a^3 Y} = k\frac{Q}{\pi a^2} \int_0^{\pi} \frac{[(\eta Sin\alpha - Cos\theta)\hat{i} + \eta Cos\alpha \hat{k} - aSin\theta \hat{j}]d\theta}{Y}$$

The electric field components are:

$$E_x = k\frac{Q}{\pi a^2}\int_0^\pi \frac{[\eta Sin\alpha - Cos\theta]d\theta}{Y} = k\frac{Q}{\pi a^2}\int_0^\pi \frac{\eta Sin\alpha d\theta}{Y} - k\frac{Q}{\pi a^2}\int_0^\pi \frac{Cos\theta d\theta}{Y}$$

(Equ. B.8)

$$E_z = k\frac{Q}{\pi a^2}\int_0^\pi \frac{\eta Sin\alpha d\theta}{Y}$$

The integrations are only on θ, so all other terms are constant and for simplicity, these can be took out of the integration.

$$I_1 = \int_0^\pi \frac{d\theta}{Y}$$

(Equ. B.9)

$$I_2 = \int_0^\pi \frac{Cos\theta d\theta}{Y}$$

Here α is within 0-π.

The numerical solution of these integral for the convergence of the electric field result is done as in [71-74]. It shows that:

$$(1-\chi)I_1 \approx \pi - (\pi - \sqrt{2})\chi$$

(Equ. B.10)

$$(1-\chi)I_2 \approx \sqrt{2}\chi$$

Plug the values of Y, χ and the integral results in Equ. B.9 in the electric field Equ. B.5.

$$E_x = k\frac{Q}{\pi a^2}\left\{\frac{\eta Sin\theta}{(1+\eta^2)^{3/2}}\frac{\pi - \dfrac{2(\pi-\sqrt{2})\eta Sin\theta}{1+\eta^2}}{1-\dfrac{2\eta Sin\theta}{1+\eta^2}} - \frac{1}{(1+\eta^2)^{3/2}}\frac{\dfrac{2\sqrt{2}\eta Sin\theta}{1+\eta^2}}{1-\dfrac{2\eta Sin\theta}{1+\eta^2}}\right\}$$

(Equ. B.11)

$$E_z = k\frac{Q}{\pi a^2}\left\{\frac{\eta Cos\theta}{(1+\eta^2)^{3/2}}\frac{\pi - \dfrac{2(\pi-\sqrt{2})\eta Sin\theta}{1+\eta^2}}{1-\dfrac{2\eta Sin\theta}{1+\eta^2}}\right\}$$

B.3. Reduced Electric Field and Electron Density measurement

The reduced electric field is measured from the ratio of the second positive system of nitrogen (B state) and the first negative system of nitrogen (C state) for the

band head of 0-0 transition as in [75-82]. For this measurement, it is considered that the excitation of the nitrogen is mainly due to the direct electron excitation. The excitation rate coefficient of these two bands is calculated by using Bolsig+ Boltzmann equation solver following the same process as in [83-85]. The measured local reduced electric field in the plasma jet along the jet axis is shown in Fig. B.3. The maximum local reduced electric field is 350 Td at 1.12 cm of the jet axis. Along the transition phase, the local reduced EF increases like the velocity curve. From the gas kinetic modeling, the mobility of electron for different amount of gas composites (He/N_2/O_2) and reduced electric field are also calculated. The amount of air mixture in helium is estimated from [86]. Figure B.4 shows the mobility of electron for differen amount of air admixture in the effect of different reduced electric fields. The electron mobility is height for the lower reduced EF. For 1% of the air admixture with helium, the electron mobility is lower than the electron mobility in the helium gas mixture with 5-20% of air. This electron mobility decreases rapidly from the reduced EF of 10 Td until the reduced electric field of 50 Td. From this point the electron mobility increases with reduced EF for the 1% and 5% of the air admixture with helium. This rate of increament is higher for the 1% air than the 5% air admixture with helium. For the air admixture of 10%, the mobility is almost the constant with increased reduced EF, and it slowly decreases with reduced EF for the air admixture of 20%. The electron density is estimated as in Chapter V.3.3, by using the local EF and the electron mobility, which is found by solving the Boltzmann transport equation. The electron density shown in Fig. B.5 is in the order of 10^{11} cm^{-3}. Along the propagation phase, the electron density is almost constant and it shows a little increase of the electron density at the end of the jet. The electron density estimated for different feed gas flow rates by using a dielectric probe is shown in Fig. B.6. The average electron density is height at the gas flow rate of 3.4 l/min. At the same operating conditions (AV = 5 kV, PW = 500 ns, and f = 4 kHz) with a changed gas flow rate, the longest plasma jet has been generated for the GFR of 3.4 l/min.
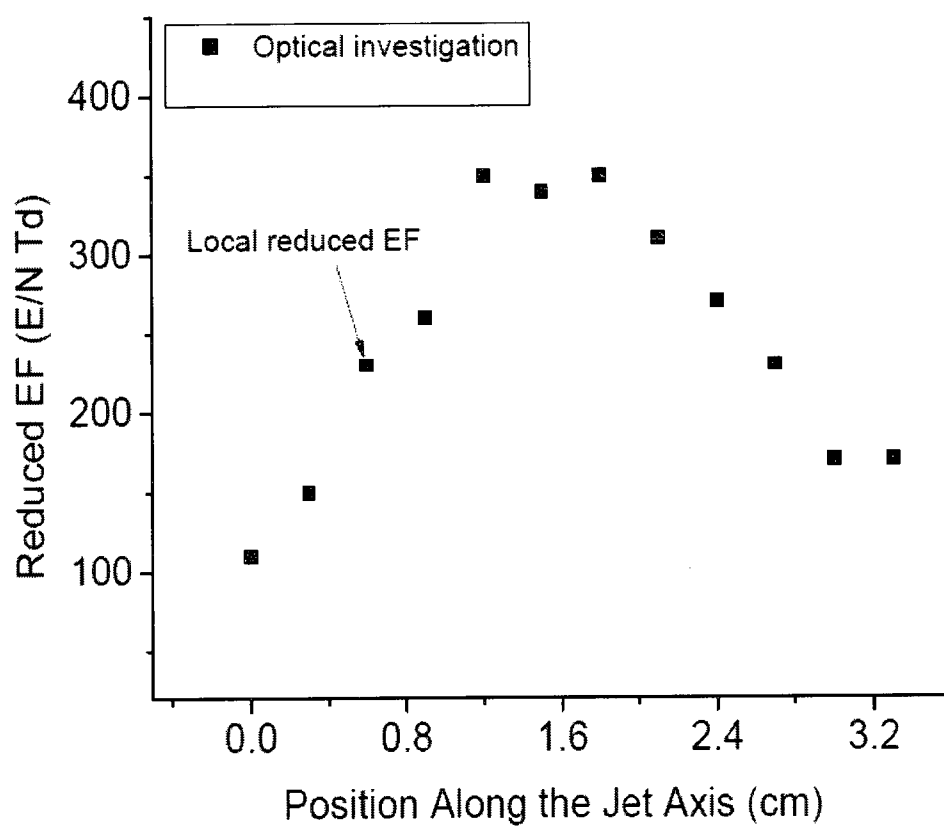
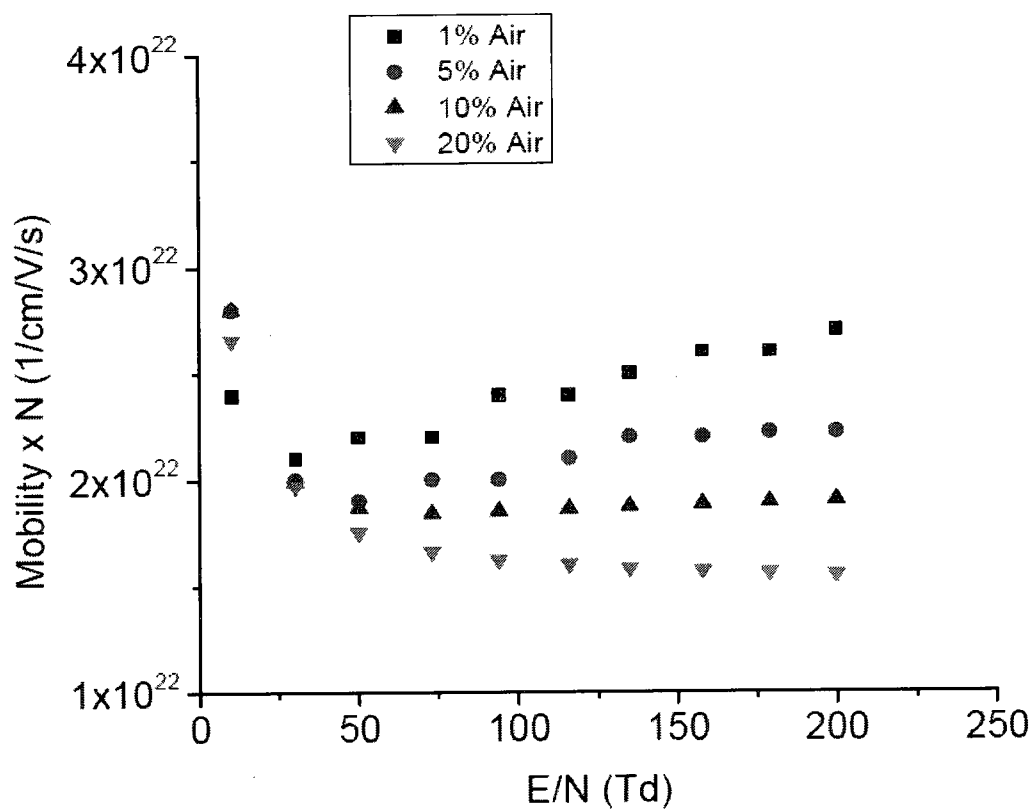Fig. B.3. Local reduced electric field of plasma jet along the jet axis.

Fig. B.4. Electron mobility in the discharge channel for different reduced electric field and for different amount of air admixture.
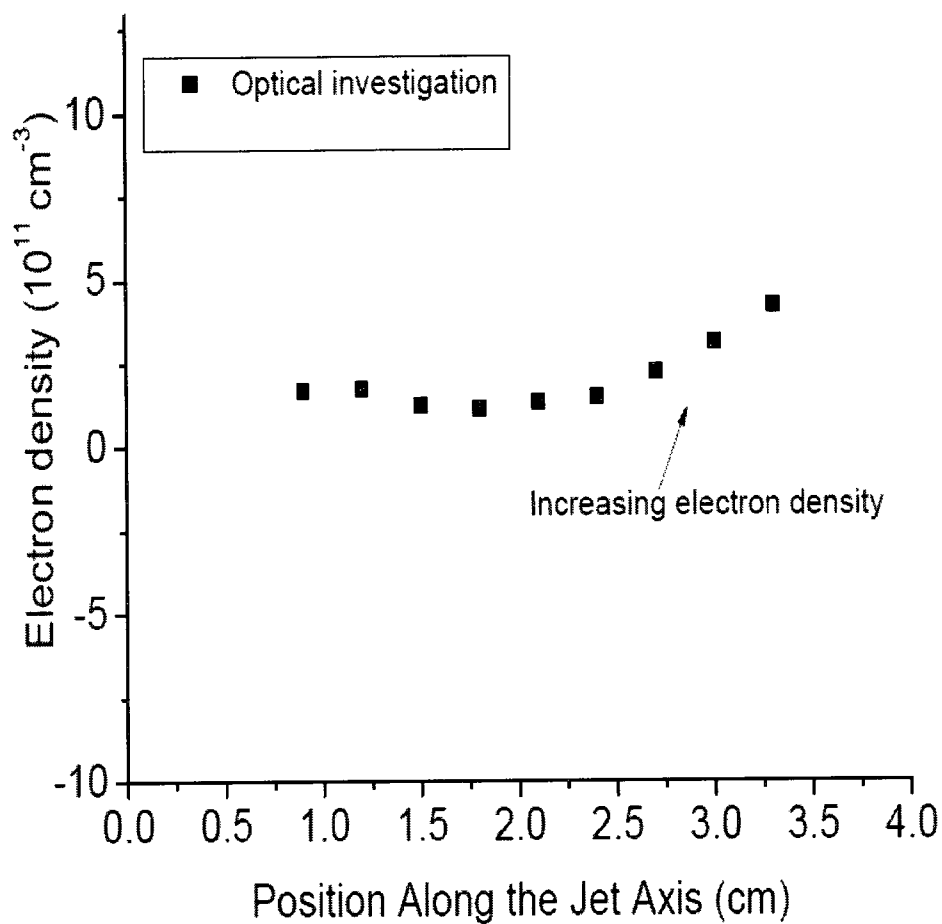
FIG. B.5. Electron density in the plasma jet along the jet axis for the operating AV = 6 kV, PW = 500 ns, and f = 4 kHz.
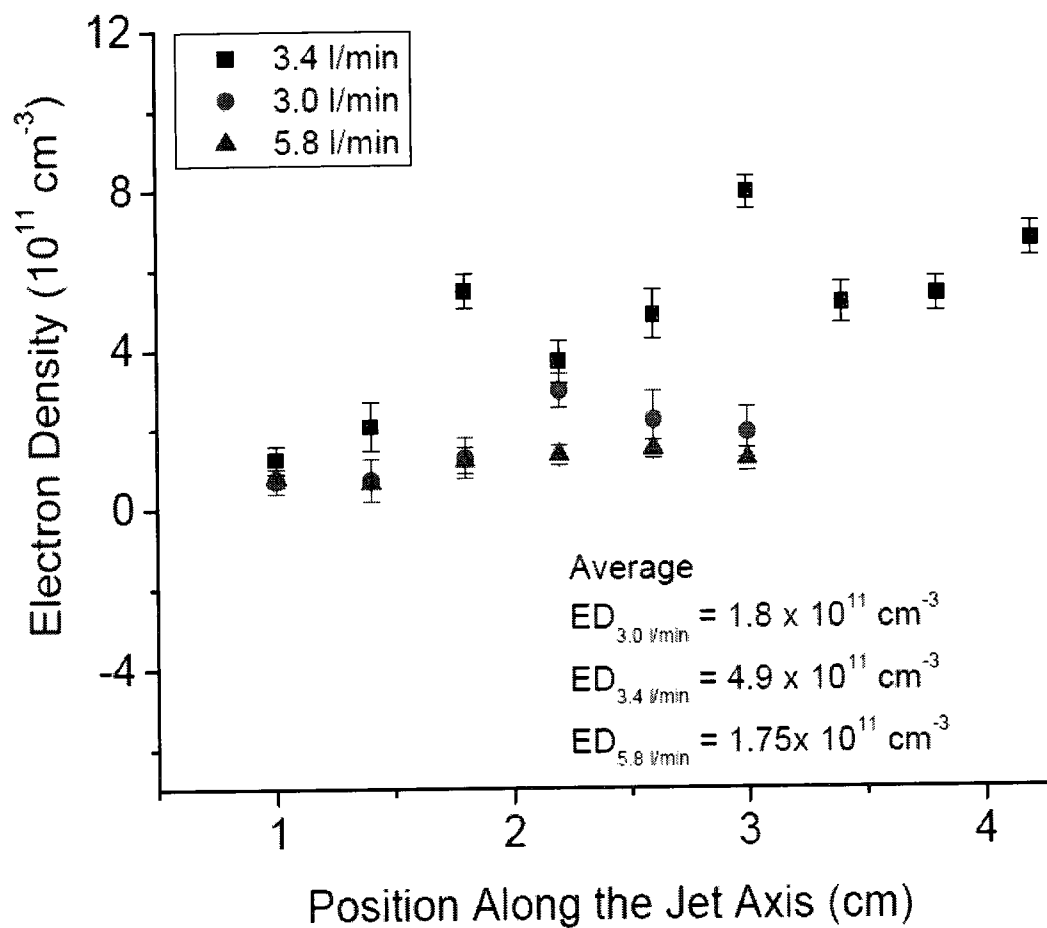
FIG. B.6. Electron density estimated by using a dielectric probe for different feed gas flow rate.

VITA

Education

2010 (summer)   Ph.D., Electrical and Computer Engineering,
                Old Dominion University, USA.

2001   M.Sc., Physics, Dhaka University, Bangladesh.

1998   B.Sc., Physics, Dhaka University, Bangladesh.

Publications

Peer-Reviewed Journal Publications

- N. Mericam-Bourdet, M. Laroussi, **A. Begum**, E. Karakas, "**Experimental Investigations of the Plasma Bullets**", *Appl. Phys. D: Appl. Phys.* **42** 5 (2009)

- E. Karakas, **A. Begum**, M. Laroussi, "**A Positive C orona-Based Ion Wind Generator**", *IEEE Transactions on Plasma Science*, **36** 3 (2008)

Conference Presentations

1. **A. Begum**, E. Karakas, M. Laroussi, " Jet velocity measurement by using electrical and optical techniques" *International Conference on Plasma Science (ICOPS)*, June 15-19, 2010, Norfolk, USA (Oral).

2. **A. Begum**, M. Laroussi, "Electrical diagnostic of plasma jet along the jet axis" *International Conference on Plasma Science (ICOPS)*, June 15-19, 2010, Norfolk, USA (Poster)

3. M. Laroussi, **A. Begum**, E. Karakas, J. Jarrige,Nicolas Mericam-Bourdet and S. Dhali, "Physical and Chemical charectarestics of Plasma bullet" *International conference of phenomanon in ionized gas (ICPIG)* July, 12-17, 2009, Maxico. (Contributed Paper)

4. **Asma Begum**, Erdinc Karakas, Mounir Laroussi, "Formation and Contraction of the Plasma Bullets Emitted by a Pulsed Plasma Jet" *International Conference on Plasma Science (ICOPS)*, May 31-June 5, 2009, California, USA (Oral).

5. M. Laroussi, **A. Begum**, and E. Karakas, "Role of The Species Generated by Plasma Jets in the Formation of The Plasma Bullets" *International Conference on Plasma Science (ICOPS)*, May 31-June 5, 2009, California, USA (Poster).

6. E. Karakas, **A. Begum**, and M. Laroussi, "Effects of Fluid Flow on the Characteristics of an Atmospheric Pressure Low Temperature Plasma Jet" *International Conference on Plasma Science (ICOPS)*, San Diego, California (2009)

7. E. Karakas, **A. Begum**, M. Lemaster, M. Laroussi, G. McCombs, M. Darby and W. Hynes "Experimental Investigations of Plasma Bullets and their Effect on Streptococcus mutans" *The Second International Conference on Plasma Medicine*, March 16-20, 2009, Texas, USA.

8. M. Laroussi, E. Karakas, and **A. Begum**, "Experimental investigation of ring shaped plasma bullets emitted by pulsed plasma jet" *IEEE international Pulsed Power Plasma Conference*, June 29-July 2, 2009, Washington, USA (Contributed paper)

9. **A. Begum**, E. Karakas, M, Laroussi, " Formation and Propagation of the plasma Bullets emitted by Pulsed Plasma Jet" *Gaseous Electronic Conference*, October 13-17, 2008, Dallas, Texas, USA

10. **Asma Begum**, Erdinc Karakas, Nicolas Mericam-Bourdet, and Mounir Laroussi, "Dynamics of the Plasma Bullets Emitted by a Pulsed Plasma Jet", *Gordon Research Conference (GRC) on Plasma Processing Science*, Mount Holyoke College, July 13-19, 2008, South Hadley, Massachusetts, USA.

11. **A. Begum**, N. Mericam-Bourdet, E. Karakas , S. K. Dhali, and M. Laroussi, "Investigation of the Plasma Bullets Generated by Low Temperature Plasma Jets", **International Conference on Plasma Science (ICOPS)**, June 15-19, 2008, Karlsruhe, Germany (Poster).

12. E. Karakas, **A. Begum**, M. Laroussi, "Experimental Measurements of an Ionic Wind Generated by a Positive Corona Discharge", **International Conference on Plasma Science (ICOPS)**, June 15-19, 2008, Karlsruhe, Germany (Poster).